Osteology of the axial skeleton of *Aucasaurus garridoi* (Coria, Chiappe and Dingus 2002): phylogenetic and paleobiological inferences

Mattia Antonio Baiano [Corresp., 1, 2, 3, 4], **Rodolfo Coria** [3, 5], **Luis M Chiappe** [6], **Virginia Zurriaguz** [7], **Ludmila Coria** [5]

[1] Consejo Nacional de Investigaciones Científicas y Técnicas (CONICET), Buenos Aires, Argentina

[2] Museo Municipal Ernesto Bachmann, Villa el Chocón, Argentina

[3] Universidad Nacional de Río Negro, General Roca, Argentina

[4] School of Life Sciences/, Chinese University of Hong Kong, Hong Kong, China

[5] Museo Municipal Carmen Funes, Plaza Huincul, Argentina

[6] Dinosaur Institute, Natural History Museum of Los Angeles County, Los Angeles, United States of America

[7] Instituto de Investigación en Paleobiología y Geología (IIPG), General Roca, Argentina

Corresponding Author: Mattia Antonio Baiano
Email address: mbaiano@unrn.edu.ar

Aucasaurus garridoi is an abelisaurid theropod from the Anacleto Formation (lower Campanian, Upper Cretaceous) of Patagonia, Argentina. The holotype of *Aucasaurus garridoi* includes cranial material, axial elements, and almost complete fore- and hind limbs. Here we present a detailed description of the axial skeleton of this taxon, along with some paleobiological and phylogenetic inferences. The presacral elements are somewhat fragmentary, although these show features shared with other abelisaurids. The caudal series, to date the most complete among brachyrostran abelisaurids, shows several autapomorphic features including the presence of pneumatic recesses on the dorsal surface of the anterior caudal neural arches, a tubercle lateral to the prezygapophyses of mid caudal vertebrae, a prominent tubercle on the lateral rim of the transverse processes of the caudal vertebrae, and the presence of a small ligamentous scar near the anterior edge of the dorsal surface in the anteriormost caudal transverse processes. The detailed study of axial skeleton of *Aucasaurus garridoi* has also allowed us to identify characters that could be useful for future studies attempting to resolve the internal phylogenetic relationships of Abelisauridae. Computed tomography scans of some caudal vertebrae show pneumatic traits in neural arches and centra, and thus the first reported case for an abelisaurid taxon. Moreover, some osteological correlates of soft tissues present in *Aucasaurus* and other abelisaurids, especially derived brachyrostrans, underscore a previously proposed increase in axial rigidity within the Abelisauridae clade.

Osteology of the axial skeleton of *Aucasaurus garridoi* (Coria, Chiappe and Dingus 2002): phylogenetic and paleobiological inferences

Mattia A. Baiano[1,2,3,4], Rodolfo A. Coria[4,5], Luis Chiappe[6], Virginia Zurriaguz[7], Ludmila Coria[5]

[1] Consejo Nacional de Investigaciones Científicas y Técnicas (CONICET), Buenos Aires, Argentina

[2] Área Laboratorio e Investigación, Museo Municipal "Ernesto Bachmann", Villa El Chocón, Neuquén, Argentina

[3] School of Life Sciences, The Chinese University of Hong Kong, Shatin, Hong Kong SAR, China

[4] Universidad Nacional de Río Negro (UNRN), General Roca, Río Negro, Argentina

[5] Museo Municipal "Carmen Funes", Av. Córdoba 55, (8318) Plaza Huincul, Neuquén, Argentina

[6] Dinosaur Institute, Natural History Museum of Los Angeles County, 900 W Exposition Blvd, (90007) Los Angeles, California, USA

[7] Instituto de Investigación en Paleobiología y Geología (IIPG). Universidad Nacional de Río Negro. Consejo Nacional de Investigaciones Científicas y Tecnológicas (CONICET). Av. Roca 1242, (8332) General Roca, Río Negro, Argentina.

Corresponding author:

Mattia Baiano

Calle Dr. Natali s/n, Villa El Chocón, Neuquén, Q8311AZA, Argentina

Email addresses: mbaiano@unrn.edu.ar

ABSTRACT

Aucasaurus garridoi is an abelisaurid theropod from the Anacleto Formation (lower Campanian, Upper Cretaceous) of Patagonia, Argentina. The holotype of *Aucasaurus garridoi* includes cranial material, axial elements, and almost complete fore- and hind limbs. Here we present a detailed description of the axial skeleton of this taxon, along with some paleobiological and phylogenetic inferences. The presacral elements are somewhat fragmentary, although these show features shared with other abelisaurids. The caudal series, to date the most complete among brachyrostran abelisaurids, shows several autapomorphic features including the presence of pneumatic recesses on the dorsal surface of the anterior caudal neural arches, a tubercle lateral to the prezygapophyses of mid caudal vertebrae, a prominent tubercle on the lateral rim of the transverse processes of the caudal vertebrae, and the presence of a small ligamentous scar near the anterior edge of the dorsal surface in the anteriormost caudal transverse processes. The detailed study of axial skeleton of *Aucasaurus garridoi* has also allowed us to identify characters that could be useful for future studies attempting to resolve the internal phylogenetic relationships of Abelisauridae. Computed tomography scans of some caudal vertebrae show pneumatic traits in neural arches and centra, and thus the first reported case for an abelisaurid taxon. Moreover, some osteological correlates of soft tissues present in *Aucasaurus* and other abelisaurids, especially derived brachyrostrans, underscore a previously proposed increase in axial rigidity within the Abelisauridae clade.

KEYWORDS: Theropoda; Abelisauridae; Brachyrostra; Late Cretaceous; Anacleto Formation; Patagonia; Phylogeny; Pneumaticity

INTRODUCTION

Abelisauridae is among the best known groups of non-avian theropods that reached the end of the Cretaceous (Bonaparte, 1985; Wilson *et al*., 2003; Krause *et al*., 2007; Novas *et al*., 2010; Gasparini *et al*., 2015). Abelisaurids are mostly known from Gondwanan landmasses, which have provided the best record in terms of abundance and specimen completeness (e.g. Krause *et al*., 2007; Novas *et al*., 2013; Zaher *et al*., 2020). In contrast, the Laurasian record is scanty; it is mostly derived from the Cretaceous of France (Buffetaut, Mechin & Mechin-Salessy, 1988; Le Loeuff & Buffetaut, 1991; Accarie *et al*., 1995; Allain & Pereda-Suberbiola, 2003; Tortosa *et al*., 2014), although some putative abelisaurids have been reported from the Cretaceous of Hungary and Spain (Ösi, Apesteguía & Kowalewski, 2010; Ösi & Buffetaut, 2011; Isasmendi *et al*., 2022).

Since they were firs discovered, abelisaurids were recognized as having a peculiar cranial anatomy and by the stricking difference between their appendicular and axial skeleton when compared to that of other theropods. In particularly, the axial skeleton shows traits, mostly in the vertebrae, which are unique of this group. Among Gondwanan abelisaurids, several taxa are known to preserved axial elements (e.g. *Ekrixinatosaurus*, *Ilokelesia*, *Pycnonemosaurus*; Coria & Salgado, 2000; Kellner & Campos, 2002; Calvo, Rubilar-Rogers & Moreno, 2004), but only seven taxa have preserved complete portions (articulated or semi-articulated) of the vertebral series: *Aucasaurus*, *Eoabelisaurus*, *Carnotaurus*, *Majungasaurus*, *Skorpiovenator*, *Spectrovenator*, and *Viavenator* (Bonaparte, Novas & Coria, 1990; Coria, Chiappe & Dingus, 2002; O'Connor, 2007; Canale *et al*., 2009; Pol & Rauhut, 2012; Filippi *et al*., 2016; Zaher *et al*.,

2020). Among them, detailed osteological descriptions of the vertebral column have been provided for *Carnotaurus* (Méndez, 2014a), *Majungasaurus* (O'Connor, 2007), and *Viavenator* (Filippi *et al*., 2016).

Here, we have carried out a detailed description of the axial skeleton of the holotype of *Aucasaurus garridoi* (MCF-PVPH-236), which is the second detailed study of the anatomy of this abelisaurid after the study of its braincase (Paulina-Carabajal, 2011). The axial skeleton of MCF-PVPH-236 is composed of cervical, dorsal, and caudal vertebrae, cervical and dorsal ribs, gastralia, and haemal arches. In spite of Coria, Chiappe & Dingus (2002) proposing a valid diagnosis for *Aucasaurus*, after the discovery of new abelisaurid species in the ensuing 20 years, we propose a new revised diagnosis using information from the axial skeleton. An exhaustive comparison between *Aucasaurus* and other abelisaurids, especially Argentinian specimens, has allowed us to detect several anatomical traits of the axial skeleton shared by these taxa, thus strengthening of Abelisauridae and adding new data for future phylogenetic analyses. We have also used (CT) scans of some caudal vertebrae to visualize their internal structure. We thus offer the first CT data of the axial skeleton of Abelisauridae, and investigate its pneumaticity. Finally, our detailed study of the axial anatomy has revealed traits in *Aucasaurus* and other brachyrostran abelisaurids that are functionally related to increased rigidity of the axial skeleton.

Institutional abbreviations: MACN, Museo Argentino de Ciencias Naturales "Bernardino Rivadavia", Buenos Aires, Argentina; **MAU**, Museo Municipal Argentino Urquiza, Rincón de Los Sauces, Argentina; **MCF**, Museo Carmen Funes, Plaza Huincul, Argentina; **MHNA**, Muséum d'Histoire Naturelle d'Aix-en-Provence, Aix-en-Provence, France; **MMCh**, Museo Municipal "Ernesto Bachmann", Villa El Chocón, Argentina; **MPCA**, Museo Provincial Carlos

Ameghino, Cipolletti, Argentina; **MPCN**, Museo Paleontológico de Ciencias Naturales, General Roca, Argentina; **MPEF**, Museo Paleontologico Egidio Feruglio, Trelew, Argentina; **MPM**, Museo Regional Provincial "Padre Manuel Jesús Molina", Río Gallego, Argentina; **MUC**, Museo Universidad Nacional del Comahue, Neuquén, Argentina; **UNPSJB**, Universidad Nacional de Patagonia San Juan Bosco, Comodoro Rivadavia, Argentina.

MATERIALS AND METHODS

The axial skeleton of the holotype of *Aucasaurus garridoi* (MCF-PVPH-236) includes the atlas and fragments of the cervical vertebrae, the second to seventh dorsal vertebrae, fragmentes of posterior dorsal vertebrae, the complete sacrum, the first to thirteenth caudal vertebrae, posterior caudal vertebrae, cervical and dorsal ribs, gastralia, and the first to thirteenth haemal arches (Fig. 1). We conducted a detailed comparison of MCF-PVPH-236 with several theropods, particular Argentinian abelisauroids. In the case of specimens where the position of the vertebrae was confidently identified, comparisons with *Aucasaurus* were using the same vertebral element. However, in those cases in which the position of specific axial elements was not known with certainty, comparisons were carried out at a more regional level: anterior, middle, and posterior (see Discussion). The Table 1 shows all taxa used in the present study (examined directly or whose data was taken from the literature). We followed the anatomical nomenclature of Wilson (1999, 2012) and Wilson *et al*. (2011) to describe laminae and fossae. These structures are spelled out when first mentioned in the text (plus acronym), subsequently they are cited only using their acronyms.

All measurements were taken using a digital calliper (Supporting Information, Table S1-S3) and images for figures (both single pothographs and photogrammetry renderings) were captured using a Nikon 3100 digital camera.

To test the phylogenetic position of *Aucasaurus* based on new axial information, we carried out an analysis based on the most recently studies of Ceratosauria (Tortosa *et al*., 2014; Filippi *et al*., 2016; Rauhut & Carrano, 2016; Baiano, Coria & Cau, 2020; Baiano *et al*., 2021, 2022; Aranciaga Rolando *et al*., 2021; Gianechini *et al*., 2021; Cerroni *et al*., 2022). We added 11 (7 new and 4 from other sources) to the data matrices of Baiano *et al*. (2022) and Cerroni *et al*. (2022); we also added 3 new taxa (*i.e.*, *Kurupi*, *Thanos*, and the Abelisauridae indet. MPM 99). The resulting data matrix consisted of 246 characters and 46 taxa (Supporting Information, Data S1). Moreover, we have improved the matrix providing new scorings for the following characters for *Aucasaurus*: 96, 98, 107, 112, 115, 116, 117, 120, 121, 123, 123, 128, 134, 136, 137. We also re-scored two characters in *Aucasaurus* (ch. 119 from "1" to "?"; ch. 133 from "0&1" to "1"). The data matrix (Supporting Information, Data S2) was edited with MESQUITE 3.61 (Maddison & Maddison, 2019). The analysis was performed using TNT 1.5 (Goloboff, Farris & Nixon, 2008; Goloboff and Catalano, 2016), conducting a traditional search through 1000 replicates of Wagner trees (saving 10 trees per replicate) followed by tree bisection–reconnection (TBR) branch swapping. The memory to store all most parsimonious trees (MPTs) was implemented to 50000. The MPTs obtained were submitted to a second round of TBR. All characters were weighted equally. To detect possible unstable taxa, we performed the IterPCR procedure (Pol & Escapa, 2009), and used Bremer support and Jackniffe value through the pcrjack.run script to assess nodal support (Pol & Goloboff, 2020).

We CT scanned six caudal vertebrae (*i.e.*, first, fifth, sixth, ninth, twelfth, and thirteenth) to investigate their internal structure. The CT scans was performed using a Toshiba Aquilion Lightnight 16/32 scanner, in the Sanatorio Plaza Huincul in Plaza Huincul (Neuquén Province, Argentina). The CT scans were carried out along the transversal, coronal, and sagittal planes with the following settings: 120 kVp, 50 mA, and slices each 5-mm. The number of slices for each vertebra is: first: 36 coronal slices, 11 transversal slices, and 23 sagittal slices; fifth and sixth: 44 coronal slices, 12 transversal slices, and 23 sagittal slices; ninth: 30 coronal slices, 9 transversal slices, and 23 sagittal slices; twelfth and thirteenth: 36 coronal slices, 7 sagittal slices, and 19 sagittal slices. The slices were observed using the K-PACS software produced by Ebit (ESAOTE).

FIGURE 1 (NEAR HERE)

Figure 1. **Axial skeleton of *Aucasaurus garridoi***. Lateral right view of the axial elements of the holotype MCF-PVPH-236. Scale bar: 1 m. Silhouette modified from Scott Hartman (https://www.skeletaldrawing.com/).

Table 1. Taxa used for anatomical comparisons.

SYSTEMATIC PALAEONTOLOGY

Dinosauria Owen, 1842

Saurischia Seeley, 1887

Theropoda Marsh, 1881

Ceratosauria Marsh, 1884

Abelisauroidea (Bonaparte & Novas), 1985

Abelisauridae Bonaparte & Novas, 1985

Brachyrostra Canale, Scanferla, Agnolín & Novas, 2009

Aucasaurus Coria, Chiappe & Dingus, 2002

Etymology

The generic name was established by Coria, Chiappe & Dingus (2002) in reference to Auca Mahuevo, the fossil locality in which the holotype was found, with the Greek suffix -σαῦρος (sauros), lizard or reptile.

Diagnosis

As for the species.

Aucasaurus garridoi Coria, Chiappe & Dingus 2002

Type species and etymology

The name of the type species was erected in recognition to geologist Alberto Garrido, who discovered the holotype.

Holotype

MCF-PVPH-236, Museo Carmen Funes (Plaza Huincul, Neuquén Province, Argentina), a partial skeleton including cranial, axial, and appendicular elements (see Coria, Chiappe & Dingus, 2002).

190

191 *Locality and Horizon*

192 Auca Mahuevo paleontological site (Chiappe *et al*., 1998), near Mina La Escondida, in the
193 northeastern corner of the Neuquén Province, Argentina. The holotype was recovered from strata
194 belonging to the Anacleto Formation (lower Campanian, Upper Cretaceous), Río Colorado
195 Subgroup, Neuquén Group of the Neuquén Basin. Sedimentological and stratigraphic
196 descriptions of these strata and of the Anacleto Formation are provided elsewhere (see Dingus *et*
197 *al*., 2000; Coria, Chiappe & Dingus, 2002; Garrido, 2010a, b).

198

199 *Comments on the original diagnosis*

200 The original diagnosis established by Coria, Chiappe & Dingus (2002) was largely based on
201 morphological comparisons with *Carnotaurus* and mentioning only one autapomorphy (i.e.,
202 anterior haemal arches with proximally opened neural canal). Here, we expand the diagnosis to
203 include the following unique features of the axial skeleton: 1) atlas with a subcircular articular
204 surface; 2) interspinous accessory processes extended to sacral and caudal neural spine; 3)
205 presence of a tubercle lateral to the prezygapophysis of mid caudal vertebrae (a similar structure
206 is mentioned in *Aoniraptor*; Motta *et al*., 2016); 4) presence of pneumatic foramina laterally to
207 the base of the neural spine in the anterior caudal vertebrae; 5) presence of a prominent tubercle
208 and extensive rugosity on the lateral rim of the transverse processes of caudal vertebrae fourth to
209 twelfth; 6) presence of a small ligamental scar near the anterior edge of the dorsal surface in the
210 anteriormost caudal transverse processes; 7) distinct triangular process located at the fusion point
211 of posterior middle gastralia. In addition, according to Coria, Chiappe & Dingus (2002), the skull
212 of *Aucasaurus* differs from that of *Carnotaurus sastrei* in having a longer and lower rostrum,

frontal swells instead of horns, and a sigmoidal outline of the dentigerous margin of the maxilla. Several postcranial differences also distinguish *Aucasaurus garridoi* from *Carnotaurus sastrei*: a less developed coracoidal process, a forelimb relatively longer, a humerus with a slender and craniocaudally compressed shaft and well-defined condyles, and a proximal radius lacking a hooked ulnar process.

DESCRIPTION AND COMPARISONS

Cervical Vertebrae (Fig. 2, 3): An almost complete atlas and several cervical fragments are preserved. The most notable piece is a right neural arch that could belong to the fifth cervical vertebra. The other remains are identified as part of isolated epipophyses.

Atlas (Fig. 2; Supporting Information, Table S1): The atlas preserves the intercentrum with a fused portion of the right neurapophysis (Fig. 2A-C). In anterior view (Fig. 2A), the articular surface for the occipital condyle is strongly concave and subcircular, which differs from the slightly transversely wider than tall atlas of *Skorpiovenator* and *Viavenator*, and from the strongly dorsoventrally compressed atlas of *Carnotaurus*, *Ceratosaurus*, and some tetanurans (e.g. *Allosaurus*, *Sinraptor*). The concave dorsal edge preserves the odontoid process in artculation. The right neurapophysis is directed dorsolaterally, and a hook-shaped process directed anteromedially on its ventromedial part seems less developed than in *Ceratosaurus*, *Majungasaurus*, *Skorpiovenator*, *Viavenator*, and *Carnotaurus*. The absence of prezygapophyses suggests that *Aucasaurus* lacked a protoatlas as in *Majungasaurus*, *Skorpiovenator*, *Viavenator*, and *Carnotaurus*.

In posterior view (Fig. 2B), the articular surface is flat as in *Viavenator*, but different from the convex surface in *Ceratosaurus*, *Carnotaurus*, and some tetanurans (e.g. *Allosaurus*,

Sinraptor). The posterior articular surface is stepped due to two parapophyseal processes located on the ventral edge. In this view, the pneumatic internal arrangement can be visualized through a break in the odontoid process. There are several small chambers, resembling a camellate condition.

In lateral view (Fig. 2C), the surface has a rectangular outline and is slightly dorsoventrally concave, although it slightly narrows ventrally. The neurapophysis is firmly fused to the intercentrum and there are no visible sutures. The posterior border of the neurapophysis forms a ridge that ends ventrally in the intercentrum.

In ventral view (Fig. 2D), the surface presents two ventrally directed processes as seen in *Skorpiovenator*, *Viavenator*, and *Carnotaurus*, which could be interpreted as parapophysis-like structures for rib articulation. However, in *Aucasaurus* these processes are separated by a more superficial groove than in *Viavenator* and *Carnotaurus*.

In dorsal view (Fig. 2E), the poor preservation of the neurapophyses prevents either the evaluation of its extension, or an assessment of the morphology of the postzygapophyses and medial processes. The preserved portion of the neurapophysis has an oval cross-section, although it narrows slightly anteriorly. The neurapophysis is slightly twisted with its greater axis anteromedially-posterolaterally directed. A fragment of the odontoid process is preserved on the dorsal part of the atlas. It has a triangular shape in dorsal view, different from the more circular outline of this structure in *Ceratosaurus*, *Masiakasaurus*, *Majungasaurus*, *Thanos*, and *Carnotaurus*. Therefore, this is here considered an autapomorphy of *Aucasaurus*. The dorsal surface of odontoid is concave, while the lateral and ventral surfaces are strongly convex to fit in the dorsal edge of the intercentrum.

FIGURE 2 (NEAR HERE)

Figure 2. **Atlas of *Aucasaurus garridoi* MCF-PVPH-236**. In anterior (A), posterior (B), right lateral (C), ventral (D), and dorsal (E) views. Abbreviations: amp, anteromedial process; ic, intercentrum; nrp, neurapophysis; od, odontoid; vp, ventral process. Scale bar: 5 cm.

Middle cervical vertebra (Cv-05?) (Fig. 3A-C): Only the right lateral portion of the neural arch is preserved. In anterior view, the prezygapophysis has a flat, dorsomedially sloping facet as in *Dahalokely*, *Carnotaurus*, *Ilokelesia*, *Majungasaurus*, *Skorpiovenator*, *Viavenator*, and Abelisauridae indet. MPM 99.

In lateral view (Fig. 3A), a well-defined epipophyseal-prezygapophyseal lamina (eprl) connects the prezygapophysis with the epipophysis, separating the lateral part of the transverse process from the dorsal part of the neural arch, as in other abelisauroids (e.g. Carrano & Sampson, 2008). This lamina, although broken in some parts, is straight as in *Majungasaurus* and *Carnotaurus*, but unlike *Viavenator* where is concave, or *Dahalokely* where it is strongly convex. Furthermore, in *Aucasaurus*, the posteriormost part of the eprl is dorsally directed, probably reaching the epipophysis. The transverse process is triangular in outline and directed ventrally. It has a flat, lateral surface with a straight prezygodiapophyseal lamina (prdl) and a concave postzygodiapophyseal lamina (podl). The latter is developed as a faint crest (Fig. 3B), which is a condition observed in abelisaurids such as *Skorpiovenator* and *Ilokelesia*. The postzygapophysis is partially preserved and positioned 1.5 cm from the podl. The postzygapophysis has a flat articular facet, is directed ventrolaterally, and is anteroposteriorly longer than mediolaterally wide (Fig. 3B). However, the medial border is partially broken, suggesting that it also extended medially with a drop-like outline. The base of an epipophysis is preserved dorsally to the postzygapophysis.

In dorsal view (Fig. 3C), a slight depression separates the prezygapophysis from a robust spinoprezygapophyseal lamina (sprl) that preserves only the base. This lamina has an anterolateral-posteromedial orientation. The prezygapophysis shows a drop-like outline, having the widest part located laterally as other abelisaurids (e.g. *Dahalokely*, *Carnotaurus*, *Ilokelesia*, *Majungasaurus*, *Viavenator*).

Other cervical remains (Fig. 3D-G)*:* Several fragments of epipophyses are preserved. Two of them contacting to each other (Fig. 3D, E). The dorsal edges of the epipophyses are slightly convex, transversely thicker than the body and with a rough surface. At least one epipophysis shows anterior and posterior processes as in *Noasaurus*, *Rahiolisaurus*, *Viavenator*, *Carnotaurus*, and Abelisauridae indet. MPM 99, in contrast to other abelisaurids that present only a posterior process (e.g. *Ilokelesia*, *Skorpiovenator*, *Spectrovenator*).

An epipophysis probably belonging to either the eighth or the ninth cervical vertebra is preserved (Fig. 3F, G). It has an anteroposteriorly reduced posterior process. Beneath it, the postzygapophysis is partially crushed. Most likely, the epipophyses had medially converging anterior processes. The hypertrophied epipophyses of *Aucasaurus* and other abelisaurids (e.g. *Viavenator*, *Carnotaurus*) served as the point of origin of the *m. complexus* (on the anterior process), and the attachment point of the *m. longus colli dorsalis* (on the posterior process) (Snively & Russell, 2007; González, Baiano & Vidal, 2021).

FIGURE 3 (NEAR HERE)

Figure 3. **Cervical vertebra fragments of *Aucasaurus garridoi* MCF-PVPH-236**. In lateral (A, G, E), ventral (B), dorsal (C), and medial (D, F) views. Abbreviations: ape, anterior process of epipophysis; eprl, epipophyseal prezygapophyseal lamina; podl, postzygodiapophyseal lamina;

poz, postzygapophysis; ppe, posterior process of epipophysis; prz, prezygapophysis; sprl, spinoprezigapophyseal lamina; tp, transverse process. Scale bar: 5 cm.

Dorsal Vertebrae (Fig. 4-7): The preserved dorsal vertebrae are very fragmentary. A series of articulated anterior dorsal vertebrae are regarded to range from the second to the seventh dorsal based on both the morphology of the neural spines and the position of the parapophyses. In addition, a posterior dorsal vertebra, a posterior vertebral centrum, and several distal fragments of posterior dorsal neural spines are also preserved.

Second dorsal vertebra (D2; Fig. 4A, B; Fig. 5A-D; Supporting Information, Table S1): The second dorsal vertebra is badly preserved. The centrum is severely cracked and transversely crashed. Part of the anterior articular surface and the lateral surface are missing. The neural arch is almost entirely missing, except for the neural spine, which was posteriorly displaced.

The anterior articular surface is concave and dorsoventrally higher than transversely wide, probably due to taphonomic deformation. The right parapophysis is partially preserved. It is low and probably had a dorsoventral elliptical outline as in *Carnotaurus*, *Dahalokely*, *Skorpiovenator*, and *Xenotarsosaurus*. The posterior articular surface seems to be a little more complete than the anterior one (Fig. 4A, B). It is strongly concave and shows an elliptical contour probably due lateral compression. The ventral surface shows neither a groove nor a keel (Fig. 5A, B) as in *Dahalokely*, *Skorpiovenator*, and *Xenotarsosaurus*, but unlike *Elaphrosaurus* and *Majungasaurus* where there is a faint keel. Conversely, *Carnotaurus* and *Viavenator* have two longitudinal crests converging posteriorly.

The neural spine is transversely wider than anteroposteriorly long, being less than one third of the centrum length as in *Carnotaurus*, *Skorpiovenator*, and *Viavenator*, but shorter than in *Dahalokely*. The lateral surface of the spine is slightly concave anteroposteriorly (Fig. 4A, B), thus the anterior and posterior edges are more laterally protuding. The neural spine is distally thick and presents a reduced anterior process for the insertion of interspinous ligaments. This process is separated from the rest of the spine by two lateral grooves. In dorsal view (Fig. 5C, D), a small process projects posteriorly.

Third dorsal vertebra (D3; Fig. 4A, B; Fig. 5A-D; Supporting Information, Table S1): The third dorsal vertebra is better preserved than the preceeding one, although it presents a significant transversal deformation and several fractures.

The anterior articular surface of the centrum is slightly concave but the articulation with the previously vertebra prevents us to evaluate further anatomical features. In lateral view (Fig. 4A, B), the anterior and posterior rims are parallel to each other. The parapophysis is positioned more dorsally than the previous vertebra and is elliptical in outline as in *Eoabelisaurus*, *Majungasaurus*, *Skorpiovenator*, and *Carnotaurus*, but its ventral part is slightly narrower anteroposteriorly than the dorsal one. The long axis of the parapophysis is slightly inclined posteriorly as in *Carnotaurus* and *Masiakasaurus*, but different from the dorsoventrally oriented parapophysis of *Eoabelisaurus* and *Majungasaurus*. Posterodorsally to the parapophysis and below the neurocentral suture, there is an anteroposterior oval fossa on the lateral surface. In the anterior corner of that fossa, there is a circular pleurocoel, which in turn is separated dorsally from two other small foramina by a septum. An anterior pleurocoel is also present in *Carnotaurus*, *Majungasaurus*, and *Skorpiovenator* (the latter have also a posterior one). In

353 posterior view, the articular surface is covered by the centrum of the next vertebra. However, a
354 reduced part is exposed, showing a concave surface. In ventral view (Fig. 5A, B), the surface has
355 neither a keel nor a groove as *Eoabelisaurus* and *Skorpiovenator*; in contrast, a faint keel is
356 present in *Elaphrosaurus*.

357 The anterior surface of the neural spine has a dorsal process that protrudes anteriorly for
358 the anchorage of interspinous ligaments. In lateral view (Fig. 4A, B), the right transverse process
359 is not preserved. However, the anterior centrodiapophyseal lamina (acdl), the posterior
360 centrodiapophyseal lamina (pcdl) and the centrodiapophyseal fossa (cdf) (or the
361 centroparapophyseal fossa; cpaf) are visible. The neural spine is anteroposteriorly longer than the
362 previous one, with a square cross-section, but it is shorter than the half of the centrum length as
363 in *Carnotaurus* and *Majungasaurus*, whereas in *Eoabelisaurus* is slightly longer. Laterally, the
364 anterodorsal process for the interspinous ligaments is visible. The two lateral grooves that
365 separate this process from the rest of the dorsal neural spine are deeper than in the D2 (Fig. 5C,
366 D). The interspinous ligamental process is also present in *Carnotaurus* and *Eoabelisaurus*, but
367 more ventrally positioned than in *Aucasaurus* and *Skorpiovenator*. Lateral to the interspinous
368 ligamental process, there is another process projected anteriorly as in *Eoabelisaurus*. In posterior
369 view, only the right postzygapophysis can be observed, which, despite being articulated with the
370 prezygapophysis of the next vertebra, seems to be anteroposteriorly longer than transversely
371 wide.
372
373 *Fourth dorsal vertebra* (D4; Fig. 4A, B; Fig. 5A-D; Supporting Information, Table S1): The
374 centrum of the fourth dorsal vertebra is slightly anteroposteriorly larger than that of the D3 (Fig.
375 4A, B). Both articular surfaces are slightly concave and, despite the deformation, probably was

dorsoventrally taller than transversely wide. The lateral surface of the centrum presents a wide fossa with a pleurocoel located more centrally than that of the D3, unlike *Carnotaurus*, *Majungasaurus*, *Skorpiovenator*, *Viavenator*, and the Abelisauridae indet. MAU-Pv-LI 665, which hold a more anterior pleurocoel, whereas *Rajasaurus* lacks pneumatic opening in the centrum of this dorsal. The parapophysis is shifted more dorsally, between the centrum and neural arch, as in *Carnotaurus*, *Eoabelisaurus*, *Rajasaurus*, *Skorpiovenator*, and the Abelisauridae indet. MAU-Pv-LI 665, but different than in *Viavenator* that holds parapophyses entirely on the neural arch and more laterally projected. The ventral surface lacks keel or groove (Fig. 5A, B), as in *Carnotaurus*, *Eoabelisaurus*, but unlike *Viavenator* that has a shallow groove, and the Abelisauridae indet. MAU-Pv-LI 665 that holds a longitudinal keel.

In anterior view, only the neural spine is visible, which is transversely narrower than that of the D3. The anterodorsal process of the neural spine for the interspinous ligaments is conspicuous and has a rough surface, as in *Viavenator* but unlike *Carnotaurus*, *Eoabelisaurus*, *Majungasaurus* where it is poorly developed, or even absent in *Skorpiovenator*.

In lateral view (Fig. 4A, B), the ventral terminus of the right acdl and pcdl are visible and diverge from each other, reaching the arch pedicels. These laminae frame a triangular centrodiapophyseal (or centroparapophyseal) fossa. The right prezygapophysis is articulated with the postzygapophysis of the D3, preventing to see its morphology. However, it seems to be anteroposteriorly longer than mediolaterally wide and tilted medially. The prezygapophysis does not have any ventral process, attributable as the lateral wall of the hypantrum, such as the one present in *Carnotaurus* and *Skorpiovenator*. This condition differs from *Eoabelisaurus*, *Majungasaurus*, and *Viavenator* that have an incipient ventral process. The lateral surface of the neural spine is slightly concave and it is the first neural spine that is longer than transversely

399 wide, as in *Eoabelisaurus*, *Majungasaurus*, and *Skorpiovenator*. This condition differs from the
400 wider than long neural spine of *Carnotaurus*, whereas in *Viavenator* is square in cross-section.
401 The dorsal end of the neural spine presents a transversal thickening and a marked anterodorsal
402 process for the interspinous ligaments. This structure is anteriorly projected, unlike the neural
403 spine of D3 where it protrudes dorsally over the dorsal surface of the neural spine. The two
404 grooves that separate it from the neural spine are deep, different from *Carnotaurus*,
405 *Eoabelisaurus*, *Majungasaurus*, *Skorpiovenator*, and *Viavenator* where there are no grooves.
406 In posterior view, only the right postzygapophysis, articulated with the prezygapophysis
407 of D5, was preserved. As in the preceeding vertebrae, the postzygapophysis is longer than wide
408 and the articular facet is slightly ventrolaterally oriented, differing from the horizontal
409 postzygapophyses of *Majungasaurus*, *Rajasaurus*, *Carnotaurus*, *Skorpiovenator*, *Viavenator*,
410 and the Abelisauridae indet. MAU-Pv-LI 665.
411 In dorsal view (Fig. 5C, D), the neural spine has a Y-shaped outline, due to the lateral
412 grooves separating the anterior process and a strong concavity between two partially broken
413 posterior processes. This morphology differs from that of other abelisaurids, since these taxa
414 either lack or have a reduced interspinous ligamental process. Furthermore, in *Aucasaurus* the
415 anterior process for the interspinous ligaments is anteroposterior longer than in other
416 abelisaurids.
417
418 *Fifth dorsal vertebra* (D5; Fig. 4A, B; Fig. 5A-D; Supporting Information, Table S1): In the fifth
419 dorsal vertebra the centrum is almost completely preserved (although deformed), whereas the
420 neural arch is incomplete. Also, this vertebra presents an anterior diagenetical displacement of
421 the neural spine (Fig. 4A, B).

The anterior and posterior articular surfaces are concave and elliptical in outline with their long axis directed dorsoventrally, as in *Eoabelisaurus*, *Majungasaurus*, *Skorpiovenator*, and the Abelisauroidea indet. CPP 893, but different from *Carnotaurus* and *Viavenator* where the centrum is subcircular. The lateral surfaces of the centrum hold shallower fossae than in D4, and it lack pleurocoels (Fig. Fig. 4A, B), as in *Eoabelisaurus* and *Majungasaurus*, but in contrast to *Carnotaurus*, *Skorpiovenator*, *Viavenator*, and the Abelisauroidea indet. CPP 893 where there are fossae with pleurocoels. The parapophysis is located on the neural arch, as in *Carnotaurus*, *Eoabelisaurus*, *Majungasaurus*, *Skorpiovenator*, *Viavenator*, and the Abelisauroidea indet. CPP 893. The ventral facet has neither a groove nor a keel (Fig. 5A, B), as in *Eoabelisaurus*, *Skorpiovenator*, and *Viavenator*, but different from the longitudinal crest present in *Carnotaurus*.

In anterior view, like in the previous vertebrae, the articulation prevents the evaluation of various morphological characteristics of the neural arch. Ventrolateral to the right prezygapophysis there is a shallow centroprezygapophyseal fossa (cprf). This fossa is incipient in *Carnotaurus* and absent in *Eoabelisaurus*, *Majungasaurus*, and *Viavenator*. The prezygapophyses are subquadrangular and the articular facets are directed slightly dorsolaterally, as in *Carnotaurus*, *Eoabelisaurus*, *Majungasaurus*, *Skorpiovenator*, *Viavenator*, and the Abelisauroidea indet. CPP 893. The prezygapophysis of *Aucasaurus* lacks the ventral columnar process present in *Carnotaurus*, *Majungasaurus*, *Skorpiovenator*, *Viavenator*, and the Abelisauroidea indet. CPP 893. The anterior process for the interspinous ligaments of the neural spine is present, but it is less developed than that of the D4.

In lateral view (Fig. Fig. 4A, B), the prezygapophysis lacks a ventral process, which is present in *Carnotaurus* and *Skorpiovenator.* Despite both transverse processes are lost, the anterior centroparapophyseal lamina (acpl) is visible. This lamina is robust and ends dorsally into

445 the parapophysis. The parapophysis is not located in its original position, due to a dorsal and
446 posterior displacement. However, it is a pendant structure as in other abelisaurids. The
447 parapophysis has an oval contour, as in *Carnotaurus*, *Eoabelisaurus*, *Skorpiovenator*, and
448 *Viavenator*. The neural spine, as mentioned above, is displaced anteriorly. It is dorsoventrally
449 taller than in the D4, and the thick distalmost portion is separated from the rest of the spine by a
450 subhorizontal step. The presence of several anteroposteriorly directed ridges gives the surface of
451 this area of the neural spine a rough appearance. The process for the interspinous ligaments is
452 located at the same level of the dorsal rim of the neural spine, and the lateral grooves are
453 shallower than in the D4, as in *Viavenator* and the Abelisauroidea indet. CPP 893. In
454 *Carnotaurus* this process is more ventrally located, whereas it is absent in *Eoabelisaurus*,
455 *Majungasaurus*, and *Skorpiovenator*. In posterior view, only the surface of the neural spine can
456 be seen; this has the same transverse thickness of the anterior portion, and it becomes wider
457 towards its distal end.
458 In dorsal view (Fig. Fig. 5C, D), the neural spine is transversely thick and anteroposterior
459 longer than that of the D4. The dorsal surface of the neural spine is slightly convex transversely.
460 The outline of the dorsal surface is rectangular, with the lateral rims diverging slightly
461 posteriorly. The posterior rim is concave, due to the presence of the base of two posteriorly
462 directed processes.
463
464 *Sixth dorsal vertebra* (D6; Fig. 4A, B; Fig. 5A-D; Supporting Information, Table S1): The sixth
465 dorsal vertebra has preserved part of the centrum and the neural arch. The centrum is as high as
466 long and is slightly larger than D2-D5 vertebrae, as seen in *Carnotaurus* and *Majungasaurus*.
467 The anterior and posterior articular surfaces are strongly concave compared with the anterior

vertebrae, and they are ovally outlined. The lateral fossa of the centrum (Fig. 4A, B), such as D5, is shallow and lacks pneumatic foramina, as in *Majungasaurus*, but different from *Carnotaurus* and *Skorpiovenator*, which have lateral pleurocoels. Ventrally (Fig. Fig. 5A, B), despite the deformation, no groove or keel are observed as in *Eoabelisaurus* and *Skorpiovenator*, but unlike the D6 of *Carnotaurus* that has a pronounced keel.

The neural arch is badly damaged and crushed. In anterior view, the neural spine is transversely wider than the D5, and the anterior process for the interspinous ligaments reaches the dorsal table of the spine. In lateral view (Fig. 4A, B), the surface is eroded and only the parapophysis is distinguishable. It is partially broken and displaced anterodorsally. The neural spine is fully displaced anteriorly, being positioned almost entirely dorsally to the D5 centrum. It is anteroposteriorly long, exceeding half of the length of the vertebral centrum as in *Carnotaurus* and *Skorpiovenator*, but different from *Majungasaurus* where it is much smaller. The distal portion of the neural spine is transversely expanded with faint lateral ridges directed anteroposteriorly. The anterior process for the interspinous ligaments is partially broken; however, it is separated from the spine table.

In posterior view, only the right postzygapophysis can be distinguished, which is partially articulated with the next prezygapophysis. It seems to be longer anteroposteriorly than transversely wide, and the articular facet is directed ventrally, as in *Eoabelisaurus* and *Skorpiovenator*, but unlike *Carnotaurus* that has ventromedially oriented prezygapophyses. In dorsal view (Fig. 5C, D), the neural spine is transversely wider and the lateral rims diverge more posteriorly than the D5. It shows a posterior concavity that probably separated two posteriorly directed processes.

Seventh dorsal vertebra (D7; Fig. 4A, B; Fig. 5C, D: Supporting Information, Table S1)*:* Only the right prezygapophysis and neural spine are preserved of this vertebra. The prezygapophysis is partially articulated to the preceding postzygapophysis (Fig. 4A, B). It is longer than wide, and the articular facet is slightly directed dorsolaterally, as in *Carnotaurus* and *Viavenator*, but different than the horizontal prezygapophyses present in *Majungasaurus*, or the dorsomedially oriented condition shown in *Dahalokely*. The neural spine shows the same size as the neural spine of the D6, and the anterior process for the interspinous ligaments is conspicuous (Fig. 4A, B). The distalmost portion of the neural spine is thick and holds several longitudinal crests. In dorsal view (Fig. 5C, D), the neural spine shows a triangular outline, and the right posterior process is visible.

FIGURE 4 (NEAR HERE)

Figure 4. **Photographs and line drawings of the anterior dorsal vertebrae of *Aucasaurus garridoi* MCF-PVPH-236**. In lateral (A) view. Abbreviations: 2dns, second dorsal neural spine; 7dns, seventh dorsal neural spine; acpl, anterior centroparapophyseal lamina; D2-D6, second to seventh dorsal vertebrae; iap, interspinous accessory process; ilp, interspinous ligament process; pl, pleurocoel; pp, parapophysis; prz, prezygapophysis; tp, transverse process. Scale bar: 5 cm.

FIGURE 5 (NEAR HERE)

Figure 5. **Photographs and line drawings of the anterior dorsal vertebrae of *Aucasaurus garridoi* MCF-PVPH-236**. In ventral (A, B), and dorsal (C, D) views. Abbreviations: D2-D7, second to seventh dorsal vertebrae; iap, interspinous accessory process; ilp, interspinous ligament process. Scale bar: 5 cm.

Posterior dorsal vertebrae (Fig. 6, 7; Supporting Information, Table S1): Only some disarticulated elements corresponding to the posterior portion of the dorsal series are preserved. Despite their taphonomic deformation, some characteristics of the preserved centra and neural spines indicate that these elements belong to the most distal dorsal vertebrae. One isolated centrum is spool-shaped (Fig. 6A-F), with slightly concave and subcircular articular surfaces (Fig. 6A, B). The lateral surfaces have a shallow fossa, and there is a pleurocoel on each side (Fig. 6C, D). Dorsally, there are no signs of the neurocental suture (Fig. 6E), thus the centrum was separated from the neural arch after their fusion. The ventral surface lacks either a groove or keel (Fig. 6F).

Another vertebra (Fig. 6G-K), probably more distal than the centrum described previously, preserves part of both centrum and neural arch. The anterior and posterior articular surfaces are concave with a slightly oval outline (Fig. 6G, H). In lateral view (Fig. 6I, J), there is a deep fossa, just below the neurocentral suture, without a pneumatic foramen, as in the posterior dorsals of *Dahalokely*, *Eoabelisaurus*, *Huinculsaurus*, *Ilokelesia*, *Majungasaurus*, *Niebla*, and *Skorpiovenator* but different than in *Carnotaurus*, *Viavenator*, and the Abelisauridae indet. MPCN-PV-69, in which central fossae bear pleurocoels. The ventral surface lacks either a groove or a keel (Fig. 6K). The neural arch is crushed, and only the neural spine was preserved, which is anteroposteriorly shorter than the neural arch (Fig. 6I, J).

Several isolated dorsal neural spines were found (Fig. 7A-F), preserving approximately their dorsal halves. All of them have a smaller anteroposterior extension than the one observed in the seventh neural spine. Reduced neural spines in the posterior portion of the dorsal series, especially in the last three ones, are also present in *Carnotaurus* and *Majungasaurus*. All recovered neural spines have the anterior processes for the interspinous ligaments (Fig. 7A-C),

which are separated from the dorsal table of the neural spines by two shallow lateral grooves. Theses processes reach dorsally the distal rim, as in *Dahalokely*, *Majungasaurus*, *Skorpiovenator*, and *Viavenator*. However, the posterior dorsals of *Carnotaurus* have a more ventrally placed process. All neural spines have a thickened distal end, with a marked lateral step and several lateral longitudinal ridges (Fig. 7D-F). A similar condition is also present in *Carnotaurus* and *Viavenator*, whereas in *Dahalokely*, *Majungasaurus* and *Skorpiovenator* this dorsal swallowness is lesser developed, and absent in *Eoabelisaurus*. The dorsal surface is transversely and strongly convex anteroposteriorly. In dorsal view (Fig. 7D-F), the neural spines seem to have a Y-like outline, tapering anteriorly. In the posterior end, two lateral interspinous accessory processes are present (completely preserved only in one neural spine). These processes are finger-like shaped and posteriorly directed (Fig. 7B, C, E, F). This structure was proposed as an autapomorphic condition for *Viavenator* (Filippi *et al*., 2016) and considered as an accessory interspinous articulation. This feature differs from the dorsal expansion of the neural spines present in other abelisauroids such as *Elaphrosaurus*, *Dahalokely*, and *Huinculsaurus*.

FIGURE 6 (NEAR HERE)

Figure 6. **Posterior dorsal vertebrae of *Aucasaurus garridoi* MCF-PVPH-236**. In anterior (A, G), posterior (B, H), lateral (C, D, I, J), dorsal (E), and ventral (F, K) views. Abbreviations: ns, neural spine; pl, pleurocoel. Scale bar: 5 cm.

FIGURE 7 (NEAR HERE)

Figure 7. **Distal fragments of dorsal neural spines of *Aucasaurus garridoi* MCF-PVPH-236**. In dorsal (A-C), and left lateral (D-F) views. Abbreviations: iap, interspinous accessory process; ilp, interspinous ligament process. Scale bar: 5 cm.

562

563 *Sacrum* (Fig. 8; Supporting Information, Table S1): The sacrum is partially preserved and the
564 vertebral centra suffered some degree of deformation. The entire right side was found fused with
565 the right ilium, while the left side is fully exposed, except for the third vertebral centrum, which
566 is fused and covered by the pubic peduncle of the ilium and part of the iliac peduncle of the
567 pubis (Fig. 8A). The sacrum is composed of six vertebrae, as in *Eoabelisaurus*, *Carnotaurus* and
568 *Masiakasaurus*, but different from the sacrum of *Majungasaurus*, and some tetanurans, which
569 includes only five vertebrae. Although partially deformed, all six vertebral centra are fused
570 forming an unique structure (Fig. 8A, B) as observed in *Ceratosaurus*, *Carnotaurus*,
571 *Elaphrosaurus*, *Eoabelisaurus*, *Rahiolisaurus*, *Skorpiovenator*, and several Patagonian
572 indeterminate abelisaurids (MAU-Pv-LI 547, MCF-PVPH-237, MMCh-PV 69, MPCN-PV-69),
573 and possibly *Berberosaurus* and *Huinculsaurus*. Other abelisauroids, such as *Majungasaurus*
574 (although adult individuals from that species are unknown), *Masiakasaurus*, *Rajasaurus*, and
575 *Vespersaurus*, have a partially fused sacrum. Despite the deformation, the anterior surface of the
576 first centrum is slightly concave and is dorsoventrally higher and mediolaterally wider than the
577 remaining sacral centra. From the second to fifth sacral vertebra, the centra are transversally
578 narrower and dorsoventrally lower than the first and sixth sacral vertebra, as observed in almost
579 all ceratosaurians (e.g. *Berberosaurus*, *Ceratosaurus*, *Elaphrosaurus*, *Carnotaurus*,
580 *Skorpiovenator*). Whereas, in *Rahiolisaurus* this constriction is present from the third sacral
581 centrum backwards; such a feature is apparently absent in *Majungasaurus*. *Aucasaurus* has
582 apneumatic sacral centra, and the lateral walls are flat or slightly concave, as in other
583 abelisauroids.

584 In lateral view (Fig. 8A), the sacrum is arched giving a concave outline to the ventral rim
585 of the centra as in *Berberosaurus*, *Carnotaurus*, *Elaphrosaurus*, *Masiakasaurus*, *Skorpiovenator*,
586 and the Abelisauridae indet. MAU-Pv-LI 547, whereas in *Rahiolisaurus* this arching is less
587 defined. Conversely, *Eoabelisaurus*, *Majungasaurus*, and *Rajasaurus* show a rather horizontal
588 ventral margin. The lateral surfaces of the centra have shallow longitudinal fossae lacking
589 pleurocoels, as in *Carnotaurus*, and *Majungasaurus*, and the indeterminate abelisaurids MAU-
590 Pv-LI 547, MMCh-PV 69, and MPCN-PV-69. The neural arches are partially preserved and are
591 fused to each other, creating a median axial wall. Unfortunately, the right side is fused to the
592 ilium preventing us from getting additional morphological information, such as the presence or
593 absence of fossae and laminae.
594 A fragment of the right rib of the first sacral vertebra was identified, and it is positioned
595 just beneath the transverse process. This portion of the rib is dorsoventrally taller than
596 anteroposteriorly long, different from the posterior sacral ribs, which are longer. Four left sacral
597 ribs have be identified, being the fourth one the best preserved (the other three are poorly
598 preserved). This rib is robust and holds a fossa on the ventral surface.
599 The neural spines of all sacral vertebrae are completely fused to one another forming a
600 continuous shelf, as in *Skorpiovenator*, *Carnotaurus*, Abelisauridae indet. MAU-Pv-LI 547, and
601 possibly *Majungasaurus*. *Eoabelisaurus* also possesses fused sacral neural spines, albeit it differs
602 from more derived abelisaurids in that it lacks a dorsal shelf. Moreover, the sacral neural spines
603 are transversely thin but with thicker distal ends. Several anteroposteriorly directed grooves and
604 ridges stand out on the laterodorsal edge of the spines. In *Aucasaurus*, the fused neural spines are
605 visible laterally above the dorsal edge of the ilium, as in *Eoabelisaurus*, *Majungasaurus*,

606 *Carnotaurus*, and Abelisauridae indet. MAU-Pv-LI 547, but unlike *Elaphrosaurus* and
607 *Skorpiovenator* where the sacrum is hidden by the ilia.
608 In ventral view (Fig. 8B), at least five of the sacral centra can be distinguished. In this
609 view, the transverse constriction of the middle portion of the sacrum is clearly visible. The
610 ventral surface of the vertebrae lack grooves or ridges, as seen in *Eoabelisaurus*, *Skorpiovenator*,
611 and *Carnotaurus*.
612 In posterior view (Fig. 8D), the sixth sacral centrum has a posterior articular surface that
613 is slightly concave and has an oval contour, being dorsoventrally taller than transversely wide.
614 This vertebra has also the greatest posterior surface when compared to the other sacral vertebrae.
615 In dorsal view (Fig. 8E, F), the transverse processes of the second through the fifth neural
616 arches are fused to the ilium some two centimeters away from the dorsal rim, whereas the first
617 transverse process contact the medial wall more ventrally. Moreover, the second up to the fifth
618 sacral vertebra have transverse processes nearly horizontally directed. Conversely, the transverse
619 processes of the sixth sacral are dorsally inclined, due to the ventral position of this vertebra with
620 respect the anterior ones. The transverse processes of the third through the fifth sacral vertebrae
621 are anteroposteriorly longer than the other sacral transverse processes (Fig. 8F). In addition to be
622 fused with the ilium, the transverse processes are fused each other at their distalmost ends,
623 leaving a medial passage (Fig. 8F), as in *Masiakasaurus* and *Skorpiovenator*. The dorsal part of
624 the neural spines form a continuous co-ossified table and among them are visible two anterior
625 and posterior interspinous processes that contact each other, as in *Carnotaurus*, *Skorpiovenator*,
626 and Abelisauridae indet. MAU-Pv-LI 547.
627
628 FIGURE 8 (NEAR HERE)

Figure 8. **Sacrum of *Aucasaurus garridoi* MCF-PVPH-236**. In lateral (A, B), ventral (C), posterior (D), and dorsal (E, F) views. Colored dashed lines marking the anterior and posterior rims of the third to fifth transverse processes. Abbreviations: 1sc-6sc, first to sixth sacral centra; 4sr, fourth sacral rib; 1stp-5stp, first to fifth sacral transverse processes; IL, ilion; ns, neural spine. Scale bar: 10 cm.

Caudal vertebrae (Fig. 9-21; Supporting Information, Table S1): MCF-PVPH-236 includes the first to thirteenth anterior caudal vertebrae that were found completely articulated (with their corresponding haemal arches), two posterior caudal vertebrae, and several isolated remains such as fragmentary neural spines and transverse processes. In general, there is a reduction in the general size of the centrum towards the posterior region, a transverse narrowing of the neural arch in the area of the pedicels in the distal anterior elements (between the seventh and tenth vertebra), and a posterior displacement of the neural spine towards the rear of the tail. The transverse processes are transversely wide, with a ratio higher than 1.3 with respect to the length of the centrum. Sutures between neural arches and vertebral centra are completely obliterated in all caudal vertebrae.

First caudal vertebra (Fig. 9; Supporting Information, Table S1): The first caudal vertebra is well-preserved. The centrum has a concave anterior surface and an oval outline with its greater axis dorsoventrally directed (Fig. 9A), as in *Eoabelisaurus* and *Skorpiovenator*, but different from *Carnotaurus* in which the articular surface has a circular outline. In lateral view (Fig. 9B, E), a pleurocoel is absent and instead, there is an extensive anteroposterior depression just beneath the neurocentral suture, as in *Carnotaurus*. In *Skorpiovenator*, this depression is shallow,

whereas it is absent in all caudal vertebrae in *Eoabelisaurus* and the Abelisauridae indet. MPM 99. In this view, the centrum has a parallelogram outline, since the anterior margin is slightly concave and the posterior margin slightly convex, as in *Eoabelisaurus*, *Skorpiovenator*, and *Carnotaurus*. The posterior surface is also concave and elliptical with the greater axis dorsoventrally directed (Fig. 9D), as in *Skorpiovenator*, but unlike *Kurupi* and *Carnotaurus* in which the surface is transversely wider than dorsoventrally high. The ventral end of the posterior surface bears the articular facet for the first haemal arch. In ventral view (Fig. 9F), the surface lacks a groove, depression, or ridge, as in *Eoabelisaurus*, *Kurupi*, *Skorpiovenator*, and *Carnotaurus*; in contrast, the surface is grooved in *Dilophosaurus*, *Ceratosaurus*, and *Majungasaurus*.

In anterior view (Fig. 9A), the neural canal shows an elliptical outline, different from the circular shape seen in *Carnotaurus*. The hypantrum is transversely reduced and the prezygapophyses are close to each other, as in *Eoabelisaurus* and *Carnotaurus*. It is likely that the articulation between the last sacral vertebra and the first caudal vertebra allowed limited lateral movements. The prezygapophyses (the right one is partially broken) have a nearly vertical orientation, as in *Eoabelisaurus* and *Carnotaurus*. The prezygodiapophyseal (prdl) and sprl laminae are lost due to weathering. The spinoprezygapophyseal fossa (sprf) is deep but transversely narrow, different from the shallower fossa present in *Eoabelisaurus* or the wider fossa in *Kurupi*. A septum divides the sprf in two areas. Laterally to the prezygapophyses, the prezygapophyseal centrodiapophyseal fossae (prcdf) are shallow depressions. These fossae are also present in *Carnotaurus* but forming shallow concavity, whereas in *Eoabelisaurus* the surface is flat without depression. In this view, the transverse processes have a strong laterodorsal inclination, at an angle of approximately 48°, as in *Eoabelisaurus* and *Carnotaurus*

675 whereas in *Kurupi* and *Skorpiovenator* the transverse processes show an inclination less than
676 30°. The neural spine is transversely thin; it widens distally forming a terminal bulge, as in
677 *Eoabelisaurus* and *Carnotaurus*. This terminal bulge appears absent in the caudal vertebrae of
678 *Ceratosaurus*.

679 In lateral view (Fig. 9B, E), the prezygapophyses and postzygapophyses do not exceed
680 the anterior and posterior rims of the centrum, respectively, as in *Skorpiovenator* and
681 *Carnotaurus* but unlike *Dilophosaurus*, *Ceratosaurus*, and *Eoabelisaurus* where they are
682 projected beyond the rims of the centrum. Ventrally, the transverse processes exhibit a
683 centrodiapophyseal lamina (cdl) that splits ventrally in the acdl and pcdl that are poorly
684 developed, as in *Kurupi*. In *Aucasaurus* and other abelisaurids, such as *Skorpiovenator* and
685 *Carnotaurus*, the first and the remaining caudal vertebrae lack pneumaticity ventral to these
686 laminae. The cdl ends laterally with a well-marked ridge, as in *Skorpiovenator* and *Carnotaurus*,
687 which is absent in *Eoabelisaurus*. A depression separates this crest from another accessory ridge
688 that is also directed anteroposteriorly, as in *Carnotaurus*. The neural spine, in lateral view, it is
689 almost perpendicular to the centrum and shows a rectangular outline with the dorsal rim directed
690 anterodorsally/posteroventrally. In contrast, in *Carnotaurus* and *Eoabelisaurus* the neural spine
691 is inclined posteriorly, projecting beyond the posterior surface of the centrum. At the dorsalmost
692 portion of this vertebra, the neural spine presents anteroposteriorly directed ridges and furrows
693 for ligamental anchorage. The neural spine is the half of the anteroposterior length of the neural
694 arch at its base, different from *Ceratosaurus*, *Carnotaurus* and *Eoabelisaurus* where it is longest.

695 In dorsal view (Fig. 9C), the transverse processes are posteriorly inclined with respect to
696 the neural spine, surpassing the posterior surface of the centrum, as in *Eoabelisaurus*, *Kurupi*,
697 *Skorpiovenator*, and *Carnotaurus*. Although partially broken, the transverse processes hold, at

the lateral edge, the anterior awl-like processes as in *Carnotaurus*. These processes are totally absent in all the caudal vertebrae of *Eoabelisaurus* and *Majungasaurus*. In the posterodorsal portion of the transverse process, there is a V-shaped rugosity, also present in *Carnotaurus* albeit much weaker. Between this scar and the lateral border of the transverse process, the dorsal surface is slightly concave. The anterior rim of the transverse processes is concave, whereas the posterior one is almost straight, as in *Carnotaurus* and *Skorpiovenator* but unlike *Eoabelisaurus* where both rims are straight. In the middle of the anterodorsal surface of the transverse processes, a possibly ligamentous scar is present, different from the prominent spur observed in *Kurupi*. This trait is here considered autapomorphic for *Aucasaurus garridoi* (see Discussion). There are two anteriorly directed, dorsal processes of the neural spine absent in *Eoabelisaurus* and *Carnotaurus*.

In posterior view (Fig. 9D), the neural canal is wider dorsally than ventrally. There is a small depression posterior at the entry of the neural canal. The hyposphene is prominent and formed by the union of the intrapostzygapophyseal laminae that arise ventrally to the postzygapophyses, as in several ceratosaurians (e.g. *Ceratosaurus*, *Carnotaurus*, *Kurupi*). Laterally to the hyposphene, the postzygapophyseal centrodiapophyseal fossae (pocdf) are shallow and hold a pneumatic foramen (see Discussion). These fossae are also shallow in all the anterior caudal vertebrae of *Carnotaurus*, *Eoabelisaurus*, *Skorpiovenator*, and *Viavenator*, although they lack pneumatic foramina. Unlike *Carnotaurus*, *Aucasaurus* lacks centropostzygapophyseal laminae (cpol) that delimit ventrally the pocdf. The postzygapophyses are partially preserved, and the articular surfaces are directed ventrolaterally, as in *Ceratosaurus*, *Carnotaurus*, and *Skorpiovenator*, whereas in *Dilophosaurus* they are directed ventromedially. Laterally to the postzygapophyses, the podl are low. Dorsal to the postzygapophyses, the

721 spinopostzygapophyseal laminae (spol) are robust and join dorsally on the posterior surface of
722 the neural spine. Between these last two laminae and the postzygapophyses the
723 spinopostzygapophyseal fossa (spof) are transversely narrow, as in *Carnotaurus*, whereas in
724 *Skorpiovenator* this fossa is wider.
725
726 FIGURE 9 (NEAR HERE)
727 Figure 9. **First caudal vertebra of *Aucasaurus garridoi* MCF-PVPH-236**. In anterior (A),
728 lateral (B, E), dorsal (C), posterior (D), and ventral (F) views. Abbreviations: acdl, anterior
729 centrodiapophyseal lamina; apltp, anterior process of lateral transverse process; cdl,
730 centrodiapophyseal lamina; dr, dorsal roughness; ha, hypantrum; hy, hyposphene; iap,
731 interspinous accessory process; ldvc, lateral depression of vertebral centrum; lrcdl, lateral ridge
732 of centrodiapophyseal lamina; nc, neural canal; ns, neural spine; pcdl, posterior
733 centrodiapophyseal lamina; pf, pneumatic foramen; poz, postzygapophysis; prz,
734 prezygapophysis; spof, spinopostzigapophyseal fossa; spol, spinopostzigapophyseal lamina; sprf,
735 spinoprezigapophyseal fossa; tp, transverse process; vlrtp, ventrolateral ridge of the transverse
736 process. Scale bar: 10 cm.
737
738 *Second caudal vertebra* (Fig. 10; Supporting Information, Table S1): The second vertebra is
739 almost completely preserved, lacking only the anterior ends of the prezygapophyses and the
740 distal half of the neural spine. The centrum has an elliptical anterior articular surface being taller
741 than wide (Fig. 10A), as in *Eoabelisaurus* and *Skorpiovenator* but different from *Carnotaurus*
742 where it is wider than tall. Ventrally to the anterior articular surface, a low rim represents the
743 contact area for the haemal arch. As in the first caudal vertebra, the lateral surfaces lack
744 pleurocoels (Fig. 10B), although there is a depression below the neurocentral suture. Conversely,

745 the second caudal vertebra of *Carnotaurus* and *Skorpiovenator* lack such depression on the
746 lateral surface of the centrum. As in the first caudal vertebra, in lateral view the centrum has a
747 parallelogram-shaped outline. The posterior articular surface is smaller than the anterior one
748 (Fig. 10D), although it has the same oval outline, unlike *Carnotaurus* that has an almost circular
749 outline. The posterior contact surface for the haemal arch is more extensive with respect to the
750 anterior facet. The ventral surface has a longitudinal groove that extends along the entire surface
751 (Fig. 10F), and is laterally bounded by two low ridges. Whereas, in *Carnotaurus* the ventral
752 surface is smooth without groove or ridges.

753 In anterior view (Fig. 10A), the neural canal has a circular outline. The prezygapophyses
754 are almost completely lost, thus the shape cannot be observed. Although, they possibly were
755 oriented medially with an inclination of 60° from the horizontal plane, as *Eoabelisaurus* and
756 *Carnotaurus*. The hypantrum is partially preserved, with an almost complete right wall. This
757 structure is wider than in the previous vertebra. In *Aucasaurus*, laterally to the prezygapophyses
758 there are neither foramina nor concavities, as in *Skorpiovenator*. Despite the sprl are partially
759 broken they seem low, delimiting a dorsoventrally deep sprf. There is a median septum in the
760 bottom of the sprf. The transverse processes continue to show a pronounced dorsal inclination
761 (although the right one is more dorsally inclined due to the diagenetic deformation), as in
762 *Eoabelisaurus* and *Carnotaurus*. In contrast, in *Skorpiovenator* the transverse processes are
763 approximately horizontal. In *Aucasaurus* the neural spine is partially preserved and is
764 transversely thin.

765 In lateral view (Fig. 10B, E), the lateral rims of the transverse processes have a
766 pronounced roughness. Ventral to the transverse processes there is a well-developed cdl that
767 occupies the entire ventral surface of the transverse process, as *Carnotaurus*. This condition

768 differs from *Skorpiovenator* where the cdl is mainly developed in the anteroventral portion of the
769 transverse process, forming a shallow depression in the posterior portion. Moreover, this lamina
770 ends in the lateral end abruptly with an anteroposteriorly directed ridge (as in the first caudal
771 vertebra). As observed in the first caudal vertebra, there is another accessory lateral ridge located
772 almost in the lateral edge of the transverse processes. Ventral to the transverse processes there
773 are no pneumatic foramina or fossae, holding only a shallow concavity that separates the acdl
774 from the pcdl, as in *Carnotaurus* and *Skorpiovenator*, while in *Eoabelisaurus* these two laminae
775 are poorly developed. The transverse processes present a considerable posterior inclination, since
776 they project beyond the centrum, as in *Skorpiovenator* and *Carnotaurus*. Only the base of the
777 neural spine is preserved, making it impossible to observe the morphology of the dorsal region.
778 In dorsal view (Fig. 10C), the lateral rim of the transverse processes have the typical awl-
779 shaped anterior process, while the left transverse (the left is partially broken). Moreover, in this
780 view the lateral rim is slightly convex and is visible the lateral roughness. A small process is also
781 present in the posterolateral end of the transverse processes, although it does not have the same
782 development as the same process present in some abelisaurids, such as *Ekrixinatosaurus*,
783 *Ilokelesia*, and *Skorpiovenator*. This reduced posterior process is absent in *Carnotaurus*. On the
784 posterolateral end the V-shaped scar is conspicuous, whereas in the second caudal vertebra of
785 *Carnotaurus* it is less-marked. The longitudinal scar on the middle of the transverse processes is
786 less pronounced than the previous vertebra. The anterior and posterior rims of the transverse
787 processes have a slightly sigmoid outline. The preserved portion of the neural spine is
788 transversely narrow with a leaf like contour in cross-section, being the posterior portion wider
789 than the anterior one. In *Aucasaurus*, the transverse processes are less posteriorly inclined than
790 *Carnotaurus*.

In posterior view (Fig. 10D), the neural canal has a triangular outline and is dorsovetrally taller than the first caudal vertebra. The hyposphene is lost, but it was conspicuous. As in the first caudal vertebra, the pocdf are shallow and have a pneumatic foramen, which is absent in *Eoabelisaurus* and *Carnotaurus*. The postzygapophyses are partially broken, with the articular facets ventrolaterally oriented. The spol delimit a rectangular spof that is transversely narrower and anteroposteriorly shallower than the previous vertebra, unlike *Carnotaurus* where this fossa remains deep and wide.

FIGURE 10 (NEAR HERE)

Figure 10. **Second caudal vertebra of *Aucasaurus garridoi* MCF-PVPH-236**. In anterior (A), lateral (B, E), dorsal (C), posterior (D), and ventral (F) views. Abbreviations: acdl, anterior centrodiapophyseal lamina; apltp, anterior process of lateral transverse process; cdl, centrodiapophyseal lamina; ha, hypantrum; haaf, haemal arch articular facet; hy, hyposphene; ldvc, lateral depression of vertebral centrum; lrcdl, lateral ridge of centrodiapophyseal lamina; nc, neural canal; ns, neural spine; pcdl, posterior centrodiapophyseal lamina; pf, pneumatic foramen; poz, postzygapophysis; ppltp, posterior process of lateral transverse process; prz, prezygapophysis; spof, spinopostzigapophyseal fossa; spol, spinopostzigapophyseal lamina; sprf, spinoprezigapophyseal fossa; tp, transverse process; vg, ventral groove; vlrtp, ventrolateral ridge of the transverse process. Scale bar: 10 cm.

Third caudal vertebra (Fig. 11; Supporting Information, Table S1): The third caudal vertebra was almost completely preserved, lacking only the anterior ends of the prezygapophyses, part of the neural spine, and the anterior and posterior ends of the lateral border of the left transverse process. The anterior articular surface of the centrum is elliptical in outline with its long axis

oriented dorsoventrally (Fig. 11A), as in *Eoabelisaurus* and *Skorpiovenator*. This morphology differs from *Carnotaurus* which has a circular contour. In lateral view (Fig. 11B), the neurocentral suture is obliterated. The centrum has the depression just below the neurocentral suture, which is absent in *Carnotaurus*. The anterior and posterior margin of the centrum are slightly concave and convex, respectively, giving to it a parallelogram-shaped outline, as in *Eoabelisaurus* and *Carnotaurus*. The posterior articular surface is elliptical in outline with its long axis oriented dorsoventrally (Fig. 11D), as in *Carnotaurus*. On the posteroventral end, the contact surface for the haemal arch is wide and has an inclination of 40°. In ventral view (Fig. 11F), the centrum holds a longitudinal groove, which is absent in *Carnotaurus*, *Eoabelisaurus*, and *Skorpiovenator*.

In anterior view (Fig. 11A), the neural arch is narrower transversely than the previous vertebra. The entry of the neural canal has a circular outline. Despite the hypantrum is almost completely lost, it can be inferred that it was dorsoventrally high, as in *Carnotaurus* but unlike *Eoabelisaurus* where the hypantrum is low. Only the left prezygapophysis is partially preserved, showing a dorsomedial inclination of the articular facet higher than 60°, different from *Eoabelisaurus* and *Carnotaurus* that have a lower inclination. The sprl are completely weathered, except for a portion at the base of the neural spine, thus we cannot estimated the depth and width of the sprf. However, this fossa lacks of the middle septum observed in *Carnotaurus*. The transverse processes have a dorsal inclination higher than 45°, as in *Carnotaurus* but different from *Eoabelisaurus* and *Skorpiovenator* where they show a lower inclination. The neural spine preserves only its basal third. The preserved portion of neural spines is transversely thin, as in *Eoabelisaurus*, *Skorpiovenator*, and *Carnotaurus*, and shows a leaf-shaped contour in cross-section.

838 In lateral view (Fig. 11B, E), the lateral edge of the transverse process is markedly
839 roughened. The cdl ends laterally with an anteroposteriorly directed crest, and laterally to this
840 crest a shallow depression is present. Ventral to the cdl, the cdf separates a well-developed acdl
841 from the pcdl, as in *Carnotaurus*, whereas in *Eoabelisaurus* both laminae are reduced. Dorsal to
842 the anterior pedicels, the prcdf are deep but without pneumatic foramina. In *Aucasaurus*, the
843 transverse processes have a significant posterior inclination surpassing the posterior articular
844 surface of the centrum, as in *Skorpiovenator* and *Carnotaurus* but unlike *Eoabelisaurus* where
845 the transverse processes are laterally directed. Although incomplete, the neural spine does not
846 exhibit the posterior orientation observed in *Carnotaurus*.
847 In dorsal view (Fig. 11C), the transverse processes exhibit the anteriorly directed awl-
848 shaped processes, although the left one is almost lost. On the posterolateral corner, the transverse
849 processes lack the posterior processes present in the second caudal vertebra. The right transverse
850 process shows a marked posterolateral rugosity, whereas the middle scar is poorly developed.
851 The anterior and posterior rims are sinusoidal, as in *Skorpiovenator*. In this view, the neural
852 spine is leaf-shaped in cross-section with the widest part located anteriorly.
853 In posterior view (Fig. 11D), the neural canal entry is dorsoventrally higher than
854 transversely wide. The hyposphene, although partially broken, is more conspicuous than in the
855 previous caudal vertebrae. Lateral to the hyposphene, the pocdf are shallow and have pneumatic
856 foramina. The postzygapophyses are partially preserved, and have a lateroventral orientation, as
857 in *Skorpiovenator* and *Eoabelisaurus*, contrasting with the almost horizontal orientation in
858 *Carnotaurus*. The spof is narrower than the previous vertebrae. The neural spine is wide at the
859 base, thinning towards the distal portion.
860
861 FIGURE 11 (NEAR HERE)

Figure 11. **Third caudal vertebra of *Aucasaurus garridoi* MCF-PVPH-236**. In anterior (A), lateral (B, E), dorsal (C), posterior (D), and ventral (F) views. Abbreviations: acdl, anterior centrodiapophyseal lamina; apltp, anterior process of lateral transverse process; cdf, centrodiapophyseal fossa; cdl, centrodiapophyseal lamina; dr, dorsal roughness; ha, hypantrum; haaf, haemal arch articular facet; hy, hyposphene; ldvc, lateral depression of vertebral centrum; lrcdl, lateral ridge of centrodiapophyseal lamina; lrtp, lateral rugosity of transverse process; nc, neural canal; ns, neural spine; pcdl, posterior centrodiapophyseal lamina; pocdf, postzygapophyseal centrodiapophyseal fossa; poz, postzygapophysis; prcdf, prezygapophyseal centrodiapophyseal fossa; prz, prezygapophysis; spof, spinopostzigapophyseal fossa; spol, spinopostzigapophyseal lamina; sprf, spinoprezigapophyseal fossa; vg, ventral groove; vlrtp, ventrolateral ridge of the transverse process. Scale bar: 10 cm.

Fourth caudal vertebra (Fig. 12; Supporting Information, Table S1): The fourth caudal vertebra only lost the distal end of the neural spine. The anterior articular surface of the centrum is elliptical in outline being taller than wide (Fig. 12A), as in *Eoabelisaurus*, *Skorpiovenator*, and *Carnotaurus*. Laterally (Fig. 12B), the surface shows a deep depression below the neurocentral suture without pneumatic foramina. The anterior and posterior rims of the lateral surface remains concavo/convex and slightly tilted anteriorly, as in *Eoabelisaurus* and *Carnotaurus*, while *Skorpiovenator* has a more rectangular outline. The posterior articular surface shows a less pronounced concavity with respect to the anterior one, and its contour is elliptical, being taller than wide (Fig. 12D), as in *Skorpiovenator* and *Carnotaurus*. The posteroventral surface for articulation of the haemal arch is wide. Despite the ventral surface of the centrum is partially collapsed, the longitudinal groove is present (Fig. 12F).

In anterior view (Fig. 12A), the neural canal has a dorsoventral elliptical outline, different from the circular shape seen in *Carnotaurus*. We cannot estimate the size and shape of the hypantrum, since its lateral walls were lost. The prezygapophyses are partially preserved and have a medial inclination greater than 60°, as *Skorpiovenator* but unlike *Eoabelisaurus* and *Carnotaurus* where the prezygapophyses are less inclined. The sprf has transverse narrower than the two previous vertebrae, whereas sprl are not preserved. The transverse processes have a dorsal inclination greater than 45°, as in *Carnotaurus* and unlike *Eoabelisaurus* and *Skorpiovenator* that have less inclined transverse processes. The neural spine is partially preserved, probably the first two thirds, narrowing towards the distal portion.

In lateral view (Fig. 12B, E), the lateral rim of the transverse processes is thick, showing a marked roughness with the presence of several tubercles. This rugosity and thickening of the lateral border of the transverse process is absent in *Carnotaurus* and *Skorpiovenator*. Lateral to the cdl and the longitudinal ridge, the surface has a conspicuous accessory ridge and is strongly concave due to a ventral bowing of the lateral end. The fourth caudal vertebra of *Carnotaurus* has the accessory ridge but lacks the ventral bowing. The cdf is deep, as in *Skorpiovenator*, whereas *Eoabelisaurus* has a shallow cdf and low acdl and pcdl. The prcdf is deeper than the second and third caudal vertebrae, as in *Eoabelisaurus* and *Skorpiovenator*. In this view, the transverse processes are poorly posteriorly directed, as in *Eoabelisaurus* but different from *Skorpiovenator* and *Carnotaurus* where the transverse processes surpass the caudal centrum. The neural spine is anteroposteriorly longer than the previous vertebrae, as occurs in *Eoabelisaurus* y *Skorpiovenator*. Moreover, in *Aucasaurus* and mentioned abelisaurids the neural spine has a length of two thirds with respect the neural arch.

907 In dorsal view (Fig. 12C), the transverse processes lack the posterior process of the lateral
908 margin. The awl-like anterior process of the transverse process is more slender than in the fourth
909 vertebra, and is more anteriorly developed than *Skorpiovenator*. The anterior rim of the
910 transverse processes is sinusoidal, whereas the posterior one is slightly convex, unlike
911 *Skorpiovenator* where both rims are straight. The lateral rim has a sinusoidal shape, being the
912 posterior half convex and the anterior half concave, different from the straight rim observed in
913 *Skorpiovenator*. The posterolateral rugosity is conspicuous. The scar present in the middle of the
914 transverse process, near the anterior border, is no longer present. The neural spine is leaf-shaped
915 in cross-section.

916 In posterior view (Fig. 12D), the outline of the neural canal entry is taller than wide and
917 triangular in outline. The hyposphene is prominent and subtriangular, unlike *Eoabelisaurus* that
918 has a reduced hyposphene. Laterally to the hyposphene, the pocdf are shallow with a pneumatic
919 foramen, which is absent in *Eoabelisaurus* and *Skorpiovenator*. The postzygapophyses are
920 partially broken, they are ventrolaterally oriented and anteroposteriorly short, as in *Carnotaurus*
921 but different from *Eoabelisaurus* and *Skorpiovenator* where the postzygapophyses are longer.
922 Despite the bad preservation of the spol, they are low mounds, implying a reduced spof with
923 respect to the previous anterior caudal vertebrae, as in *Eoabelisaurus* and *Carnotaurus*.

924

925 FIGURE 12 (NEAR HERE)

926 Figure 12. **Fourth caudal vertebra of *Aucasaurus garridoi* MCF-PVPH-236**. In anterior (A),
927 lateral (B, E), dorsal (C), posterior (D), and ventral (F) views. Abbreviations: acdl, anterior
928 centrodiapophyseal lamina; apltp, anterior process of lateral transverse process; cdf,
929 centrodiapophyseal fossa; cdl, centrodiapophyseal lamina; dr, dorsal roughness; haaf, haemal
930 arch articular facet; hy, hyposphene; ldvc, lateral depression of vertebral centrum; lrcdl, lateral

ridge of centrodiapophyseal lamina; lrtp, lateral rugosity of transverse process; nc, neural canal; ns, neural spine; pcdl, posterior centrodiapophyseal lamina; pocdf, postzygapophyseal centrodiapophyseal fossa; poz, postzygapophysis; prcdf, prezygapophyseal centrodiapophyseal fossa; prz, prezygapophysis; spof, spinopostzigapophyseal fossa; spol, spinopostzigapophyseal lamina; sprf, spinoprezigapophyseal fossa; vg, ventral groove. Scale bar: 10 cm.

Fifth caudal vertebra (Fig. 13; Supporting Information, Table S1): The fifth and sixth caudal vertebrae are fused together with the proximal part of the fifth haemal arch, probably due to a pathology that occurred in an early ontogenetic stage, since the sizes of both centra are smaller than the preceding and subsequent vertebrae. The anterior articular surface of the centrum is oval in outline with the long axis dorsoventrally directed (Fig. 13A), as in fifth caudal vertebra of *Eoabelisaurus* and *Skorpiovenator*. The facet for the haemal arch contact is wide. On both sides, the depression below the neurocentral suture is shallow (Fig. 13B). The anterior rim of the lateral facet is partially broken, although it appears to be concave. A vertical furrow marks the posterior rim, which divide the fifth caudal centrum for the sixth one. The posterior articular surface is not visible, although it appears to have an oval outline, as in *Eoabelisaurus* and *Skorpiovenator* but unlike the circular outline in *Kurupi*. The posteroventral end is not visible, due to the pathological fusion with the haemal arch. Ventrally (Fig. 13F), a longitudinal groove is present, as in *Kurupi*.

In anterior view (Fig. 13A), the hypantrum is wide and high dorsoventrally, whereas in *Eoabelisaurus* is low. The prezygapophyses are nearly vertically positioned, thus its articular facet are oriented almost completely medially, as in *Skorpiovenator* but different from *Eoabelisaurus* and *Carnotaurus* in which the prezygapophyses are dorsomedially oriented. The

954 sprf is transversely and anteroposteriorly reduced with respect to the previous vertebrae.
955 *Aucasaurus* lacks the septum that divide the sprf in two subfossae observed in *Carnotaurus*. The
956 transverse processes are dorsally directed with an inclination of 60°, as in *Carnotaurus* and
957 different from *Eoabelisaurus*, *Kurupi*, and *Skorpiovenator* that show a lesser inclination. The
958 neural spine is transversely thin and presents a distal swelling, as in *Skorpiovenator* and
959 *Carnotaurus*, whereas it is absent in *Eoabelisaurus*.
960 In lateral view (Fig. 13B, E), the lateral rim of the right transverse process (the left one is
961 broken) shows a pronounced roughness, which is absent in the fifth caudal vertebra of
962 *Skorpiovenator* and *Carnotaurus*. However, it does not show the ventral torsion of the lateral rim
963 of the fourth caudal vertebra. Moreover, the depression between the lateral rim of the transverse
964 process and the lateral crest of the cdl is shallower than the fourth caudal vertebra. The cdl is
965 prominent and ends laterally with an oblique ridge, which is longitudinal directed in *Carnotaurus*
966 and absent in *Skorpiovenator*. The prcdf is deep but without pneumatic foramina. The transverse
967 processes are significantly posterior directed extending beyond the posterior articular surface, as
968 in *Skorpiovenator* and *Carnotaurus* but different from *Eoabelisaurus* where the transverse
969 processes are directed laterally. In lateral view, the neural spine is almost complete, is
970 anteroposteriorly shorter and dorsoventrally lower than the previous vertebrae. A similar
971 condition is observed in *Eoabelisaurus*, whereas in *Skorpiovenator* the neural spine is
972 anteroposteriorly longer. In *Aucasaurus*, there is a low process in the ventral portion of the
973 anterior and posterior rims of the neural spine, as in *Carnotaurus*. The dorsal swelling of the
974 neural spine shows lateral striae, probably designed for ligament attachment.
975 In dorsal view (Fig. 13C), the transverse processes have a sinusoidal lateral rim, as in
976 *Carnotaurus* and different from a straight lateral rim observed in *Majungasaurus* and

977 *Skorpiovenator*. In *Aucasaurus*, the awl-like process of the lateral rim of the transverse process is
978 anteroposteriorly reduced compared to the previous vertebrae. Conversely, in *Skorpiovenator*
979 this structure increase slightly in size. *Aucasaurus* shows a concave anterior rim and sinusoidal
980 posterior rim of the transverse process. The scar at the posterolateral corner is more marked than
981 *Carnotaurus*. The transverse process is anteroposteriorly reduced compared to the previous
982 caudal vertebrae. At the base of the neural spine, especially on the right side, there is a small
983 pneumatic foramen. The dorsal swelling of the neural spine is rectangular in contour. The neural
984 spine preserves only one of the anteriorly directed processes, and the posterior ones are missing.
985 These processes possibly are present in *Carnotaurus* but absent in *Eoabelisaurus* and
986 *Skorpiovenator*.
987
988 *Sixth caudal vertebra* (Fig. 13; Supporting Information, Table S1): As previously mentioned, the
989 sixth caudal vertebra is fused to the fifth one. Consequently, the morphology of the anterior
990 surface of the sixth caudal is not discernible. However, it seems to have an oval outline being
991 taller than wide, as in *Eoabelisaurus* and *Skorpiovenator*. In lateral view (Fig. 13B), despite the
992 collapsed right side, the centrum lacks depression below the neurocentral suture. The posterior
993 rim of the centrum remains convex. The posterior surface presents a concavity more pronounced
994 with respect to all previous vertebrae and is elliptical in outline with its major axis directed
995 dorsoventrally (Fig. 13D), as in *Eoabelisaurus*. In ventral view (Fig. 13F), a low keel runs across
996 the surface anteroposteriorly, bounding, on the left, a longitudinal groove.
997 Due to the fusion with its preceding vertebra, it is not possible to observe the morphology
998 of the anterior portion of the neural arch. In lateral view (Fig. 13B, E), the prezygapophyses
999 show a strong medial inclination being greater than 60º, as in *Skorpiovenator* but unlike

Eoabelisaurus and *Carnotaurus* that shows a lower inclination. The left transverse process is partially preserved lacking the distal end, whereas the right one is broken at the base, therefore it is not possible to appreciate the morphology of the lateral end. In the ventral part of the transverse process, a conspicuous cdl is visible giving to the transverse process a triangular cross-section, as in *Skorpiovenator* and *Carnotaurus*. The cdf is deep, bounded anterior and posteriorly by prominent acdl and pcdl. The neural spine is almost complete, and it is anteroposteriorly slender than the fifth caudal vertebra. The dorsal part of the spine is laterally thickened, with longitudinal scars for ligament attachment.

In dorsal view (Fig. 13C), the neural spine holds the anterior processes, whereas lost the posterior ones. These processes and the lateral swelling of the distal part of the neural spine are absent in *Eoabelisaurus* and *Skorpiovenator*. The preserved portion of both transverse processes has a slightly concave anterior rim and a sigmoid posterior one. Moreover, the transverse processes are projected beyond the centrum. The pneumatic foramina present at the base of the neural spine are anteriorly placed with respect to the previous vertebra.

In posterior view (Fig. 13D), the neural canal has an elliptical outline. Dorsally to the canal, the hyposphene is dorsoventrally reduced but transversely wider than the previous vertebrae, as in *Eoabelisaurus* and *Carnotaurus*. *Aucasaurus*, unlike *Eoabelisaurus*, has straight lateral surfaces of the hyposphene, whereas they are concave in the Jurassic taxon. The pocdf include a pneumatic foramen, absent in *Eoabelisaurus* and *Skorpiovenator*. The spof is reduced to a fissure; this condition differs from a wider fossa in *Eoabelisaurus*, whereas in *Skorpiovenator* disappear. The postzygapophyses have a lateroventral orientation and they do not surpass posteriorly the centrum. The transverse processes show a strong dorsal inclination, as in

Carnotaurus, but they differ from *Eoabelisaurus* and *Skorpiovenator* in that the latter have a lesser dorsal inclination.

FIGURE 13 (NEAR HERE)

Figure 13. F**ifth and sixth caudal vertebrae of *Aucasaurus garridoi* MCF-PVPH-236**. In anterior (A), lateral (B, E), dorsal (C), posterior (D), and ventral (F) views. Abbreviations: 5cv, fifth caudal vertebra; 6cv, sixth caudal vertebra; apltp, anterior process of lateral transverse process; cdl, centrodiapophyseal lamina; dr, dorsal roughness; ha, hypantrum; har, haemal arch; haaf, haemal arch articular facet; hy, hyposphene; iap; interspinous accessory process; lrcdl, lateral ridge of centrodiapophyseal lamina; lrtp, lateral rugosity of transverse process; nc, neural canal; ns, neural spine; pf, pneumatic foramen; poz, postzygapophysis; prcdf, prezygapophyseal centrodiapophyseal fossa; prz, prezygapophysis; spof, spinopostzigapophyseal fossa; spol, spinopostzigapophyseal lamina; sprf, spinoprezigapophyseal fossa; tp, transverse process; vg, ventral groove; vlrtp, ventrolateral ridge of the transverse process. Scale bar: 10 cm.

Seventh caudal vertebra (Fig. 14; Supporting Information, Table S1): The seventh caudal vertebra lacks only the left transverse process. The centrum dorsoventrally lower than the previous vertebrae. The anterior surface has an oval outline and almost flat (Fig. 14A). In *Aucasaurus*, the anterior articular facet for the haemal arch of this vertebra is transversely and dorsoventrally wider than the anterior vertebrae. In lateral view (Fig. 14B), the surface lacks of the depression below the neurocentral suture, as in *Skorpiovenator*. The anterior and posterior rims are straight and parallel to each other, giving a subrectangular contour. In posterior view (Fig. 14D), the surface is oval with the articulation facet for the haemal arch anteroposteriorly wide, as in *Kurupi*. In ventral view (Fig. 14F), the groove runs anteroposteriorly along the entire

surface, unlike *Kurupi* where is appreciable only near the contact surfaces for the haemal arches. Laterally and posterior to the groove, there are nutrient foramina.

In anterior view (Fig. 14A), the neural arch is transversely narrower than the anterior vertebrae. The neural canal is tall with an oval outline. Like the previous vertebrae, the preserved portion of the prezygapophyses show a strong medial orientation, as observed in *Skorpiovenator* but different from *Eoabelisaurus* and *Carnotaurus* where they show a lesser medial inclination. The hypantrum is not preserved but we consider it was reduced, based on the reduction of the hyposphene of the sixth vertebra. The sprf is laterally narrow and the sprl, although partially preserved, are reduced compared to the most anterior vertebrae. In *Aucasaurus*, the transverse processes have the same dorsal inclination of the fifth and sixth vertebrae, as in *Carnotaurus* whereas *Eoabelisaurus*, *Kurupi*, and *Skorpiovenator* have lesser inclined the transverse processes. The neural spine shows lateral expansion in its most dorsal portion, which is absent in *Eoabelisaurus*, *Skorpiovenator*, and *Carnotaurus*.

In lateral view (Fig. 14B, E), the prdl is prominent with a posterior displacement of the transverse process, as in *Skorpiovenator* but unlike *Eoabelisaurus* in which the transverse process occupies a central position with respect to the neural arch. Ventrally to the transverse process, the lateral rim of the process has a rough texture. The anteroposterior ridge that marks where the cdl ends is less marked than in the previous vertebrae. Whereas, the accessory ridge is prominent as in *Kurupi*. The acdl and pcdl are well-developed, bounding a deep cdf, as in *Kurupi*. Anterior to the acdl, the prcdf occupies almost half of the anteroposterior length of the neural arch, unlike *Eoabelisaurus* where it is less developed. The anterior process of the base of the neural spine is more conspicuous than the previous vertebrae, while the posterior one is only partially preserved. These processes are absent in the same vertebra of *Eoabelisaurus* and

Skorpiovenator, while in *Carnotaurus* only the posterior one is observed. In the distalmost portion of the neural spine, the surface has lateral roughness, as in *Skorpiovenator*.

In dorsal view (Fig. 14C), the posterolateral scar is well-developed turning a posterior directed process. The awl-shaped anterior process is slender and anteroposteriorly long and its lateral rim is strongly sinusoidal, as in *Kurupi* and *Carnotaurus*. The anterior rim of the transverse process is concave, while the posterior one is sinusoidal. At the base of the neural spine, the pneumatic foramina have an oval contour. The neural spine is situated in the posterior half of the neural arch. The anterior and posterior processes of the neural spine are present but incomplete.

In posterior view (Fig. 14D), the neural canal shows a heart-like outline. The hyposphene is reduced with respect to the sixth vertebra but still prominent, as in *Kurupi*. Laterally to the hyposphene, the pocdf has a reduced pneumatic foramen, which is absent in *Eoabelisaurus*, *Skorpiovenator*, and *Carnotaurus*. The postzygapophyses are poorly preserved therefore it is impossible to deduce size and shape. The spof, as in the sixth caudal vertebrae, is a fissure, whereas in *Eoabelisaurus* it is transversely wider.

FIGURE 14 (NEAR HERE)

Figure 14. **Seventh caudal vertebra of *Aucasaurus garridoi* MCF-PVPH-236**. In anterior (A), lateral (B, E), dorsal (C), posterior (D), and ventral (F) views. Abbreviations: acdl, anterior centrodiapophyseal lamina; apltp, anterior process of lateral transverse process; cdf, centrodiapophyseal fossa; cdl, centrodiapophyseal lamina; dr, dorsal roughness; ha, hypantrum; haaf, haemal arch articular facet; hy, hyposphene; iap; interspinous accessory process; lrcdl, lateral ridge of centrodiapophyseal lamina; lrtp, lateral rugosity of transverse process; nc, neural canal; ns, neural spine; pcdl, posterior centrodiapophyseal lamina; pf, pneumatic foramen; poz,

postzygapophysis; prcdf, prezygapophyseal centrodiapophyseal fossa; prz, prezygapophysis; spof, spinopostzigapophyseal fossa; sprf, spinoprezigapophyseal fossa; sprl, spinoprezigapophyseal lamina; vg, ventral groove. Scale bar: 10 cm.

Eighth caudal vertebra (Fig. 15; Supporting Information, Table S1): The eighth caudal vertebra is almost completely preserved, lacking only the left transverse process. In anterior view (Fig. 15A), the centrum shows a similar morphology of the seventh caudal vertebra, except for a more pronounced concavity of the articular surface. In lateral view (Fig. 15B), as in the previous vertebra the centrum has a subrectangular outline. Despite the collapsing of the lateral surfaces, they lack the depression below the neurocentral suture. In posterior view (Fig. 15D), the articular surface is broken on the left side, although it shows a drop-like outline due to narrowing of the dorsal portion, unlike *Eoabelisaurus* and *Skorpiovenator* that have an oval contour. The articulation surface with the haemal arch is wide. In ventral view (Fig. 15F), the longitudinal groove is deeper towards the posterior end of the surface, forming two low tubercles in correspondence of the articular facet for the haemal arch. These tubercles are observed in all following vertebrae.

In anterior view (Fig. 15A), the neural arch is transversely narrow. The prezygapophyses have an almost vertical orientation, and the hypantrum is dorsoventrally deep although it is transversely narrower than the seventh vertebra. A similar condition is observed in *Skorpiovenator*, whereas *Eoabelisaurus* has lesser inclined prezygapophyses and a reduced hypantrum. The sprf is shallower and laterally reduced than the previous vertebra. The right transverse process is less dorsally inclined than the seventh caudal vertebrae, whereas in

Eoabelisaurus it is horizontal. The neural spine shows a transverse reduction of the dorsal swelling.

In lateral view (Fig. 15B, E), the transverse processes are positioned on the posterior portion of the neural arch, as in *Skorpiovenator* but different from *Eoabelisaurus* that has centrally positioned transverse processes. The awl-like processes is partially preserved on the right side. The lateral rim of the transverse process is ornamented by roughness. On the ventral surface of the transverse process, the accessory ridge is rugose. The cdl is less prominent than the previous vertebrae, and the acdl and pcdl are low, as in *Skorpiovenator*. The prcdf is shallow but anteroposteriorly long. The neural spine is anteroposteriorly reduced than the seventh caudal vertebra, and positioned on the posterior half of the neural arch. The anterior process of the basal neural spine was partially preserved, giving to the latter an L-like shape. The dorsal end of the neural spine has several longitudinal ridges.

In dorsal view (Fig. 15C), the transverse process is mediolaterally larger than the previous vertebra. The posterolateral process is reduced to a scar. The prezygapophyses slightly surpass the centrum. The pneumatic foramina present at the base of the neural spine are conspicuous. The dorsal swelling is transversely reduced when compared with the seventh caudal vertebra.

In posterior view (Fig. 15D), the hyposphene is dorsoventrally low, and the postzygapophyses are partially broken. The foramen inside the pocdf is reduced with respect to previous vertebrae. The spof is a fissure, unlike in *Eoabelisaurus* where this fossa is subcircular.

FIGURE 15 (NEAR HERE)

Figure 15. **Eighth caudal vertebra of *Aucasaurus garridoi* MCF-PVPH-236**. In anterior (A), lateral (B, E), dorsal (C), posterior (D), and ventral (F) views. Abbreviations: apbns, anterior

process of basal neural spine; apltp, anterior process of lateral transverse process; cdl, centrodiapophyseal lamina; dr, dorsal roughness; haaf, haemal arch articular facet; hy, hyposphene; lrcdl, lateral ridge of centrodiapophyseal lamina; lrtp, lateral rugosity of transverse process; nc, neural canal; ns, neural spine; pocdf, postzygapophyseal centrodiapophyseal fossa; poz, postzygapophysis; prcdf, prezygapophyseal centrodiapophyseal fossa; prz, prezygapophysis; spof, spinopostzigapophyseal fossa; spol, spinopostzigapophyseal lamina; sprf, spinoprezigapophyseal fossa; sprl, spinoprezigapophyseal lamina; vg, ventral groove. Scale bar: 10 cm.

Ninth caudal vertebra (Fig. 16; Supporting Information, Table S1): The ninth caudal vertebra is complete excepting the neural spine. The centrum shows a circular outline of the anterior surface and the surface is strongly concave due to a marked rim (Fig. 16A), unlike *Eoabelisaurus* and *Skorpiovenator* that have an oval anterior contour. In lateral view (Fig. 16B), the anterior and posterior rims of the centrum are slightly convex. In posterior view (Fig. 16D), the surface, like the anterior one, has a circular outline and is strongly concave due to a prominent rim, different from the oval outline present in *Eoabelisaurus* and *Skorpiovenator*. The posterior facet for the haemal arch is wide. The ventral groove is deep and slightly wider than the previous vertebrae (Fig. 16F).

In anterior view (Fig. 16A), the hypantrum is lacking. The prezygapophyses have a medial inclination greater than 60°, as *Skorpiovenator*. The sprf is transversely narrow, anteroposteriorly long, and has a septum on the bottom, unlike *Eoabelisaurus* that has a reduced and circular fossa. In *Aucasaurus* the sprl is reduced to low mound. The transverse processes

show the same dorsal inclination of the eighth caudal vertebra. The neural spine is preserved only at the base.

In lateral view (Fig. 16B, E), the prezygapophyses are projected dorsally and anteriorly, surpassing the anterior rim of the centrum. This dorsal inclination increases in posterior caudal vertebrae. The transverse processes slightly exceed the posterior rim of the centrum. The lateral border of the transverse process has an irregular surface due to the presence of a marked roughness, especially for the presence of a conspicuous tubercle. That tubercle is present up to the twelfth caudal vertebra. The cdl ends laterally at the lateral rim of the transverse process, and is no longer separated in the acdl and pcdl. For this reason, the cdf disappear, different from *Eoabelisaurus* where the acdl, pcdl, and cdf are still present. The prcdf extends far the half of the neural arch, whereas in *Eoabelisaurus* is anteroposteriorly reduced. The postzygapophyses do not exceed the centrum posteriorly.

In dorsal view (Fig. 16C), the pneumatic foramina at the base of the neural spine are wider than the previous vertebrae. The posterolateral scar of the transverse processes is present but incipient. The awl-like process is still well-developed. The lateral rims of the transverse processes are sinusoidal.

In posterior view (Fig. 16D), the hyposphene is poorly developed, and the postzygapophyses are ventrolaterally oriented. The spof has a fissure-like morphology and is dorsoventrally reduced with respect to eighth caudal vertebra, unlike the shallow depression observed in *Eoabelisaurus*. The pocdf are shallow and holds a small pneumatic foramen.

FIGURE 16 (NEAR HERE)

Figure 16. **Ninth caudal vertebra of *Aucasaurus garridoi* MCF-PVPH-236**. In anterior (A), lateral (B, E), dorsal (C), posterior (D), and ventral (F) views. Abbreviations: apltp, anterior

process of lateral transverse process; cdl, centrodiapophyseal lamina; haaf, haemal arch articular facet; hy, hyposphene; lrtp, lateral rugosity of transverse process; nc, neural canal; ns, neural spine; pf, pneumatic foramen; pocdf, postzygapophyseal centrodiapophyseal fossa; poz, postzygapophysis; prcdf, prezygapophyseal centrodiapophyseal fossa; prz, prezygapophysis; spof, spinopostzigapophyseal fossa; spol, spinopostzigapophyseal lamina; sprf, spinoprezigapophyseal fossa; sprl, spinoprezigapophyseal lamina; vg, ventral groove. Scale bar: 10 cm.

Tenth caudal vertebra (Fig. 17; Supporting Information, Table S1): The tenth caudal vertebra lacks the neural spine and the left transverse process. In anterior view, the centrum shows a circular outline and, as in the ninth caudal vertebra, has a marked rim giving the surface an accentuated concavity (Fig. 17A), unlike an oval surface in *Eoabelisaurus*. The lateral surface has a subrectangular outline with straight anterior and posterior rims (Fig. 17B). In posterior view (Fig. 17D), the presence of a fragment of the following vertebra prevents the observation of the articular surface, although the contour seems to be circular, different from the oval shape shown by *Eoabelisaurus*. In ventral view (Fig. 17F), the facet for the haemal arch articulation is reduced and the two low ridges bound the groove.

In anterior view (Fig. 17A), the neural canal is reduced and shows a circular outline. The prezygapophyses are partially broken, although they were reduced in size and strongly medially oriented. The sprf is anteroposteriorly reduced with respect to the ninth caudal vertebra and presents the vestige of a septum in its posteriormost portion, whereas in *Eoabelisaurus* this fossa is a shallow depression. The transverse processes have a dorsal inclination of 30°.

In lateral view (Fig. 17B, E), the prezygapophyses are slightly dorsally directed and surpass anteriorly the centrum. The right transverse process still presents a rugose accessory ridge on the ventral surface. The awl-like anterior process is conspicuous. Moreover, the posterior end of the transverse process has a reduced posteriorly projected process. The cdl is low, and the prcdf is reduced to an anteroposteriorly extended depression, different from *Eoabelisaurus* where the cdl is well-developed and the prcdf is deeper. In *Aucasaurus*, the pocdf is shallow, although a pneumatic foramen is present.

In dorsal view (Fig. 17C), the lateral rim of the transverse process has a pronounced tubercle on its middle portion. The posterolateral scar is barely developed. The transverse process is reduced anteroposteriorly with respect the previous vertebra, and the anterior and posterior rims are slightly concave, unlike *Eoabelisaurus* where the anterior rim is convex and the posterior one is sinusoidal. The foramina at the base of the neural spine are deep and wide, being the right one slightly wider. In posterior view (Fig. 17D), the neural canal has a circular outline. It is not possible to observe the morphology of the neural spine, spol, spof, and postzygapophyses because they are poorly preserved.

FIGURE 17 (NEAR HERE)

Figure 17. **Tenth caudal vertebra of *Aucasaurus garridoi* MCF-PVPH-236**. In anterior (A), lateral (B, E), dorsal (C), posterior (D), and ventral (F) views. Abbreviations: apltp, anterior process of lateral transverse process; cdl, centrodiapophyseal lamina; dr, dorsal roughness; haaf, haemal arch articular facet; lrcdl, lateral ridge of centrodiapophyseal lamina; lrtp, lateral rugosity of transverse process; nc, neural canal; ns, neural spine; pf, pneumatic foramen; prcdf, prezygapophyseal centrodiapophyseal fossa; prz, prezygapophysis; sprf, spinoprezigapophyseal fossa. Scale bar: 10 cm.

Eleventh caudal vertebra (Fig. 18; Supporting Information, Table S1): As in the preceding vertebra, the eleventh caudal vertebra lacks the neural spine and left transverse process. In anterior view (Fig. 18A), the surface is circular in outline, and ventrally the facet for the haemal arch articulation is greatly reduced, whereas in *Eoabelisaurus* the anterior contour is slightly oval. In lateral view (Fig. 18B), the anterior and posterior rims of the centrum are slightly convex. In posterior view (Fig. 18D), the articular surface is strongly concave and in its ventral end the surface for contact with the haemal arch is wider than the anterior one. In ventral view (Fig. 18F), the groove is anteroposteriorly reduced than the tenth vertebra, running for three quarter of the whole surface.

In anterior view (Fig. 18A), the neural canal is circular. The prezygapophyses, even though incomplete, are further away from each other than in the preceding vertebrae. However, the articular facet of the prezygapophyses are medially directed. The sprf disappear from this vertebra, as in *Eoabelisaurus*. The right transverse process is almost horizontally directed.

In lateral view (Fig. 18B, E), the prezygapophyses exceed anteriorly the centrum, as in *Eoabelisaurus*. The transverse process has the same morphology and orientation of the tenth caudal vertebra. The prcdf is shallow and anteroposteriorly reduced, as in *Eoabelisaurus*. The cdl is poorly developed and the accessory ridge of the transverse process is still present.

In dorsal view (Fig. 18C), the transverse process shaft is shorter than the previous vertebra. The anterior and posterior rims of the transverse processes are concave, but lack a posterior process. The posterolateral scar is barely developed. The lateral border of the transverse process is anteroposteriorly longer than the neural arch. The left pneumatic foramen at the base

of the neural spine is wider than the right one. The postzygapophyses are partially preserved, surpassing the posterior rim of the centrum such as in *Eoabelisaurus*.

In posterior view (Fig. 18D), the pneumatic foramen of the pocdf disappears. A deep fossa stands out between the postzygapophyses, forming a shelf dorsally to the neural canal. This fossa is absent in all the middle caudal vertebrae of *Eoabelisaurus*.

FIGURE 18 (NEAR HERE)

Figure 18. **Eleventh caudal vertebra of *Aucasaurus garridoi* MCF-PVPH-236**. In anterior (A), lateral (B, E), dorsal (C), posterior (D), and ventral (F) views. Abbreviations: apltp, anterior process of lateral transverse process; dr, dorsal roughness; haaf, haemal arch articular facet; lrtp, lateral rugosity of transverse process; nc, neural canal; ns, neural spine; pf, pneumatic foramen; poz, postzygapophysis; prz, prezygapophysis; vg, ventral groove. Scale bar: 10 cm.

Twelfth and Thirteenth caudal vertebrae (Fig. 19; Supporting Information, Table S1): The twelfth and thirteenth caudal vertebrae remain articulated. The right prezygapophysis, most of the neural spine, and the left transverse process are missing in the twelfth vertebra. The thirteenth caudal vertebra has lost most of the neural spine, the two transverse processes, the postzygapophyses and the posterior half of the centrum. The anterior articular surface of the centrum of both vertebra is circular in outline (Fig. 19A), although it appears slightly wider than tall with respect to the eleventh caudal vertebra. Conversely, *Eoabelisaurus* shows an oval outline. In lateral view (Fig. 19B), both vertebrae have a flat surface without pleurocoels or depressions. The posterior articular surface of the twelfth caudal vertebra seems to have a circular outline. In ventral view (Fig. 19F), both vertebrae have the groove that runs anteroposteriorly for three quarter of the surface.

In anterior view (Fig. 19A), the articular surfaces of the prezygapophyses are widely spaced and are strongly medially inclined (being almost vertical in the thirteenth caudal vertebra), unlike *Eoabelisaurus* where they have a lesser medial inclination. The neural canal opens 2 cm away from the dorsal rim of the anterior articular surface. The transverse processes have an approximately 10° to 15° dorsal inclination,

In lateral view (Fig. 19B, E), the prezygapophyses are anterodorsally projected, surpassing the centrum anteriorly. Moreover, they have a rugose protuberance directed dorsolaterally. A similar structure is also present in *Aoniraptor* (Motta *et al*., 2016). The transverse process of the twelfth caudal vertebra is almost identical, in shape and morphology, to the previous vertebra. The neural spine is positioned in the posterior half of the neural arch and is "L"-shaped, since there is a low ridge that runs anteriorly from the neural spine to a small process. The right postzygapophysis of the twelfth caudal vertebra arises posterodorsally, ending with the posteriormost portion almost horizontally. Moreover, it exceeds the centrum posteriorly. Conversely, *Eoabelisaurus* has postzygapophyses that do not exceed the centrum.

In dorsal view (Fig. 19C), the pneumatic foramina at the neural spine base disappear in both vertebrae, replace by shallow depressions. The right transverse process of twelfth caudal vertebra has anterior and posterior borders straight and parallel to each other. The awl-like process is conspicuous, surpassing the anterior surface of the centrum. In this view, the lateral rim of the transverse is markedly sinusoidal with the presence of a prominent tubercle. The posterolateral scar is reduced to a low prominence. In posterior view, the twelfth caudal vertebra has a fossa between the two postzygapophyses, as in the previous one; this region is not preserved in thirteenth caudal vertebra (Fig. 19D).

FIGURE 19 (NEAR HERE)

Figure 19. **Twelfth and thirteenth caudal vertebrae of *Aucasaurus garridoi* MCF-PVPH-236**. In anterior (A), lateral (B, E), dorsal (C), posterior (D), and ventral (F) views. Abbreviations: 12cv, twelfth posterior vertebra; 13cv, thirteenth posterior vertebra; apltp, anterior process of lateral transverse process; dr, dorsal roughness; haaf, haemal arch articular facet; ltprz, lateral tubercle of prezygapophysis; lrtp, lateral rugosity of transverse process; nc, neural canal; ns, neural spine; poz, postzygapophysis; prz, prezygapophysis; vg, ventral groove. Scale bar: 10 cm.

Posterior caudal vertebrae: The holotype of *Aucasaurus garridoi* MCF-PVPH-236 includes two incomplete posterior centra. Both elements were partially separated from the neural arch and preserved only a portion of a concave and circular outlined anterior articular surface, different from *Elemgasem* that shows oval outlines. The anterodorsal surfaces of the centra preserved the base of the prezygapophyses. Laterally, the centra have a low anteroposteriorly directed ridge with no pits or depressions. The ventral surface shows a faint anteroposteriorly directed ridge bounded laterally by two grooves, in proximity to the articular facet for the haemal arch.

Other caudal vertebrae remains (Fig. 20, 21): Two isolated neural spines (Fig. 20A-D), are interpreted as belonging to some of the anterior caudal vertebrae due to their anteroposterior length, reduced transverse width, and morphology of their distal end. In anterior view, both spines are transversely narrow with an expanded distal end.

In lateral view (Fig. 20A, B), the distalmost portion of both neural spines is dorsally convex. In addition, they presents several longitudinal grooves and ridges on the lateral surface of the expanded portion. This distal swelling is separated from the ventral part of the neural spine

by a marked step. The anterior and posterior rims are rugose due to the attachment of interspinous ligaments. In dorsal view (Fig. 20C, D), both anterior and posterior interspinous processes are visible. The anterior processes are separated by a concavity deeper than the posterior ones.

Two differently-sized isolated transverse processes (Fig. 21A-D) are interpreted as belonging to anterior caudal vertebrae. The anterior awl-like processes are well-developed (Fig. 21A, B). The lateral rims are convex, rugose and turn somewhat ventrally. In the posterolateral corner, the scar is conspicuous. In ventral view (Fig. 21 C, D), the cdl ends laterally in the anteroposteriorly directed ridge.

FIGURE 20 (NEAR HERE)

Figure 20. **Caudal neural spines of *Aucasaurus garridoi* MCF-PVPH-236**. In lateral (A, B) and dorsal (C, D) views. Abbreviations: iap; interspinous accessory process. Scale bar: 5 cm.

FIGURE 21 (NEAR HERE)

Figure 21. **Caudal transverse processes of *Aucasaurus garridoi* MCF-PVPH-236**. In dorsal (A, B) and ventral (C, D) views. Abbreviations: apltp, anterior process of lateral transverse process; cdl, centrodiapophyseal lamina; dr, dorsal roughness; lrcdl, lateral ridge of centrodiapophyseal lamina; lrtp, lateral rugosity of transverse process. Scale bar: 5 cm.

Cervical ribs (Fig. 22): The cervical ribs are fragmentary, since preserved only two proximal ends. These two elements are similar in morphology, differing slightly in size (Fig. 22A, B). Both fragments preserved up to where the tuberculum and capitulum split, although lacking the articular portions, and the base of the anterolateral process. Thus, the proximal end of the

1348 cervical ribs shows a triradiate morphology. Based on their morphology, we considered that
1349 these ribs belong to the posterior portion of the neck, between the seventh and the ninth element.
1350 In fact, the preserved ribs of *Aucasaurus* are similar to the seventh to ninth cervical ribs of
1351 *Carnotaurus* and *Majungasaurus*, since the dorsolateral processes of these elements is reduced to
1352 a low mound in all specimens. The dorsal rim of the cervical fragments is sinusoidal due to the
1353 presence of the dorsolateral process, while the ventral one is concave. Moreover, *Aucasaurus*
1354 (like in *Carnotaurus* and *Majungasaurus*) has a subrectangular-shaped proximal end of the
1355 posterior ribs in lateral view, whereas other large theropods have a subtriangular proximal end
1356 (e.g. *Allosaurus*, *Tyrannosaurus*).
1357
1358 FIGURE 22 (NEAR HERE)
1359 Figure 22. **Proximal fragments of two cervical ribs of *Aucasaurus garridoi* MCF-PVPH-23**.
1360 In lateral (A, B) views. Abbreviations: alp, anterolateral process; cap, capitulum; dlp,
1361 dorsolateral process; tub, tuberculum. Scale bar: 5 cm.
1362
1363 *Dorsal ribs* (Fig. 23): Several dorsal rib fragments are preserved (Fig. 23A-G), some
1364 corresponding to the anterior region of the trunk and others to the abdominal region (Fig. 23A-C,
1365 E-G). Additionally, several tubercula are preserved separate from the rib shafts (Fig. 23D). The
1366 dorsal ribs of *Aucasaurus* present well-defined tuberculum and capitulum, and the tuberculum
1367 separated from the capitotubercular lamina as in *Majungasaurus*, but unlike *Carnotaurus* and the
1368 Abelisauridae indet. MAU-Pv-LI 665 where the tubercula are in line with the lamina or slightly
1369 offset. The articular surfaces of the tubercula and capitula are oval in outline, although the
1370 former is broader. The capitotubercular lamina is thin and has a more pronounced concavity than
1371 in *Carnotaurus*. The capitula are triangular in lateral view, widening towards the rib shaft (Fig.

23A). Pneumatic foramina are not observed, as in *Majungasaurus* but unlike *Carnotaurus*, *Ceratosaurus*, *Masiakasaurus*, and the Abelisauridae indet. MAU-Pv-LI 665 that have pneumatic dorsal ribs. Anteriorly and posteriorly, intercostal ridges runs from the tuberculum towards the shaft (Fig. 23A-C), as in *Niebla*. Noteworthy, it is the presence of a roughness in the proximal part of the anterior intercostal ridge that would be the area of insertion of some soft tissue. From the capitulum, a ridge runs distally on the medial portion of the shaft, giving to the proximal end a T-shaped cross-section, as in other abelisaurids (MAU-Pv-LI 665 and MMCh-PV 48). Whereas, the middle portion of the shafts have a triangular cross-section, as in *Niebla*. Distal fragments of proximal dorsal ribs show an oval cross-section, ending distally with a rectangular shape (Fig. 23E), as in *Majungasaurus*. Distal fragments of posterior ribs taper distally and someone ends with a pronounced swelling (Fig. 23F).

FIGURE 23 (NEAR HERE)

Figure 23. **Fragments of dorsal ribs of *Aucasaurus garridoi* MCF-PVPH-236**. In lateral (A, C-G) and medial (B) views. Abbreviations: cap, capitulum; ctw, capitotuberculum web; der, distal expansion of rib; drcap, distal ridge of capitulum; ir, intercostal ridge; tub, tuberculum. Scale bar: 5 cm.

Gastralia (Fig. 24): Multiple fragments of gastralia are preserved (Fig. 24A-D); some of them show the median suture between middle elements (Fig. 24A, B), others represent portions of the diaphysis of middle or lateral elements (Fig. 24C, D). Among them, two middle elements are almost completely preserved (Fig. 24A, B), lacking only the proximal end of the shafts.

The middle gastralium elements are completely fused (Fig. 24A, B), creating an angle of approximately 80°. In ventral or dorsal view, the shafts of the middle elements have a sinusoidal

morphology, being laterally convex in their proximal half and laterally concave in their distal half. In the left middle element, a ventrolateral groove is the site where articulated the lateral element (Fig. 24A), such as observed in several theropods (e.g. Norell & Makovicky, 1997; Chure, 2000; Allain & Chure, 2002; Claessens, 2004). The shaft of these gastralia has a cylindrical shape for almost its whole length; however, there is a wing-like process with a rugose surface in the distal portion of the shaft (Fig. 24A, B). This medially directed process has a cross-section with teardrop-shaped outline.

The two middle elements forms a distal process with a triangular outline and with the apex directed ventrodistally (Fig. 24A, B). This process forms a dorsal platform, possibly contacting the following middle gastralia, unlike the imbricate-type system observed in tyrannosaurids and allosaurids (Claessens, 2004). *Poekilopleuron* and possibly *Juravenator* have a distal process (Allain & Chure, 2002; Chiappe & Göhlich, 2010), which is less developed than *Aucasaurus*. A chevron-shaped morphology with an acute angle is typical of the posteriormost gastralia in several theropods, such as in *Acrocanthosaurus*, *Poekilopleuron*, *Tyrannosaurus*, or *Troodon* (Harris, 1998; Chure, 2000; Allain and Chure, 2002; Claessens, 2004). However, these taxa lack the triangular distal process observed in *Aucasaurus*.

FIGURE 24 (NEAR HERE)

Figure 24. **Gastralia of *Aucasaurus garridoi* MCF-PVPH-236**. In ventral (A, C, D) and dorsal (B) views. Abbreviations: dpg, distal process of gastralia; g, groove; mfg, medial fusion of gastralia; mpg, medial process of the gastralium. Scale bar: 5 cm.

Haemal arches (Fig. 25, 26; Supporting Information, Table S2): Twelve haemal arches are preserved in articulation with their corresponding vertebrae (Fig. 25A-H3; Fig. 26A-E3). A

proximal fragment of a more distal haemal arch and three fragments from the middle portion of the shaft of two distal haemal arches are also preserved. The first three haemal arches show the articular surface open proximally, with a "V"-shaped haemal canal (Fig. 25A-C, A1-C1). This morphology differs from that in *Camarillasaurus*, *Majungasaurus*, *Ilokelesia*, and *Carnotaurus* where canal is dorsally closed. This trait was originally considered an autapomorphyic condition of *Aucasaurus* (Coria, Chiappe & Dingus, 2002). In the fourth haemal arch, the proximal end is partially fused anteriorly (Fig. 25D, D1). From the fifth haemal arch until the last one preserved, the proximal end of the haemal canal is fully closed (Fig. 25E1-H1; Fig. 26A1-E1). In the first to four haemal arch, the articulation surfaces for the centra are divided in four facets, two of them directed anteroproximally and two posteroproximally (Fig. 25A-D3). Since the fifth and the following haemal arches have a completely closed canal, the articular surfaces for the centra are reduced to two facet, the first one inclined anteroproximally and the second one posteroproximally (Fig. 25E-H3; Fig. 26A1-E3).

The anteroproximal articular surface, which articulates with the posteroventral end of the previous centrum, is generally wider than the posteroproximal surface along the entire series of haemal arches. This morphology is also reflected in the size of the articular surface for the haemal arches of the centra, where the posteroventral facet is wider than the anteroventral one. Anteriorly to the anteroproximal surface and separate from it, there are two proximally directed processes. However, the separation among them is shallower posteriorly. Moreover, these two processes are connected with the haemal shaft by ridges.

In anterior view, the haemal canal of the anterior haemal arches has a triangular outline (Fig. 25A-D), whereas it shows a drop-shaped outline from the fifth to the last element (Fig. 25E-H; 26A-E). In this view, the shaft distal to the haemal canal is transversely flat or slightly

concave with the presence of a rough ridge in the middle of the surface and directed distally (Fig. 25C, D). This morphology is also observed in *Majungasaurus*, *Ilokelesia*, and *Carnotaurus*, but unlike *Camarillasaurus* where there is a groove that crosses the entire anterior surface of the shaft.

In lateral view, the proximal end of all haemal arches have a triangular outline (Fig. 25A2-H2, A3-H3; Fig. 26A2-E2, A3-E3), due to the anterior and posterior projections of the articular surface. Distally to the proximal rim, the surface is proximodistally concave, due to the lateral bowing of the proximal articular surface. The shaft is straight in the anteriormost haemal arches; whereas it is curved posteriorly, resulting in convex anterior and concave posterior rims, in the remaining haemal arches. The lateral surfaces of the shaft show an anteroposterior convexity throughout the series.

In posterior view, there are two processes (visible at least in the first to four haemal arch; Fig. 25A1-D1) positioned distally to the posteroproximal articular surface and connect distally to the shaft with a ridge. The haemal canals of the first to third element end distally in a rough ridge that runs the whole length of the shaft (Fig. 25B1). From the fourth haemal arch, a groove replaces the crest that reaches the half of the length of the shaft thus disappearing distally (Fig. 25E1, H1), as in *Ilokelesia*, *Carnotaurus*, and *Camarillasaurus*. The shaft of the first to four haemal arches shows a triangular cross-section proximally, while it converts in an oval cross-section distally. The remaining haemal arches show a heart-shaped cross-section of the proximal portion of the shaft, whereas they have a lenticular cross-section of the distal end.

The morphology of the fifth and sixth haemal arches stand out among the entire series in that their size does not follow the normal posterior size reduction (Fig. 25E-F3). In fact, the fifth haemal arch is more robust than the other ones, whereas the sixth haemal arch is reduced in size

when compared to other haemal arches. Therefore, the morphology of these two haemal arches is likely the consequence of the pathology observed in the fifth and sixth caudal vertebrae. The three distal haemal arch fragments correspond to the distal part of a haemal channel with the proximal portion of the shaft, and two fragments of shafts that present the proximodistal groove on the posterior surface.

FIGURE 25 (NEAR HERE)

Figure 25. **First to eighth haemal arches of *Aucasaurus garridoi* MCF-PVPH-236**. In anterior (A-H), posterior (A1-H1), and lateral (A2-H2; A3-H3) views. Abbreviations: afcc, articular facet for the caudal centrum; arha, anterior ridge of haemal arch; hc, haemal canal; pgha, posterior groove of the haemal arch; prha, posterior ridge of the haemal arch. Scale bar: 5 cm.

FIGURE 26 (NEAR HERE)

Figure 26. **Ninth to thirteenth haemal arches of *Aucasaurus garridoi* MCF-PVPH-236**. In anterior (A-E), posterior (A1-E1), and lateral (A2-E2; A3-E3) views. Abbreviations: hc, haemal canal; pgha, posterior groove of the haemal arc. Scale bar: 5 cm.

Further comparisons

We compare the caudal series of *Aucasaurus* with other taxa in which the precise position of the vertebrae is uncertain; comparisons exclude the autapomorphic traits of *Aucasaurus garridoi*, which are unique to this taxon.

Several named and unnamed abelisaurids preserved caudal elements, allowing a direct comparison with *Aucasaurus*. The specimen Abelisauridae indet. MPM 99 preserves three anterior caudal vertebrae, one of the proximal portion of the tail and the other two vertebrae from

the mid-posterior portion of the anterior region of the tail. *Aucasaurus* differs from Abelisauridae indet. MPM 99 in having the transverse processes strongly dorsally inclined; in the latter specimen these processes are slightly dorsally inclined or horizontally directed. Conversely to *Aucasaurus*, Abelisauridae indet. MPM 99 has straight and smooth lateral rims of the transverse processes. However, the caudal neural spine in Abelisauridae indet. MPM 99 presents a widening of the dorsal end with two reduced dorsal processes directed anteriorly and posteriorly, as in *Aucasaurus*. In addition, both specimens share the presence of the awl-like projection of the transverse processes, a marked posterior scar on the dorsal surface of the processes, prominent cdl, acdl, and pcdl, and the presence of a groove on the ventral surface of the centrum.

The holotype of *Ekrixinatosaurus* (MUCPv 294) includes several anterior and middle caudal vertebrae. *Aucasaurus* and *Ekrixinatosaurus* share a well-developed hyposphene in the anterior caudal vertebrae, a prominent cdl that divides ventrally in the acdl and pcdl, and a dorsal swelling of the neural spine. However, *Ekrixinatosaurus* has lesser dorsally inclined transverse processes of the anterior vertebrae, lacks the dorsal processes of the neural spine and the groove on the ventral surface of the centrum.

Tralkasaurus is a brachyrostran abelisaurid from the same litostratigraphic unit of *Huinculsaurus*, *Ilokelesia*, and *Skorpiovenator*. The holotype of *Tralkasaurus* comprises anterior caudal vertebrae that differs from *Aucasaurus* in having transverse processes lesser inclined with prominent posterior awl-like projections and a straight lateral rim.

Aucasaurus and *Viavenator* share several morphological features observable in the anterior caudal vertebrae. Both taxa have anterior caudal vertebrae with articular surfaces taller than wide, lateral surfaces of the centra with a parallelogram-shaped outline without pleurocoels. With respect to neural arches, both abelisaurids share the presence of dorsoventrally-developed

and strongly medially inclined prezygapophyses, a wide hypantrum, and the presence of a septum at the bottom of the sprf. Moreover, they have transverse processes longer than the anteroposterior length of the centra, prominent acdl, pcd, and cdl (the latter ending laterally with a ridge), the presence of a posterodorsal scar, strongly sinusoidal lateral rim, and reduced or absent posterior process (unlike basal forms such as *Ekrixinatosaurus*, *Ilokelesia*, and *Skorpiovenator*). However, *Aucasaurus* presents a deeper ventral groove on the centra and slightly more inclined transverse processes. It is noteworthy the presence of two isolated transverse processes of a indeterminate abelisaurid (MAU-Pv-LI 547) from the same geological levels of *Viavenator*, which shows a convex or sinusoidal lateral rim and a ventral longitudinal ridge similar to those in *Aucasaurus*.

Aucasaurus also shows similarities and differences with the anterior caudal vertebra of the specimen Abelisauridae indet. MACN-PV-RN 1012. In fact, both specimens have centra with a longitudinal groove on the ventral surface and lack pleurocoels on the lateral surface. The sprf in the Abelisauridae indet. MACN-PV-RN 1012 has a septum that divided it in two areas, as observed in some vertebrae of *Aucasaurus*. With respect to neural arch, Abelisauridae indet. MACN-PV-RN 1012 has a conspicuous anterior awl-like projection and a longitudinal ventrolateral ridge in the transverse processes, like in *Aucasaurus*. However, *Aucasaurus* differs from Abelisauridae indet. MACN-PV-RN 1012 in having more inclined transverse processes with straight or slightly concave posterior rims.

The anterior caudal vertebra of Abelisauridae indet. MPCN PV 69 has an overall similar morphology to the anteriormost caudal vertebrae of *Aucasaurus*. However, all the anterior caudal vertebrae of the latter (except the first) present a groove on the ventral surface of the centrum, which is absent in Abelisauridae indet. MPCN PV 69.

Abelisauroidea indet. MPEF PV 1699/1-2 constitutes of two anterior caudal vertebrae from the La Paloma Formation (Hauterivian-Barremian, Lower Cretaceous) of Chubut Province (Argentina). *Aucasaurus* and Abelisauroidea indet. MPEF PV 1699/1-2 share the presence of a groove on the ventral surface of the centra, transversely long transverse processes, a well-developed hypanthro-hyposphene articulation, and prominent cdl, acdl, and pcdl. However, *Aucasaurus* has more medially inclined prezygapophyses and a dorsal inclination of the transverse processes greater than Abelisauroidea indet. MPEF PV 1699/1-2. Although both vertebrae of this Early Cretaceous specimen show somewhat lateral expansion of the transverse processes, their fragmentary preservation prevents determining the presence of anterior awl-like projections.

The anterior caudal vertebrae of *Pycnonemosaurus* and *Aucasaurus* share a ventral groove on the centra, transverse processes with an anterior awl-like projection, and prominent hyposphene. However, the latter Brazilian abelisaurid shows lesser inclined transverse processes and prezygapophyses. *Spectrovenator* has transverse processes with evident anteroposterior awl-like processes and straight lateral rims, unlike *Aucasasurus* that has only anterior prominent awl-like projections and sinusoidal lateral rim.

With respect to *Majungasaurus*, *Aucasaurus* shares with the Malagasy abelisaurid the presence of a ventral groove on the anterior centrum, transversely long transverse processes, and a dorsal expansion of the neural spines. However, *Majungasaurus* differs from *Aucasaurus* in having lesser medial inclined prezygapophyses, transverse processes that are less dorsally inclined and lack an awl-like projection, absence of accessory processes on the dorsal neural spines, and absence of a distinct hypantrum-hyposphene articulation.

The anterior caudal centra of *Aucasaurus* differ from the anterior caudal vertebrae of *Rajasaurus* in the absence of an anteroposteriorly directed keel on the ventral surface of the latter. A second Indian taxon, *Rahiolisaurus*, has well-developed cdl, acdl, and pcdl, as in *Aucasaurus*, but the transverse processes are lesser inclined.

Arcovenator is the most complete laurasian abelisaurid to include anterior caudal vertebrae. The French abelisaurid shares with *Aucasaurus* the presence of strongly medially tilted prezygapophyses, but unlike the latter, the transverse processes are nearly horizontal and the hyposphene is reduced.

DISCUSSION

Phylogenetic analysis

The first round of our cladistics analysis recovered most parsimonious trees (MPTs) on 161 replicates of a total 1000 replicates, resulting in 1610 MPTs (10 MPTs per each replicate) with a length of 556 steps, a consistent index of 0.493, and a retention index of 0.725. However, the second round of TBR found more than 50000 MPTs, due to an overflow of trees in the memory space. The strict consensus shows a large polytomy among all ceratosaurians (Fig. 27A), and the IterPCR procedure detected 11 unstable taxa: *Afromimus*, *Berberosaurus*, *Dahalokely*, *Huinculsaurus*, *Kryptops*, *Kurupi*, *Quilmesaurus*, *Rahiolisaurus*, *Thanos*, MNN-Tig6, and the Abelisauridae indet. MPCN-PV-69. When these “wildcards” were *a posteriori* pruned, the internal relationships among Ceratosauria were better solved. Major internal clades were recovered, such as Majungasaurinae, Brachyrostra, and Furileusauria; although, some polytomies are observed among more inclusive majungasaurines and among furileusaurians (Fig. 27B). The 100 replicates of Jackniffe found 22 unstable taxa, 20 final nodes, and a nodal support

average of 72.2 (Supporting Information, Data S3). The unique node with a value of 100% is Neotheropoda. Regarding Abelisauridae, this clade is recovered with a value of 73%, whereas all internal nodes show values lower than 85% except for the node *Spectrovenator* plus more derived abelisaurids (97%) (Supporting Information, Data S3).

Previously, *Aucasaurus* has been recovered as a derived abelisaurid by several phylogenetic studies, which disagree from each other in the proposed sibling relatioships of this taxon. Most of the phylogenetic analyses regarded *Carnotaurus* as sister taxon of *Aucasaurus* (Coria, Chiappe & Dingus, 2002; Calvo, Rubilar-Rogers & Moreno, 2004; Canale *et al*., 2009, 2016; Pol & Rauhut, 2012; Farke & Sertich, 2013; Gianechini *et al*., 2015; Rauhut & Carrano, 2016; Longrich *et al*., 2017; Baiano, Coria & Cau, 2020). However, other analyses have recovered either *Abelisaurus* (Filippi *et al*., 2016; Delcourt, 2018; Cerroni *et al*., 2020; Gianechini *et al*., 2021; Agnolín *et al*., 2022) or *Niebla* (Baiano *et al*., 2022) as the closest taxon to *Aucasaurus*. Our analysis nests *Aucasaurus* in an unresolved brachyrostran furileusaurian clade, and confirms several phylogenies (e.g. Filippi *et al*., 2016; Gianechini *et al*., 2021; Baiano *et al*., 2022) recovering *Carnotaurus*, *Elemgasem*, *Genusaurus*, *Llukalkan*, *Niebla*, *Pycnonemosaurus*, and *Viavenator* (Fig. 27B) within the same clade.

Irrespective of which taxon is most closely related to *Aucasaurus*, the latter shares axial apomorphies with other abelisaurids that should be considered in future phylogenetic analyses of abelisaurids. Based on these Abelisauridae (including *Aucasaurus*) is diagnosed by having caudal vertebrae with reduced neural spines when compared to posterior dorsal vertebrae (ch. 139:1) and caudal vertebrae with well-defined anterior and posterior centrodiapophyseal laminae (ch. 141:2). Furthermore, in *Aucasaurus* the bases of the neural arch of the anterior caudals are wider than the mid-centrum (ch. 142:1), a condition shared by several abelisaurids (plus *Kurupi*

and the Abelisauridae indet. MPCN-PV-69) and *Masiakasaurus*. *Aucasaurus*, *Spectrovenator*, and more nested abelisaurids (plus *Kurupi*) have anterior and middle caudal vertebra expanded posteriorly (ch. 144:1), a condition reverted in *Majungasaurus* where they are not expanded. *Aucasaurus* shares with Majungasaurinae and Brachyrostra (plus *Kurupi*) the presence of caudal vertebrae with transverse processes that are more than 1.4 times the length of caudal centra (ch. 147:1). *Aucasaurus*, *Majungasaurus*, and Brachyrostra (plus *Dahalokely*) have cervical vertebrae with postaxial tear-shaped zygapophyses (ch. 107:1). *Aucasaurus* has tall prezygapophyses-hypantrum complex (ch. 240:1), a condition shared with the Abelisauridae indet. MPM 99, *Arcovenator*, and several brachyrostrans. Moreover, *Aucasaurus*, the Abelisauridae indet. MPM 99, and brachyrostrans present transverse processes directed dorsolaterally (ch. 244:2) (although in *Aucasaurus* and *Carnotaurus* this condition is exacerbated). Addtionally, the inclusion of *Aucasaurus* within Brachyrostra is supported by the presence of the following synapomorphies: anterior caudal vertebrae with an inclination of the prezygapophyses greater than 50° (ch. 242:1), and anterior caudal vertebrae with a ventrolateral ridge at the lateral end of the transverse processes (ch. 245:1). Finally, the inclusion of *Aucasaurus* within furileusaurians is supported by the presence of cervical epipophyses with an anterior prong (ch. 112:1; condition shared also with *Noasaurus* and *Rahiolisaurus*) and a sinusoidal lateral rim of the anterior and middle caudal vertebrae (ch. 246:2).

FIGURE 27 (NEAR HERE)

Figure 27. **Phylogenetic relationships of *Aucasaurus garridoi* MCF-PVPH-236**. The results show a quite unresolved strisct consensus (A), and a more resolved topology of the reduced consensus (B). Colored dots were used for node-based taxa, colored arrows for stem-based taxa.

Autapomorphic axial traits in *Aucasaurus*

Several traits in the cervical, dorsal, and caudal vertebrae of abelisaurids distinguish this group from any other theropod clade, however, detailed description of the axial skeleton have been produced for only a few taxa: *Carnotaurus* (Bonaparte, Novas & Coria, 1990; Méndez, 2014a), *Majungasaurus* (O'Connor, 2007), and *Viavenator* (Filippi *et al*., 2018). These studies have allowed us to identify new autapomorphic traits for *Aucasaurus*, which are discussed below.

Odontoid with a triangular outline in dorsal view (Fig. 28): The odontoid of *Aucasaurus* preserved in anatomical articulation with the dorsal surface of the atlas intecentrum. When compared to other ceratosaurian theropods (e.g. *Masiakasaurus*, *Thanos*, *Majungasaurus*, *Carnotaurus*), and even some tetanuran theropods (e.g. *Allosaurus*, *Tyrannosaurus*), the odontoid of *Aucasaurus* is more triangular in dorsal view (Fig. 28A-D).

FIGURE 28 (NEAR HERE)

Figure 28. **Photographs of autapomorphies of *Aucasaurus garridoi***. Dorsal view of the odontoids of *Aucasaurus* (A), *Carnotaurus* (B), *Thanos* (C), *Majungasaurus* (modified by O'Connor, 2007) (E), and *Masiakasaurus* (modified by Carrano, Loewen & Sertich, 2011) (D). Image not to scale.

Atlas with a subcircular articular surface (Fig. 29): This morphology of the atlas is absent in several medium and large theropods, including those abelisaurids in which the atlas is known. A transversely oval atlas is seen in *Herrerasaurs*, *Dilophosaurus*, *Ceratosaurus*, *Allosaurus*, *Sinraptor*, *Aerosteon*, and *Tyrannosaurus*, where the occipital condyle is also wider

than tall. Among abelisaurids, only *Viavenator* shows a similar condition as *Aucasaurus*, but in the former it is slightly wider than tall producing an oval contour; in *Carnotaurus* the articular surface of the atlas is strongly transversely oval (Fig. 29B, C).

Interspinous accessory processes extended to sacral and caudal neural spines (Fig. 29): The interspinous ligament scar on the neural spines of cervical and dorsal vertebrae is a feature present in several theropods (Foth *et al*., 2015; Wilson *et al*., 2016; see also the chapter Discussion). However, some ceratosaur theropods show anteriorly and/or posteriorly expanded distal end of the neural spine, giving to this spine a fan-shaped outline. Moreover, some theropods have the distal portion of the dorsal neural spines with well-developed processes. These morphologies imply some accessory interspinous ligamental insertion among consecutive vertebrae. A fan-shaped neural spine is present in the noasaurids *Elaphrosaurus* (Rauhut & Carrano, 2016) and *Huinculsaurus* (Baiano, Coria & Cau, 2020). Furthermore, fan-shaped neural spines of the dorsal vertebrae are present in several coelurosaurs, such as the compsognathids *Compsognathus*, *Sinocalliopteryx*, and *Sinosauropteryx* (Currie & Chen, 2001; Peyer, 2006; Ji *et al*., 2007). Distal accessory interspinous process can be observed in *Dilophosaurus* (Welles, 1984; Marsh & Rowe, 2020), *Dahalokely* (Farke & Sertich, 2013), and *Siats* (Zanno & Makovicky, 2013). However, a contact among consecutive accessory interspinous processes was first reported in the dorsal vertebrae of the abelisaurid *Viavenator* (Filippi *et al*., 2016; Fig. 6). In fact, Filippi and colleagues proposed this condition as an autapomorphic trait for *Viavenator*. Here we show that this condition is also present in *Aucasaurus*, although in this taxon it is present in the dorsal, sacral, and caudal vertebrae (Fig. 29D-F).

A tubercle lateral to the prezygapophysis of middle and posterior caudal vertebrae (Fig. 29): The presence of a rough tubercle on the lateral surface of the prezygapophyses of the middle and posterior caudal vertebrae is absent in other abelisaurids that preserved elements of this section of the tail (Fig. 29G). Motta *et al*. (2016) mentioned the presence of a low swelling on the lateral prezygapophyses for the megaraptorid *Aoniraptor*. Some tyrannosaurids, such as *Alioramus*, *Tarbosaurus*, and *Tyrannosaurus*, have a bulge on the ventral side of the prezygapophyses (Fig. 29H) of the posterior caudal vertebrae (Brusatte, Carr & Norell, 2012), which is different from *Aucasaurus*.

Presence of pneumatic foramina laterally to the base of the neural spine in the anterior caudal vertebrae (Fig. 29): Pneumaticity (fossae or foramina) on the dorsal surface of the neural arch is a condition present in several theropods. For instance, the noasaurid *Elaphrosaurus* and the theropod *Spinostropheus* have shallow fossae on the dorsal surface of the cervical transverse processes (Carrano & Sampson, 2008; Rauhut & Carrano, 2016). The paravian *Unenlagia* present deep fossae with internal foramina laterally to the base of the neural spine of the thirteenth dorsal vertebrae. The foramina possibly communicate with the internal neural arch. This trait is regarded as a peculiar condition for *Unenlagia*, due to the absence in other non-avian theropods (Novas *et al*., 2021; Gianechini & Zurriaguz, 2021). Considering the caudal vertebrae, few groups of theropods show pneumatic traits with external manifestation; for instance, a pleurocoel is present on the lateral surface of the centra of Megaraptora, Oviraptorosauria, Therizinosauria, and possibly *Torvosaurus* (e.g. Britt, 1991, 1993; Zhang *et al*., 2001; Xu *et al*., 2007; Zanno *et al*., 2009; Benson, Carrano & Brusatte, 2010; Balanoff & Norell, 2012). However, Megaraptora is the only clade with highly pneumatized caudal vertebrae, extending to

the centra and the neural arches (Coria & Currie, 2016; Motta *et al*., 2016; Aranciaga Rolando, Garcia Marsá & Novas, 2020). Up to now, the only theropods that have foramina on the dorsal surface of the caudal neural arches are *Acrocanthosaurus* and *Meraxes* (Fig. 29I), while *Giganotosaurus* has shallow depressions (Britt, 1993; Aranciaga Rolando, Garcia Marsá & Novas, 2020; Canale *et al*., 2022). Thus, the presence of foramina laterally to the neural spine of the anterior to middle caudal vertebrae of *Aucasaurus* (Fig. 29J, K), is considered an autapomorphic condition for this abelisaurid (see Discussion).

FIGURE 29 (NEAR HERE)

Figure 29. **Photographs of autapomorphies of *Aucasaurus garridoi***. Outline (in red dashed line) of the anterior articular surface of the atlas of *Aucasaurus* (A), *Viavenator* (B), and *Carnotaurus* (C). Interspinous accessory processes on the dorsal (D), sacral (E), and caudal (F) neural spines of *Aucasaurus*. Lateral tubercle of prezygapophysis in the middle caudal vertebrae of *Aucasaurus* (G), and ventral bulge on prezygapophysis of the posterior caudal vertebrae of *Alioramus* (modified by Brusatte, Carr & Norell, 2012) (H). Foramina on the dorsal surface of the caudal neural arch in *Meraxes* (I). Whereas, *Aucasaurus* holds pneumatic foramina on the dorsal surface of the neural arches (framed by blue dashed lines) of the ninth (J) and eleventh (K) caudal vertebrae. Image not to scale.

A marked rugosity with a prominent tubercle on the lateral rim of the transverse processes of caudal vertebrae fourth to twelfth (Fig. 30): Among abelisaurids the transverse processes of the anterior and middle caudal vertebrae take a different morphology, being extremely specialized along the Brachyrostra clade. The latter group includes abelisaurids with anteroposterior expanded lateral end of the transverse processes and a straight or concave lateral

rim (Coria & Salgado, 2000; Calvo, Rubilar-Rogers & Moreno, 2004; Canale *et al*., 2009). More derived brachyrostran, such as the furileusaurians *Aucasaurus*, *Carnotaurus*, and *Viaveator*, have extremely developed an anterior awl-like projection on the lateral end of the transverse processes. Furthermore, the lateral rim of the caudal transverse processes in these abelisaurids is extremely convex, turning in concave laterally to the awl-like processes. However, *Aucasaurus* holds evident ornamentation on the lateral rim, with the presence of a prominent tubercle and rugosity (Fig. 30A-C), whereas in *Carnotaurus* and *Viavenator* this trait is faint.

Presence of a small ligamentous scar near the anterior edge of the dorsal surface in anteriormost caudal transverse processes (Fig. 30): *Aucasaurus* also differs from other abelisaurids in having an anterodorsal scar on the middle portion of the transverse processes (Fig. 30D, E). This mark is visible especially in the caudal vertebrae first to sixth, disappearing in the rest of the caudal series. Despite this morphology seems unique among abelisaurids, the recently described *Kurupi* (Iori *et al*., 2021) is diagnosed by strikingly conspicuous, cuneiform processes located in the same area of *Aucasaurus*'s scar (Fig. 30F; see also Discussion).

Distinct triangular process located at the fusion point of posterior gastralia (Fig. 30): Among ceratosaurians, *Masiakasaurus*, *Aucasaurus*, and *Majungasaurus* are the unique taxa that preserved gastral elements, although described as paleopathological in the latter (Gutherz *et al*., 2020). The middle gastralia preserved in *Aucasaurus* are fused to each other medially, forming a conspicuous triangular, ventral process (Fig. 30G, H) that could have either articulated with the following middle gastralia or could have been a site for the insertion of ligaments of the *m. rectus abdominis*.

1745

1746 *Anterior haemal arches with the neural canal proximally open* (Fig. 30): Coria, Chiappe
1747 & Dingus (2002) mentioned the presence of proximal haemal arches with a proximal open
1748 haemal canal (Fig. 30I, J) as an autapomorphic trait in *Aucasaurus*. This statement is based on
1749 the absence of this condition in other abelisaurids. However, taphonomic or ontogenetic factors
1750 raise a note of caution regarding this interpretation. However, a taphonomic biase for this unique
1751 morphology in the first four haemal arches is discarded for two reasons: 1) the haemal arches
1752 were found perfectly articulated with the corresponding caudal vertebrae (Coria, Chiappe &
1753 Dingus, 2002; Fig. 2); 2) there is a gradually closure of the haemal canal from the first to four
1754 haemal arches. Ontogenetic causes can also be ruled out, since several external anatomical
1755 condition (e.g. obliterated vertebral neurocentral fusion, fused pelvic elements, fused distal ends
1756 of tibia and fibula with astragalocalcaneum; Baiano, 2021) and a recently histological study
1757 (Baiano & Cerda, 2022) confirm a somatic and sexual mature condition for the holotype of
1758 *Aucasaurus*. Thus, for these reasons we consider this condition a valid autapomorphy for
1759 *Aucasasurus garridoi*.

1760

1761 FIGURE 30 (NEAR HERE)

1762 Figure 30. **Photographs of autapomorphies of *Aucasaurus garridoi***. Lateral rugosity and
1763 tubercle of the transverse processes of the fourth (A), ninth (B), and eleventh (C) caudal
1764 vertebrae of *Aucasaurus* in dorsal (upper) and lateral (lower) views. Anterodorsal scar (black
1765 arrows) of the transverse processes of the first (D), and second (E) caudal vertebrae of
1766 *Aucasaurus*, and cuneiform process (black arrow) on the anterodorsal surface of the anterior
1767 caudal vertebra of *Kurupi* (F). Triangular distal process (red lines) of posterior gastralia in

ventral (G), and dorsal (H) views. Proximal portion of the first (I), and second (J) haemal arches showing a dorsally open haemal canal. Image not to scale.

Inferences about abelisauridae axial pneumaticity

CT scans show camellated tissue in the neural arches and centra (Fig. 31A-Q). The camellated tissue present in the neural arches can be also seen around the foramina at the base of the neural spine of the first, fifth, sixth, ninth, twelfth and thirteenth caudal vertebrae.

Among living tetrapods, only birds are characterized as having extensive postcranial pneumaticity, but such pneumaticity was characteristic of several groups of extinct ornithodires, including pterosaurs and non-avian saurischian dinosaurs (Owen, 1857; Seeley, 1870; Britt, 1993, 1998; O´Connor & Claessens, 2005; O´Connor, 2006; Sereno *et al*., 2008; Wedel, 2009). Within non-avian saurischians, pneumaticity has been best-studied and documented in sauropods (much less so among non-avian theropods (e.g. O'Connor, 2007; Aranciaga Rolando, Garcia Marsá & Novas, 2020; Gianechini & Zurriaguz, 2021). Postcranial skeletal pneumaticity (PSP) is often manifested by the presence of foramina piercing cortical bone, especially of vertebrae, and connecting with chambers inside these elements (O´Connor, 2006). *Aucasaurus garridoi* presents two sets of foramina: at the basis of the spine (Fig. 29J, K) and inside the pocdf (Fig. 32A-C). The first set of foramina, visible from the fifth to eleventh caudal vertebrae, is here considered an autapomorphy of this taxon. These foramina also show homogeneity in size among the right and left side (Supporting Information, Table S3). The foramina located inside the pocdf also shows homogeneity among the right and the left side, at least until the ninth vertebra (Supporting Information, Table S3). These external correlates are also in *Carnotaurus* and in a new abelisaurid from Argentina (MPEF 10826).

Although the structures described above have characteristics of pneumatic foramina (Britt, 1993), the resolution of the CT scans makes it difficult to discern a connection between these foramina and the internal chambers or camellated tissue; however, an incipient camellated tissue at the basis of the spines is visible. Unfortunately, the resolution of the CT scan also precludes to determinate the presence of internal connections between the foramina located in the postzygapophyseal centrodiapophyseal fossa (pocdf) and the internal airspaces of the vertebral centra. However, the CT scans does show what appears to correspond to camellated tissue inside all scanned vertebrae (Fig. 31I-Q).

PSP is present at least in three brachyrostran abelisaurids—*Aucasaurus*, *Kurupi*, and the Abelisauridae indet. MPM 99—with camellated tissue in the centra and the neural arches of the anterior caudal vertebrae (Fig. 33A, B). Pneumatic caudal vertebrae are so far unknown in Majungasaurinae, although only *Majungasaurus* was subjet to such type of study (O´Connor, 2007). Moreover, noasaurids such as *Masiakasaurus* or *Vesperasaurus* also have apneumatic caudal vertebrae (Carrano, Sampson & Forster, 2002; Carrano, Loewen & Sertich, 2011; Langer *et al*., 2019). Therefore, the presence of the pneumatic traits in the caudal series, at least in the anterior portion, could be a unique condition of brachyrostran abelisaurids within the clade Ceratosauria, although more studies using CT imaging are needed, especially among basal ceratosaurs, nosasaurids, majungasaurines, and more derived brachyrostrans. As to pneumatic caudal vertebrae, the other clades that have signs of pneumaticity along the tail are Carcharodontosauridae, Megaraptora, Ornithomimosauria, Therizinosauroidea, Oviraptorosauria, and possibly in *Torvosaurus* (Britt, 1991, 1993; Benson *et al*., 2012; Novas *et al*., 2013; Watanabe *et al*., 2015; Aranciaga Rolando, Garcia Marsá & Novas, 2020). However, there is a different degree of pneumaticity among these taxa, being Megaraptora the group with the highest

1814 diffusion of the pneumaticity along the caudal series, and Carcharodontosauria the lowest one
1815 (Aranciaga Rolando, Garcia Marsá & Novas, 2020; Fig. 10). Megaraptorans have extensively
1816 pneumatized neural arches and centra of anterior and middle caudal vertebrae (e.g. Aranciaga
1817 Rolando, Garcia Marsá & Novas, 2020); carcharodontosaurids show evidence of pneumatization
1818 only in the arches of the anterior vertebrae (Britt, 1993). Among other theropod groups,
1819 Ornithomimosauria shows evidence of pneumatization in only the neural arches of the anterior
1820 and middle caudal vertebrae (Watanabe *et al*., 2015), while in Therizinosauroidea, penumaticity
1821 is observed mainly in the anterior vertebrae (neural arch and centrum; e.g. Zanno *et al*., 2009;
1822 Zanno, 2010). Finally, oviraptorosaurs hold pneumatic foramina in anterior, middle, and
1823 posterior caudal centra (e.g. Xu *et al*., 2007; Balanoff & Norell, 2012). Among non-tetanuran
1824 theropods (and possibly among non-avetheropodan theropods), Brachyrostra is the unique clade
1825 that possibly counts with pneumatic caudal vertebrae, as shown in the present study. Such
1826 diversified pattern of the pneumaticity among the caudal series of different theropod groups
1827 supports hypotheses of independent evolution among these lineages (Benson *et al*., 2012).
1828 Finally, *Aucasaurus* and possibly other abelisaurid taxa show (assuming more detailed
1829 CT imaging will confirm the vertebral pneumaticity hypothesized here) the "neural arch first"
1830 pattern (Benson *et al*., 2012), where the extension of pneumaticity in the posterior axial skeleton
1831 first appears in the neural arch. This assumption is due to the location of foramina and the
1832 associated camellated tissue in the caudal vertebrae of *Aucasaurus garridoi*, and corresponds to a
1833 highly conserved pneumatization pattern in theropods (Benson *et al*., 2012).
1834
1835 FIGURE 31 (NEAR HERE)
1836 Figure 31. **Select computed tomography sections of selected caudal vertebrae of *Aucasaurus***
1837 ***garridoi***. First (A, B, I, J), fifth and sixth (C, D, K, L), ninth (E, F, N, O), and twelfth and

1838 thirteenth (G, H, P, Q) caudal vertebrae in anterior (A, C, E, G), and posterior (B, D, F, H) views.
1839 Red lines indicate sagittal sections, while blu lines indicate transverse sections. Abbreviations:
1840 ct, camellate tissue.
1841
1842 FIGURE 32 (NEAR HERE)
1843 Figure 32. **Photographs of possible external correlates of pneumaticity in *Aucasaurus***
1844 ***garridoi***. Foramina (black arrows) whitin the pocdf of the first (A), fourth (B), and ninth (C)
1845 caudal vertebrae of *Aucasaurus*.
1846
1847 FIGURE 33 (NEAR HERE)
1848 Figure 33. **Internal tissue in caudal vertebrae of two brachyrostran abelisaurids**. The
1849 camellate tissues is visible in the centrum of Abelisauridae indet. MPM 99 (A), and the
1850 transverse process of *Kurupi* (B). On the right, details of the camellate tissues in both specimens.
1851 Image not to scale.
1852
1853 **Implications for reduction of movements in the axial skeleton of abelisauridae**
1854 Skeletal stiffness and robustness in abelisaurids, especially among derived forms, was
1855 suggested by several authors and based primarily on craniocervical modifications showed by
1856 these theropods (e.g. O'Connor, 2007; Sampson & Witmer, 2007; Méndez, 2014a; Filippi *et al*.,
1857 2016; Delcourt, 2018). Some studies have proposed specific behaviors for abelisaurids based on
1858 the peculiar features of the caudal portion of the skull, cervical vertebrae, and ribs (e.g.
1859 hypertrophied high epipophyses, low neural spines, ribs with aliform processes; O'Connor, 2007;
1860 Sampson & Witmer, 2007; Delcourt, 2018; González, Baiano & Vidal, 2021). Hence, behavioral
1861 inferences, especially as related to feeding habits and intraspecific behaviors, were tested by

biomechanical analyses of the skull and/or the cervical portion of the axial skeleton (Mazzetta, Fariña & Vizcaíno, 1998; Mazzetta *et al*., 2009; Therrien, Henderson & Ruff, 2005; Snively *et al*., 2011).

The postcervical portion of the axial skeleton of abelisaurids—particularly Brachyrostra (e.g. Méndez, 2014a, b)—also has features that are related to increased axial rigidity. For instance, abelisaurids (e.g. *Majungasaurus*, *Aucasaurus*, *Carnotaurus*) have a D-shaped transverse processes, which may have increased the surface for the attachment of robust epaxial musculature. Additionally, *Viavenator* holds conspicuous longitudinal ridges on the dorsal surface of the transverse processes, from the second to the nineth dorsal (Fig. 34A, B). The indeterminate abelisaurid MAU-Pv-LI 665 also has a similar ridge in the transverse processes of the dorsals (Fig. 34C, D). These structures were insertion sites of ligaments or of strong epaxial muscles, such as *m. longissimus dorsi* and/or *m. iliocostalis*. Furthermore, *Aucasaurus* and *Viavenator* have interspinous accessory articulation on the dorsal end of the neural spine that could be the ossified supraspinous ligament. Despite Filippi *et al*., (2016) stated these accessory processes are present on the posterior portion of the dorsal series; possibly, they were present also in anterior and middle dorsal vertebrae (Fig. 34E, F). These processes articulated between vertebrae, reducing further the mobility of the trunk, turning the backbone into a single rigid structure (Filippi *et al*., 2016). Surprisingly, *Aucasaurus* holds these processes on the sacral and caudal neural spines as well.

The sacrum is generally a rigid portion of the axial skeleton, due to several anatomical aspects such as inclusion between the ilia and partially or totally fusion of vertebrae. Abelisaurids—as in *Coelophysis*, *Syntarsus*, and *Masiakasaurus*—have sacral neural spines tightly fused to one another forming an anteroposterior wall (Carrano & Sampson, 2008).

Moreover, some abelisaurids such as *Aucasasurus* and *Carnotaurus* are characterized by having a transversely expanded dorsal end of the sacral neural spines with longitudinal lateral ridges, forming a T-like structure more conspicuous than that of other ceratosaurians (e.g. *Masiakasaurus*, *Elaphrosaurus*, *Majungasaurus*; Carrano & Sampson, 2008). A similar T-like structure is recorded in the neural spines of some sauropods (Cerda *et al*., 2015; and references therein), but the origin and function of this condition is still debated. Cerda *et al*. (2015) proposed a ligamentous origin for this structure, based on histological observations of sauropod specimens. However, a cartilaginous (Bonaparte, 1996) or tendinous (Giménez, Salgado & Cerda, 2008) origin were also suggested for the supraspinous rod of the sacral neural spines. The cause or function of the supraspinous ligament ossification is so far unknown, but could be related to an effect of stressing forces in this region of the skeleton (e.g. tensile forces; Cerda *et al*., 2015); however, it is not clear to what extent this condition has an ontogenetic component (Cerda *et al*., 2015). Up to now, this portion of the sacral neural spines are unexplored histologically, but the morphological similarity among sauropods and some abelisaurids (e.g. *Aucasaurus*, *Carnotaurus*) suggest a similar origin. Thereby, the T-like structure plus the accessory interspinous processes present in the dorsal vertebra of *Viavenator* and dorsal, sacral, and caudal vertebrae in *Aucasaurus* could be the result of the supraspinous ligament ossification along the axial skeleton, as also proposed for some sauropod dinosaurs (Cerda *et al*., 2015). Further paleohistological and biomechanical studies of these structures are likely to shed additional light on the stiffening of the axial skeleton of abelisaurids, in turn aiding a better understanding of their locomotory and postural role in these theropods.

The caudal vertebrae of brachyrostran abelisaurids have been the highlighted by several studies due to the specialized morphology of their transverse processes (e.g. Persons & Currie,

2011). Whitin Brachyrostra, the caudal transverse processeses can adopt two morphology; 1) with an anteroposteriorly developed lateral end (Coria & Salgado, 2000; Calvo, Rubilar-Rogers & Moreno, 2004; Canale *et al*., 2009; Cerroni *et al*., 2020); or, 2) a lateral end with an anterior awl-like process (e.g. Bonaparte, Novas & Coria, 1990; Coria, Chiappe & Dingus, 2002; Ezcurra & Méndez, 2009; Méndez, 2014b; Filippi *et al*., 2016; Delcourt, 2017). These distinct morphologies along with other ones previously highlighted (e.g. hyposphene-hypantrum articulation, large and dorsally inclined transverse processes, robust cdl, acdl, and pcdl) suggest that the tail was rigid in at least its proximal and middle regions (Persons & Currie, 2011; Méndez, 2014b). We propose new traits of the caudal vertebrae that support a significant stiffening of the tail. The caudal vertebrae of the abelisaurids *Aucasaurus*, *Carnotaurus*, *Viavenator*, and the Abelisauridae indet. MAU-Pv-LI 547 have a rough scar near the posterolateral rim of the dorsal surface of the transverse processes (Fig. 34G-K). This scar is visible up to the twelfth caudal in *Aucasaurus* (posterior to this it is unknown due to preservation). Another scar is located more medially in *Aucasaurus*, and this structure is extremely developed in *Kurupi* (cuneiform process of transverse process in Iori *et al*., 2021) (Fig. 30F). Derived brachyrostrans (e.g. *Aucasaurus*, *Carnotaurus*, and *Viavenator*) also show a marked boundary between the *m. ilio-ischiocaudalis* and the *m. longissimus*, due to the presence of ornamentation on the lateral rim of the transverse processes (more evident in *Aucasaurus*). Finally, *Aucasaurus*, *Carnotaurus*, *Viavenator*, and other abelisaurids (e.g. MAU-Pv-LI 547, MACN-PV-RN 1012) have an accessory longitudinal ridge (vlrtp) on the lateroventral end of the transverse processes (Fig. 34L, M). These dorsal and ventral ridges and scars suggest strong attachment points of ligaments and insertion points for the epaxial and hypaxial musculature of the caudal vertebrae, such as the *m. transversospinalis*, *m. longissimus*, *m. ilio-ischiocaudalis*,

and *m. caudofemoralis*, especially the latter (Persons & Currie, 2011). We believe that such degree of caudal musculature (Persons & Currie, 2011), in addition to the overlapped lateral transverse processes (e.g. Persons & Currie, 2011; Cerroni *et al*., 2020), must have rendered an extremely rigid tail in some brachyrostran abelisaurids, an interpretation that is congruent with previously proposed paleobiological implications of some abelisaurids as fast-runners/powerful sprinters (Bonaparte, Novas & Coria, 1990; Mazzetta, Fariña & Vizcaíno, 1998; Persons & Currie, 2011). Interestingly, several authors (Dollo, 1886; Organ, 2006a) have considered the stiffness of the tail ornithopod dinosaurs, via ossified tendons, as a response to the forces generate by retractor muscles of the femur, such as the *m. caudofemoralis*, which pulls back this bone (Organ, 2006a) and gives stability to the tail (Siviero *et al*., 2020). Despite the fact that ossified tendons are so far unknown in non-avian theropods, these mineralized structures are common among birds and ornithischian dinosaurs (e.g. Organ, 2006b). These structures lead to a stiffening of the axial skeleton to store more elastic energy and to redistribute internal forces (Organ, 2006a; Organ, 2006b). Wilson *et al*. (2016) claim similar functions for the supraspinous anterior and posterior bone outgrowths (mineralized supraspinous ligament via metaplasia) of dorsal neural spines in some non-avian theropods, adding the role of these structures in avoiding the ventral collapse of the vertebral column. However, Wilson *et al*. (2016) stated that the presence of the mineralized supraspinous ligament is a body-size and ontogenetic-dependent factor, since they are present in large non-avian theropods (Foth *et al*., 2015) and increase through the ontogeny. So far, ossified tendons seem to be absent among abelisaurds but the axial skeleton of these dinosaurs shows several traits that appear analogous to ossified tendons (or the notarium and expanded synsacrum of living birds), namely, accessory interspinous processes, procumbent osteological correlates of the epaxial musculature (e.g. longitudinal ridge on the

dorsolateral surface of dorsal transverse processes), and extremely fused sacral vertebrae with a dorsal swelling of the neural spines. Further studies of the myological correlates of the vertebral column of these theropods may confirm or rebut previously proposed paleobiological inferences.

FIGURE 34 (NEAR HERE)

Figure 34. **Details of the dorsal and caudal vertebrae of several abelisaurids**. Structures on the dorsal surface of the transverse process in the second dorsal vertebra of *Viavenator* (A, B), and anterior dorsal vertebra of MAU-Pv-LI 665 (C, D). Interspinous accessory process on the dorsal neural spine of the fourth dorsal vertebra of *Viavenator* (E), and *Aucasaurus* (F). Scar (black arrows) on the dorsal surface of the mid caudal transverse processes of *Aucasaurus* (G, H), *Viavenator* (I, J), and MAU-Pv-LI 547 (K). Ventrolateral ridge (black arrows) of the transverse process in *Aucasaurus* (L), and *Viavenator* (M) (lateral ridges of centrodiapophyseal lamina indicate by red arrows). Image not to scale.

CONCLUSIONS

Our detailed study of the axial skeleton of the abelisaurid *Aucasaurus garridoi* allowed us to expand the original diagnosis of this species. On the basis of the information gathered from the axial skeleton, *Aucasaurus garridoi* is distinguished by a unique combination of characters (plus the autapomorphy proposed by Coria, Chiappe & Dingus, 2002) including (1) atlas with a subcircular articular surface; (2) interspinous accessory processes extended to sacral and caudal neural spine; (3) a tubercle lateral to the prezygapophysis of middle caudal vertebrae (a similar structure is mentioned in *Aoniraptor*, Motta *et al*., 2016); (4) presence of pneumatic foramina laterally to the base of the neural spine in the anterior caudal vertebrae; (5) a prominent tubercle and extensive rugosity on the lateral rim of the transverse processes of caudal vertebrae fourth to

twelfth; (6) presence of a small ligamentous scar near the anterior edge of the dorsal surface in the anteriormost caudal transverse processes; and (7) distinct triangular process located at the fusion point of posterior gastralia.

Our phylogenetic analysis allowed us to recognize several new axial characters, and to detect apomorphic conditions shared by *Aucasaurus* and other abelisaurid taxa. The phylogeny presented here confirms the position of *Aucasaurus* among derived abelisaurids; our results recover *Aucasaurus* as a brachyrostran furileusaurian, although in a polytomy with other abelisaurids.

The presence of a pair of foramina laterally to the neural spines, of a foramen inside the pocdf (the latter trait is shared with other abelisaurids, such as *Carnotaurus*), and the presence of camellated tissue at the basis of neural spine and internally to the caudal vertebrae, are among the most salient features of the axial skeleton of *Aucasaurus garridoi* as these maybe evidencing the extension of axial pneumaticity into the caudal series. Pneumatic caudal vertebrae have not been documented in any other abelisaurid so far; consequently, we hypothesize that the pneumaticity in the caudal section of the axial skeleton of several brachyrostran abelisaurids (e.g. *Aucasaurus*, *Kurupi*, and the Abelisauridae indet. MPM 99) was independently acquired along the Brachyrostra lineage.

We also analyse some traits that possibly increased the stiffness and reduce the movements of the axial skeleton of abelisaurids, although some of these traits—hypertrophied high epipophyses, ribs with aliform processes, D-shaped transverse processes, accessory interspinous processes on the dorsal neural spine, fused sacral spines, caudal vertebrae with well-developed hypantrum-hyposphene articulation—were previously highlighted (e.g. O'Connor, 2007; Carrano & Sampson, 2008; Persons & Currie, 2011; Méndez, 2014a, b; Filippi *et al*.,

2016; González, Baiano & Vidal, 2021). We proposed several new traits, in some cases known only for a singular taxon, that are interpreted as related to attachment points for ligaments, which in turn, would have increased rigidity of the axial skeleton. These traits include the presence of a ridge on the dorsal surface of the dorsal transverse processes (e.g. *Viavenator*) and the presence of a scar on the posterolateral portion of the dorsal surface of the caudal transverse processes (e.g. *Aucasaurus*, *Carnotaurus*, *Viavenator*).

This study is the second detailed description of the axial skeleton of an abelisaurid theropod, after O'Connor's (2007) description of *Majungasaurus*, which delves into the pneumaticity and stiffness of the vertebral column. The detailed information provided here is expected to contribute to our understanding of the paleobiology and paleoecology of abelisaurid theropods.

ACKNOWLEDGEMENTS

We want to thank D. Pol (MPEF-CONICET), J. I. Canale (MMCh-CONICET), M. Ezcurra (MACN-CONICET), J. L. Carballido (MPEF-CONICET), J. Calvo (UNCo), G. Casal (UNPSJB), L. Ibiricu (CENPAT-CONICET), M. Luna (UNPSJB), P. Chafrat (MPCN), I. A. Cerda (IIPG-CONICET), C. Aguilar (MPM), M. Gutiérrez (MCF), L. Filippi (MAU), C. Fuentes (MAU), A. Garrido (MOZ), Y. Dutour (MHNA), T. Tortosa (MHNA), M. A. Rolando (MACN-CONICET), F. V. Iori (MPMA), T. S. Marinho (UFTM), and N. E. Jalil (MNHN), for providing access to specimens under their care. To D. Pol, J. I. Canale., M. Ezcurra, S. Apesteguía (Fundación Azara-CONICET), F. Gianechini (UNSL-CONICET), M. Cerroni (MACN-CONICET), and A. Cau for their comments on an early version of the manuscript. To the Sanatorio de Plaza Huincul and the technician G. Iril for providing access to the CT-scan and for assisting us during the scanning of

2024 the *Aucasaurus* holotype. We also acknowledge CONICET, Museo Municipal Carmen Funes, and
2025 Universidad Nacional de Río Negro for logistical support. We are thankful to the reviewers XXX
2026 for their helpful and insightful comments that have improved the quality of the manuscript.

2027

2028 **REFERENCES**

2029 **Accarie H, Beaudoin B, Dejax J, Friès G, Michard Jg, Taquet P. 1995**. D´ecouverte d'un
2030 Dinosaure théropode nouveau (*Genusaurus sisteronis* n. g., n. sp.) dans l'Albien marin de
2031 Sisteron (Alpes de Haute-Provence, France) et extension au Crétacé inférieur de la lignée
2032 cératosaurienne. *Compte Rendus de l'Academie des Sciences*, *Paris, série 7 IIa* **320**: 327–334.

2033

2034 **Agnolín FL, Cerroni MA, Scanferla A, Goswami A, Paulina-Carabajal A, Halliday T, Cuff**
2035 **AR, Reuil S. 2022.** First definitive abelisaurid theropod from the Late Cretaceous of
2036 Northwestern Argentina. *Journal of Vertebrate Paleontology* **41**: e2002348.

2037

2038 **Allain R, Chure DJ. 2002**. *Poekilopleuron bucklandii*, the theropod dinosaur from the Middle
2039 Jurassic (Bathonian) of Normandy. *Palaeontology* **45:** 1107–1121.

2040

2041 **Allain R, Suberbiola XP. 2003**. Dinosaurs of France. *Comptes Rendus Palevol* **2**: 27–44.

2042

2043 **Aranciaga Rolando M, Cerroni MA, Garcia Marsà JA, Motta MJ, Rozadilla S, Brissón**
2044 **Egli F, Novas FE. 2021.** A new medium-sized abelisaurid (Theropoda, Dinosauria) from the late
2045 cretaceous (Maastrichtian) Allen Formation of Northern Patagonia, Argentina. *Journal of South*
2046 *American Earth Sciences* **105**: 102915.

Aranciaga Rolando M, Garcia Marsá JA, Novas FE. 2020. Histology and pneumaticity of *Aoniraptor libertatem* (Dinosauria, Theropoda), an enigmatic mid-sized megaraptoran from Patagonia. *Journal of Anatomy* **237:** 741–756.

Aranciaga Rolando M, Méndez A, Canale JI, Novas FE. 2022. Osteology of *Aerosteon riocoloradensis* (Sereno et al. 2008) a large megaraptoran (Dinosauria: Theropoda) from the Upper Cretaceous of Argentina. *Historical Biology* **34:** 226–282.

Baiano MA. 2021. Osteología y relaciones filogenéticas de *Aucasaurus garridoi* Coria, Chiappe y Dingus, 2002 (Dinosauria, Theropoda, Abelisauridae). Implicancias sistemáticas y paleobiogeográficas en la evolución de los abelisáuridos. Unpublished D. Phil. Thesis, Universidad Nacional del Comahue.

Baiano MA, Cerda IA. 2022. Osteohistology of *Aucasaurus garridoi* (Dinosauria, Theropoda, Abelisauridae): inferences on lifestyle and growth strategy. *Historical Biology*: 1–12.

Baiano MA, Coria RA, Cau A. 2020. A new abelisauroid (Dinosauria: Theropoda) from the Huincul formation (lower upper Cretaceous, Neuquén Basin) of Patagonia, Argentina. *Cretaceous Research* **110**: 104408.

Baiano MA, Coria RA, Canale JI, Gianechini FA. 2021. New abelisaurid material from the Anacleto Formation (Campanian, Upper Cretaceous) of Patagonia, Argentina, shed light on the

2070 diagnosis of the Abelisauridae (Theropoda, Ceratosauria). *Journal of South American Earth*
2071 *Sciences* **110**: 103402.
2072
2073 **Baiano MA, Pol D, Bellardini F, Windholz GJ, Cerda IA, Garrido AC, Coria RA. 2022**.
2074 *Elemgasem nubilus*: a new brachyrostran abelisaurid (Theropoda, Ceratosauria) from the
2075 Portezuelo Formation (Upper Cretaceous) of Patagonia, Argentina. *Papers in Palaeontology* **8:**
2076 e1462.
2077
2078 **Balanoff AM, Norell MA. 2012**. Osteology of *Khaan mckennai* (Oviraptorosauria:
2079 Theropoda). *Bulletin of the American Museum of Natural History* **2012:** 1–77.
2080
2081 **Benson RB, Butler RJ, Carrano MT, O'Connor PM. 2012**. Air-filled postcranial bones in
2082 theropod dinosaurs: physiological implications and the 'reptile'-bird transition. *Biological*
2083 *Reviews* **87**: 168–193.
2084
2085 **Benson RB, Carrano MT, Brusatte SL. 2010**. A new clade of archaic large-bodied predatory
2086 dinosaurs (Theropoda: Allosauroidea) that survived to the latest
2087 Mesozoic. *Naturwissenschaften* **97:** 71–78.
2088
2089 **Bonaparte JF. 1985**. A horned Cretaceous carnosaur from Patagonia. *National Geographic*
2090 *Research* **1:** 149–151.
2091

Bonaparte JF. 1996. Cretaceous tetrapods of Argentina. *Münchner Geowissenschaftliche Abhandlungen (A)* **30**: 73–130.

Bonaparte JF, Novas FE, Coria RA. 1990. *Carnotaurus sastrei* Bonaparte, the horned, lightly built carnosaur from the Middle Cretaceous of Patagonia. *Contributions in Science, Natural History Museum of Los Angeles County* **416**: 1–42.

Britt BB. 1991. Theropods of Dry Mesa Quarry (Morrison Formation, Late Jurassic), Colorado, with emphasis on the osteology of Torvosaurus tanneri. *Brigham Young University Geology Studies* **37**: 1–72.

Britt BB. 1993. Pneumatic postcranial bones in dinosaurs and other archosaurs. Unpublished D. Phil. Thesis, University of Calgary.

Britt BB, Makovicky PJ, Gauthier J, Bonde N. 1998. Postcranial pneumatization in *Archaeopteryx*. *Nature* **395**: 374–376.

Brochu CA. 2003. Osteology of *Tyrannosaurus rex*: insights from a nearly complete skeleton and high-resolution computed tomographic analysis of the skull. *Journal of Vertebrate Paleontology* **22**: 1–138.

Brusatte SL, Carr TD, Norell MA. 2012. The osteology of *Alioramus*, a gracile and long-snouted tyrannosaurid (Dinosauria: Theropoda) from the Late Cretaceous of Mongolia. *Bulletin of the American Museum of Natural History* **2012:** 1–197.

Buffetaut E, Mechin P, Mechin-Salessy A. 1988. Un dinosaure théropode d'affinités gondwaniennes dans le Crétacé supérieur de Provence. *Comptes rendus de l'Académie des sciences* **306**: 153–158.

Calvo JO, Rubilar-Rogers D, Moreno K. 2004. A new abelisauridae (Dinosauria: Theropoda) from northwest Patagonia. *Ameghiniana* **41:** 555–563.

Canale JI, Apesteguía S, Gallina PA, Mitchell J, Smith ND, Cullen TM, Shinya A, Haluza A, Gianechini FA, Makovicky PJ. 2022. New giant carnivorous dinosaur reveals convergent evolutionary trends in theropod arm reduction. *Current Biology* **32:** 3195–3202.

Canale JI, Cerda I, Novas FE, Haluza A. 2016. Small-sized abelisaurid (Theropoda: Ceratosauria) remains from the Upper Cretaceous of northwest Patagonia, Argentina. *Cretaceous Research* **62**: 18–28.

Canale JI, Scanferla CA, Agnolín FL, Novas FE. 2009. New carnivorous dinosaur from the Late Cretaceous of NW Patagonia and the evolution of abelisaurid theropods. *Naturwissenschaften* **96**: 409–414.

2136 **Carrano MT, Sampson SD. 2008**. The phylogeny of ceratosauria (Dinosauria: Theropoda).
2137 *Journal of Systematic Palaeontology* **6**: 183–236.
2138
2139 **Carrano MT, Loewen MA, Sertich JJ. 2011**. New materials of *Masiakasaurus knopfleri*
2140 Sampson, Carrano, and Forster, 2001, and implications for the morphology of the Noasauridae
2141 (Theropoda: Ceratosauria). *Smithsonian Contributions to Paleobiology* **95**: 1–53.
2142
2143 **Carrano MT, Sampson SD, Forster CA. 2002**. The osteology of *Masiakasaurus knopfleri*, a
2144 small abelisauroid (Dinosauria: Theropoda) from the Late Cretaceous of Madagascar. *Journal of*
2145 *Vertebrate Paleontology* **22**: 510–534.
2146
2147 **Cerda IA, Casal GA, Martinez RD, Ibiricu LM. 2015**. Histological evidence for a
2148 supraspinous ligament in sauropod dinosaurs. *Royal Society Open Science* **2**: 150369.
2149
2150 **Cerroni MA, Baiano MA, Canale JI, Agnolín FL, Otero A, Novas FE. 2022**. Appendicular
2151 osteology of *Skorpiovenator bustingorryi* (Theropoda, Abelisauridae) with comments on
2152 phylogenetic features of abelisaurids. *Journal of Systematic Palaeontology* **20:** 1–32.
2153
2154 **Cerroni MA, Motta MJ, Agnolín FL, Rolando AA, Brissón Egli F, Novas FE. 2020**. A new
2155 abelisaurid from the Huincul Formation (Cenomanian-Turonian; upper Cretaceous) of Río Negro
2156 province, Argentina. *Journal of South American Earth Sciences* **98**: 102445.
2157

Chiappe LM, Göhlich UB. 2010. Anatomy of *Juravenator starki* (Theropoda: Coelurosauria) from the late Jurassic of Germany. *Neues Jahrbuch fuer Geologie und Palaeontologie. Abhandlungen* **258**: 257–296.

Chiappe LM, Coria RA, Dingus L, Jackson F, Chinsamy-Turan A, Fox M. 1998. Sauropod dinosaur embryos from the Late Cretaceous of Patagonia. *Nature* **396**: 258–261.

Chure DJ. 2000. Observations on the morphology and pathology of the gastral basket of *Allosaurus*, based on a new specimen from Dinosaur National Monument. *Oryctos* **3**:29–37.

Claessens LP. 2004. Dinosaur gastralia; origin, morphology, and function. *Journal of Vertebrate Paleontology* **24**: 89–106.

Coria RA, Currie PJ. 2016. A new megaraptoran dinosaur (Dinosauria, Theropoda, Megaraptoridae) from the Late Cretaceous of Patagonia. *PLoS One* **11**: e0157973.

Coria RA, Chiappe LM, Dingus L. 2002. A new close relative of *Carnotaurus sastrei* Bonaparte 1985 (Theropoda: Abelisauridae) from the Late Cretaceous of Patagonia. *Journal of Vertebrate Paleontology* **22**: 460–465.

Coria RA, Currie PJ, Paulina-Carabajal A. 2006. A new abelisauroid theropod from northwestern Patagonia. *Canadian Journal of Earth Sciences* **43**: 1283–1289.

2181 **Currie PJ, Chen PJ. 2001**. Anatomy of *Sinosauropteryx prima* from Liaoning, northeastern
2182 China. *Canadian Journal of Earth Sciences* **38**: 1705–1727.
2183
2184 **Currie PJ, Zhao XJ. 1993.** A new carnosaur (Dinosauria, Theropoda) from the Jurassic of
2185 Xinjiang, People's Republic of China. *Canadian Journal of Earth Sciences* **30**: 2037–2081.
2186
2187 **Delcourt R. 2017**. Revised morphology of *Pycnonemosaurus nevesi* Kellner & Campos, 2002
2188 (Theropoda: Abelisauridae) and its phylogenetic relationships. *Zootaxa* **4276**: 1–45.
2189
2190 **Delcourt R. 2018**. Ceratosaur palaeobiology: new insights on evolution and ecology of the
2191 southern rulers. *Scientific reports* **8**: 1–12.
2192
2193 **Delcourt R, Iori FV. 2018**. A new Abelisauridae (Dinosauria: Theropoda) from São José do Rio
2194 Preto Formation, Upper Cretaceous of Brazil and comments on the Bauru Group
2195 fauna. *Historical Biology* **11:** 1–8.
2196
2197 **Depéret C. 1896**. Sur l'existence de dinosauriens sauropodes et théropodes dans le Crétacé
2198 supérieur de Madagascar. *Comptes Rendus de l'Academie des Sciences* **122**: 483–485.
2199
2200 **Dingus L, Clark J, Scott GR, Swisher CC, Chiappe LM, Coria RA. 2000**. Stratigraphy and
2201 magnetostratigraphic/faunal constraints for the age of sauropod embryo-bearing rocks in the
2202 Neuquén Group (Late Cretaceous, Neuquén Province, Argentina). *American Museum Novitates*
2203 **3290**: 1–11.

Dollo L. 1886. Note sur les ligaments ossifies des dinosauriens de Bernissart. *Archives de Biologie* **7**: 249–264.

Ezcurra MD, Méndez AH. 2009. First report of a derived abelisaurid theropod from the Bajo de la Carpa Formation (Late Cretaceous), Patagonia, Argentina. *Bulletin of Geosciences* **84**: 547–554.

Farke AA, Sertich JJ. 2013. An abelisauroid theropod dinosaur from the Turonian of Madagascar. *PloS one* **8**: e62047.

Filippi LS, Méndez AH, Juárez Valieri RD, Garrido AC. 2016. A new brachyrostran with hypertrophied axial structures reveals an unexpected radiation of latest Cretaceous abelisaurids. *Cretaceous Research* **61**: 209–219.

Filippi LS, Méndez AH, Juárez Valieri RD, Gianechini FA, Garrido AC. 2018. Osteology of *Viavenator exxoni* (Abelisauridae; Furileusauria) from the Bajo de la Carpa Formation, NW Patagonia, Argentina. *Cretaceous Research* **83**: 95–119.

Foth C, Evers SW, Pabst B, Mateus O, Flisch A, Patthey M, Rauhut OWM. 2015. New insights into the lifestyle of *Allosaurus* (Dinosauria: Theropoda) based on another specimen with multiple pathologies. *PeerJ* **3**: e940.

Garrido AC. 2010a. Estratigrafía del Grupo Neuquén, Cretácico Superior de la Cuenca Neuquina (Argentina): nueva propuesta de ordenamiento litoestratigráfico. *Revista del Museo Argentino de Ciencias Naturales nueva serie* **12**: 121–177.

Garrido AC. 2010b. Paleoenvironment of the auca mahuevo and los barreales sauropod nesting-sites (Late Cretaceous, Neuquén Province, Argentina). *Ameghiniana* **47**: 99–106.

Gasparini Z, Sterli J, Parras A, O'Gorman JP, Salgado L, Varela J, Pol D. 2015. Late Cretaceous reptilian biota of the La Colonia Formation, central Patagonia, Argentina: Occurrences, preservation and paleoenvironments. *Cretaceous Research* **54**: 154–168.

Gianechini FA, Zurriaguz VL. 2021. Vertebral pneumaticity of the paravian theropod *Unenlagia comahuensis*, from the Upper Cretaceous of Patagonia, Argentina. *Cretaceous Research* **127**: 104925.

Gianechini FA, Apesteguía S, Landini W, Finotti F, Juárez Valieri RD, Zandonai F. 2015. New abelisaurid remains from the Anacleto Formation (Upper Cretaceous), Patagonia, Argentina. *Cretaceous Research* **54**: 1–16.

Gianechini FA, Méndez AH, Filippi LS, Paulina-Carabajal A, Juárez Valieri RD, Garrido AC. 2021. A new furileusaurian abelisaurid from La Invernada (Upper Cretaceous, Santonian, Bajo de la Carpa Formation), northern Patagonia, Argentina. *Journal of Vertebrate Paleontology* **40**: e1877151.

Gilmore CW. 1920. Osteology of the carnivorous Dinosauria in the United States National Museum, with special reference to the genera *Antrodemus* (*Allosaurus*) and *Ceratosaurus*. *Bulletin of the United States National Museum* **110**: 1–159.

Giménez O, Salgado L, Cerda IA. 2008. Osteohistología de la viga supraneural del sacro del titanosaurio *Epachthosaurus sciuttoi* (Cretácico tardío del Chubut). *Naturalia Patagónica* **4**: 111–117.

Goloboff PA, Farris J, Nixon KC. 2008. TNT, a free program for phylogenetic analysis. *Cladistics* **24**: 774–786.

Goloboff PA, Catalano SA. 2016. TNT, version 1.5, with a full implementation of phylogenetic morphometrics. *Cladistics* **32**: 221–238.

González A, Baiano MA, Vidal D. 2021. Neck myology, range of motion and feeding style of *Carnotaurus sastrei* (Theropoda: Abelisauridae). In: Belvedere M, Díez Díaz V, Mecozzi B, Sardella R, eds. *Abstract book of the XVIII annual conference of the European Association of Vertebrate Palaeontologists*, online, 5th-9th July 2021. *Palaeovertebrata* **44**: 65.

Gutherz SB, Groenke JR, Sertich JJ, Burch SH, O'Connor PM. 2020. Paleopathology in a nearly complete skeleton of *Majungasaurus crenatissimus* (Theropoda: Abelisauridae). *Cretaceous Research* **115**: 104553.

Harris JD. 1998. A reanalysis of *Acrocanthosaurus atokensis*, its phylogenetic status, and paleobiographic implications, based on a new specimen from Texas. *New Mexico Museum of Natural History and Science Bulletin* **13**: 1–75.

Ibiricu LM, Baiano MA, Martínez RD, Alvarez BN, Lamanna MC, Casal GA. 2021. A detailed osteological description of *Xenotarsosaurus bonapartei* (Theropoda: Abelisauridae): implications for abelisauroid phylogeny. *Cretaceous Research* **124**: 104829.

Iori FV, de Araújo-Júnior HI, Tavares SAS, da Silva Marinho T, Martinelli AG. 2021. New theropod dinosaur from the Late Cretaceous of Brazil improves abelisaurid diversity. *Journal of South American Earth Sciences* **112**: 103551.

Isasmendi E, Torices A, Canudo JI, Currie PJ, Pereda-Suberbiola X. 2022. Upper Cretaceous European theropod palaeobiodiversity, palaeobiogeography and the intra-Maastrichtian faunal turnover: new contributions from the Iberian fossil site of Laño. *Papers in Palaeontology* **8:** e1419.

Janensch W. 1920. Über *Elaphrosaurus bambergi* und die megalosaurier aus den Tendaguru-Schichten Deutsch-Ostafrikas. *Sitzungsberichte der Gesellschaft Naturforschender Freunde zu Berlin* **8**: 226–235.

2295 **Janensch W. 1925**. Die Coelurosaurier und Theropoden der Tendaguru-Schichten Deutsch-
2296 Ostafrikas. *Palaeontographica* **7**: 1–99.
2297
2298 **Ji SA, Ji Q, Lü J, Yuan C. 2007**. A new giant compsognathid dinosaur with long filamentous
2299 integuments from Lower Cretaceous of Northeastern China. *Acta Geologica Sinica* **81**: 8–15.
2300
2301 **Kellner AWA, Campos DDA. 2002**. On a theropod dinosaur (Abelisauria) from the continental
2302 Cretaceous of Brazil. *Arquivos do Museu Nacional* **60**: 163–170.
2303
2304 **Krause DW, Sampson SD, Carrano MT, O'connor PM. 2007.** Overview of the history of
2305 discovery, taxonomy, phylogeny, and biogeography of *Majungasaurus crenatissimus*
2306 (Theropoda: Abelisauridae) from the Late Cretaceous of Madagascar. *Journal of Vértebrate*
2307 *Paleontology* **27**: 1–20.
2308
2309 **Langer MC, Martins NDO, Manzig PC, Ferreira GDS, Marsola JCDA, Fortes E, Lima R,**
2310 **Frediani Sant'Ana LC, da Silva Vidal L, da Silva Lorençato RH, Ezcurra MD. 2019**. A new
2311 desert-dwelling dinosaur (Theropoda, Noasaurinae) from the Cretaceous of south
2312 Brazil. *Scientific reports* **9**: 1–31.
2313
2314 **Lavocat R. 1955**. Sur une portion de mandibule de théropode provenant du Crétacé supérieur de
2315 Madagascar. *Bulletin du Muséum de l'Histoire Naturelle* **27**: 256–259.
2316

Le Loeuff J, Buffetaut E. 1991. *Tarascosaurus salluvicus* nov. gen., nov. sp., dinosaure théropode du Crétacé Supérieur du sud de la France. *Géobios* **24**: 585–594.

Longrich NR, Pereda-Suberbiola X, Jalil NE, Khaldoune F, Jourani E. 2017. An abelisaurid from the latest Cretaceous (late Maastrichtian) of Morocco, North Africa. *Cretaceous Research* **76**: 40–52.

Maddison WP, Maddison DR. 2019. Mesquite: a modular system for evolutionary analysis, v. 3.61.

Madsen JH. 1976. *Allosaurus fragilis*: a revised osteology. *Utah Geological and Mining Survey Bulletin* **109**: 1–163.

Madsen JH, Welles SP. 2000. *Ceratosaurus* (Dinosauria, Theropoda): a revised osteology. *Utah Geological Survey Miscellaneous* **2**: 1–80.

Marsh OC. 1877. Notice on new dinosaurian reptiles: *American Journal of Science* **14**: 514–516.

Marsh AD, Rowe TB. 2020. A comprehensive anatomical and phylogenetic evaluation of *Dilophosaurus wetherilli* (Dinosauria, Theropoda) with descriptions of new specimens from the Kayenta Formation of northern Arizona. *Journal of Paleontology* **94**: 1–103.

Martínez RD, Novas F, Ambrosio A. 2004. Abelisaurid remains (Theropoda, Ceratosauria) from southern Patagonia. *Ameghiniana* **41:** 577–585.

Martínez RD, Giménez O, Rodríguez J, Bochatey G. 1986. *Xenotarsosaurus bonapartei* nov. gen. et sp.(Carnosauria, Abelisauridae), un nuevo Theropoda de la Formación Bajo Barreal, Chubut, Argentina. *IV Congreso Argentino de Paleontología y Bioestratigrafía* **2**: 23–31.

Mazzetta GV, Fariña RA, Vizcaíno SF. 1998. On the palaeobiology of the South American horned theropod *Carnotaurus sastrei* Bonaparte. *Gaia* **15**: 185–192.

Mazzetta GV, Cisilino AP, Blanco RE, Calvo N. 2009. Cranial mechanics and functional interpretation of the horned carnivorous dinosaur *Carnotaurus sastrei*. *Journal of Vértebrate Paleontology* **29**: 822–830.

Méndez AH. 2014a. The cervical vértebrae of the Late Cretaceous abelisaurid dinosaur *Carnotaurus sastrei*. *Acta Palaeontologica Polonica* **59**: 569–579.

Méndez AH. 2014b. The caudal vertebral series in abelisaurid dinosaurs. *Acta Palaeontologica Polonica* **59**: 99–107.

Méndez AH, Filippi LS, Gianechini FA, Juárez Valieri RD. 2018. New brachyrostran remains (Theropoda, Abelisauridae) from La Invernada fossil site (Bajo de la Carpa Formation, Upper Cretaceous), northern Patagonia, Argentina. *Cretaceous Research* **83**: 120–126.

Méndez AH, Gianechini FA, Paulina-Carabajal A, Filippi LS, Juárez Valieri RD, Cerda IA, Garrido AC. 2022. New furileusaurian remains from La Invernada (northern Patagonia, Argentina): A site of unusual abelisaurids abundance. *Cretaceous Research* **129**: 104989.

Motta MJ, Aranciaga Rolando AM, Rozadilla S, Agnolín FL, Chimento NR, Brissón Egli F, Novas FE. 2016. New theropod fauna from the Upper Cretaceous (Huincul Formation) of northwestern Patagonia, Argentina. *New Mexico Museum of Natural History and Science Bulletin* **71**: 231–253.

Norell MA, Makovicky PJ. 1997. Important features of the dromaeosaur skeleton: information from a new specimen. *American Museum Novitates* **3215**: 1–28.

Novas FE, Agnolín FL, Ezcurra MD, Porfiri J, Canale JI. 2013. Evolution of the carnivorous dinosaurs during the Cretaceous: the evidence from Patagonia. *Cretaceous Research* **45**: 174–215.

Novas FE, Agnolín FL, Motta MJ, Brissón Egli F. 2021. Osteology of *Unenlagia comahuensis* (Theropoda, Paraves, Unenlagiidae) from the Late Cretaceous of Patagonia. *The Anatomical Record* **304**: 2741–2788.

Novas FE, Chatterjee S, Rudra DK, Datta PM. 2010. *Rahiolisaurus gujaratensis*, n. gen. n. sp., a new abelisaurid theropod from the Late Cretaceous of India. In: Bandyopadhyay S, ed. *New aspects of Mesozoic biodiversity*. Heidelberg: Springer Verlag, 45–62.

Novas FE, de Souza Carvalho I, Ribeiro LCB, Méndez AH. 2008. First abelisaurid bone remains from the Maastrichtian Marilia Formation, Bauru basin, Brazil. *Cretaceous Research* **29**: 625–635.

O'Connor PM. 2006. Pulmonary pneumaticity: an evaluation of soft tissue influences on the postcranial skeleton and the reconstruction of pulmonary anatomy in archosaurs. *Journal of Morphology* **267**: 1199–1226.

O'Connor PM. 2007. The postcranial axial skeleton of *Majungasaurus crenatissimus* (Theropoda: Abelisauridae) from the Late Cretaceous of Madagascar. *Journal of Vertebrate Paleontology* **27**: 127–163.

O'Connor PM, Claessens L. 2005. Basic avian pulmonary design and flow-through ventilation in nonavian theropod dinosaurs. *Nature* **436**: 253–256.

Organ CL. 2006a. Biomechanics of ossified tendons in ornithopod dinosaurs. *Paleobiology* **32**: 652–665.

Organ CL. 2006b. Thoracic epaxial muscles in living archosaurs and ornithopod dinosaurs. *The Anatomical Record* **288**: 782–793.

Osborn HF. 1905. *Tyrannosaurus* and other Cretaceous carnivorous dinosaurs. *Bulletin of the American Museum of Natural History* **21**: 259–265.

Ősi A, Buffetaut E. 2011. Additional non-avian theropod and bird remains from the early Late Cretaceous (Santonian) of Hungary and a review of the European abelisauroid record. *Annales de Paleontologie* **97**: 35–49.

Ősi A, Apesteguía S, Kowalewski M. 2010. Non-avian theropod dinosaurs from the early Late Cretaceous of Central Europe. *Cretaceous Research* **31**: 304–320.

Owen R. 1857. Monograph on the fossil Reptilia of the Wealden and Purbeck formations. Part III. Dinosauria (*Megalosaurus*). *Paleontology Society Monograph* **9**: 1–26.

Paulina-Carabajal A. 2011. Braincases of abelisaurid theropods from the Upper Cretaceous of North Patagonia. *Palaeontology* **54**: 793–806.

Persons IV WS, Currie PJ. 2011. Dinosaur speed demon: the caudal musculature of *Carnotaurus sastrei* and implications for the evolution of South American abelisaurids. *PloS one* **6**: e25763.

2429 **Peyer K. 2006**. A reconsideration of *Compsognathus* from the Upper Tithonian of Canjuers,
2430 southeastern France. *Journal of vertebrate Paleontology* **26**: 879–896.
2431
2432 **Pol D, Escapa IH. 2009**. Unstable taxa in cladistic analysis: identification and the assessment of
2433 relevant characters. *Cladistics* **25**: 515–527.
2434
2435 **Pol D, Goloboff PA. 2020**. The impact of unstable taxa in coelurosaurian phylogeny and
2436 resampling support measures for parsimony analyses. *Bulletin of the American Museum of*
2437 *Natural History* **440**: 97–115.
2438
2439 **Pol D, Rauhut OWM. 2012**. A Middle Jurassic abelisaurid from Patagonia and the early
2440 diversification of theropod dinosaurs. *Proceedings of the Royal Society B: Biological*
2441 *Sciences* **279**: 3170–3175.
2442
2443 **Reig OA. 1963**. La presencia de dinosaurios saurisquios de los “Estratos de Ischigualasto”
2444 (Mesotriásico Superior) de las provincias de San Juan y La Rioja (República Argentina).
2445 *Ameghiniana* **3**: 3–20.
2446
2447 **Rauhut OWM, Carrano MT. 2016**. The theropod dinosaur *Elaphrosaurus bambergi*, from the
2448 Late Jurassic of Tendaguru, Tanzania. *Zoological Journal of the Linnean Society* **178**: 546-–610.
2449
2450 **Rauhut OWM, Cladera G, Vickers-Rich P, Rich TH. 2003**. Dinosaur remains from the Lower
2451 Cretaceous of the Chubut group, Argentina. *Cretaceous Research* **24**: 487–497.

Sampson SD, Witmer LM. 2007. Craniofacial anatomy of *Majungasaurus crenatissimus* (Theropoda: Abelisauridae) from the late Cretaceous of Madagascar. *Journal of Vertebrate Paleontology* **27:** 32–104.

Sampson SD, Carrano MT, Forster CA. 2001. A bizarre predatory dinosaur from the Late Cretaceous of Madagascar. *Nature* **409**: 504–506.

Sánchez-Hernández B, Benton MJ. 2012. Filling the ceratosaur gap: A new ceratosaurian theropod from the Early Cretaceous of Spain. *Acta Palaeontologica Polonica* **59:** 581–600.

Seeley HG. 1870. On *Ornithopsis*, a gigantic animal of the pterodactyle kind from the Wealden. *Annals and Magazine of Natural History* **4**: 279–283.

Sereno PC, Novas FE. 1994. The skull and neck of the basal theropod *Herrerasaurus ischigualastensis*. *Journal of Vertebrate Paleontology* **13**: 451–476.

Sereno PC, Martínez RN, Wilson JA, Varricchio DJ, Alcober OA, Larsson HC. 2008. Evidence for avian intrathoracic air sacs in a new predatory dinosaur from Argentina. *PLoS one* **3**: e3303.

Siviero BC, Rega E, Hayes WK, Cooper AM, Brand LR, Chadwick AV. 2020. Skeletal trauma with implications for intratail mobility in *Edmontosaurus annectens* from a

monodominant bonebed, Lance Formation (Maastrichtian), Wyoming USA. *Palaios* **35**: 201–214.

Snively E, Russell AP. 2007. Functional morphology of neck musculature in the Tyrannosauridae (Dinosauria, Theropoda) as determined via a hierarchical inferential approach. *Zoological Journal of the Linnean Society* **151**: 759–808.

Snively E, Cotton JR, Witmer LM, Ridgely R, Theodor J. 2011. Finite Element Comparison of Cranial Sinus Function in the Dinosaur *Majungasaurus* and Head-Clubbing Giraffes. In Summer Bioengineering Conference. *American Society of Mechanical Engineers*: 1075–1076.

Therrien F, Henderson DM, Ruff CB. 2005. Bite me: biomechanical models of theropod mandibles and implications for feeding behavior. In: Carpenter K, ed. *The carnivorous dinosaurs*. Indianapolis: Indiana University Press, 179–237.

Tortosa T, Buffetaut E, Vialle N, Dutour Y, Turini E, Cheylan G. 2014. A new abelisaurid dinosaur from the Late Cretaceous of southern France: Palaeobiogeographical implications. *Annales de Paléontologie* **100**: 63–86.

Watanabe A, Eugenia Leone Gold M, Brusatte SL, Benson RB, Choiniere J, Davidson A, Norell MA. 2015. Vertebral pneumaticity in the ornithomimosaur *Archaeornithomimus* (Dinosauria: Theropoda) revealed by computed tomography imaging and reappraisal of axial pneumaticity in Ornithomimosauria. *PloS one* **10**: e0145168.

Wedel MJ. 2009. Evidence for bird-like air sacs in saurischian dinosaurs. *Journal of Experimental Zoology A* **311**: 611–628.

Welles SP. 1954. New Jurassic dinosaur from the Kayenta formation of Arizona. *Geological Society of America Bulletin* **65**: 591–598.

Welles SP. 1984. *Dilophosaurus wetherilli* (Dinosauria, Theropoda). Osteology and comparisons. *Palaeontographica. Abteilung A, Paläozoologie, Stratigraphie* **185**: 85–180.

Wilson JA. 1999. Vertebral laminae in sauropods and other saurischian dinosaurs. *Journal of Vértebrate Paleontology* **19**: 639–653.

Wilson JA. 2012. New vertebral laminae and patterns of serial variatiom in vertebral laminae of sauropod dinosaurs. *Contributions from the Museum of Paleontology, University of Michigan* **32**: 91–110.

Wilson JA, Sereno PC, Srivastava S, Bhatt DK, Khosla A, Sahni A. 2003. A new abelisaurid (Dinosauria, Theropoda) from the Lameta Formation (Cretaceous, Maastrichtian) of India. *Contributions from the Museum of Paleontology* **31:** 1–42.

Wilson JA, D'Emic MD, Ikejiri T, Moacdieh EM, Whitlock JA. 2011. A nomenclature for vertebral fossae in sauropods and other saurischian dinosaurs. *PloS one* **6**: e17114.

Wilson JP, Woodruff DC, Gardner JD, Flora HM, Horner JR, Organ CL. 2016. Vertebral adaptations to large body size in theropod dinosaurs. *PloS one* **11**: e0158962.

Xu X, Tan Q, Wang J, Zhao X, Tan L. 2007. A gigantic bird-like dinosaur from the Late Cretaceous of China. *Nature* **447**: 844–847.

Zaher H, Pol D, Navarro BA, Delcourt R, Carvalho AB, 2020. An Early Cretaceous theropod dinosaur from Brazil sheds light on the cranial evolution of the Abelisauridae. *Comptes Rendus Palevol* **19**: 101–115.

Zanno LE. 2010. Osteology of *Falcarius utahensis* (Dinosauria: Theropoda): characterizing the anatomy of basal therizinosaurs. *Zoological Journal of the Linnean Society* **158**: 196–230.

Zanno LE, Makovicky PJ. 2013. Neovenatorid theropods are apex predators in the Late Cretaceous of North America. *Nature Communications* **4**: 2827.

Zanno LE, Gillette DD, Albright LB, Titus AL. 2009. A new North American therizinosaurid and the role of herbivory in 'predatory' dinosaur evolution. *Proceedings of the Royal Society B: Biological Sciences* **276:** 3505–3511.

Zhang X, Xu X, Zhao X, Sereno P, Kuang X, Tan L. 2001. A long-necked therizinosauroid dinosaur from the Upper Cretaceous Iren Dabasu Formation of Nei Mongol, People's Republic of China. *Vertebrata PalAsiatica* **39:** 282–290.

Table 1(on next page)

Taxa used for anatomical comparisons.

1 **Table 1. Taxa used for anatomical comparisons**.

Taxa examined directly	Specimen no.	First reference
Arcovenator escotae	MHNA-PV-2011.12.5/198/213	Tortosa *et al*., 2014
Aucasaurus garridoi	MCF-PVPH-236	Coria *et al*., 2002
Carnotaurus sastrei	MACN-PV-CH 894	Bonaparte, 1985
Ekrixinatosaurus novasi	MUC Pv 294	Calvo *et al*., 2004
Elemgasem nubilus	MCF-PVPH-380	Baiano *et al*., 2022
Eoabelisaurus mefi	MPEF Pv 3990	Pol & Rauhut, 2012
Huinculsaurus montesi	MCF-PVPH-36	Baiano *et al*., 2020
Ilokelesia aguadagrandensis	MCF-PVPH-35	Coria & Salgado, 2000
Niebla antiqua	MPCN-PV-796	Aranciaga Rolando *et al*., 2021
Skorpiovenator bustingorryi	MMCh-PV 48	Canale *et al*., 2009
Tralkasaurus cuyi	MPCA-PV 815	Cerroni *et al*., 2020
Viavenator exxoni	MAU-PV-LI 530	Filippi *et al*., 2016
Xenotarsosaurus bonapartei	UNPSJB-PV 612/1-2	Martínez *et al*., 1986; Ibiricu

		et al., 2021
Abelisauridae indet.	MACN-PV-RN 1012	Ezcurra & Méndez, 2009
Abelisauridae indet.	MAU-Pv-LI 547	Méndez *et al*., 2018
Abelisauridae indet.	MAU-Pv-LI 665	Méndez *et al*., 2022
Abelisauridae indet.	MCF-PVPH-237	Coria *et al*., 2006
Abelisauridae indet.	MMCh-PV 69	Canale *et al*., 2016
Abelisauridae indet.	MPCN-PV-69	Gianechini *et al*., 2015; Baiano *et al*., 2021
Abelisauridae indet.	MPM 99	Martínez *et al*., 2004
Abelisauroidea indet.	MPEF PV 1699/1-2	Rauhut *et al*., 2003

Taxa drawn from literature	**Source**	**First reference**
Aerosteon riocoloradensis	Aranciaga Rolando *et al*., 2022	Sereno *et al*., 2008
Allosaurus fragilis	Madsen, 1976	Marsh, 1877
Camarillasaurus cirugedae	Sánchez-Hernández & Benton, 2011	Sánchez-Hernández & Benton, 2011
Ceratosaurus sp	Gilmore, 1920;	Gilmore, 1920

	Madsen & Welles, 2000	
Dahalokely tokana	Farke & Sertich, 2013	Farke & Sertich, 2013
Dilophosaurus wetherilli	Welles, 1984; Marsh & Rowe, 2020	Welles, 1954
Elaphrosaurus bambergi	Rauhut & Carrano, 2016	Janensch, 1920, 1925
Herrerasaurus ischigualastensis	Sereno & Novas, 1994	Reig, 1963
Kurupi itaata	Iori *et al*., 2021	Iori *et al*., 2021
Majungasaurus crenatissimus	O'Connor, 2007	(Depéret, 1896) Lavocat, 1955
Masiakasaurus knopfleri	Carrano *et al*., 2002, 2011	Sampson *et al*., 2001
Pycnonemosaurus nevesi	Delcourt, 2017	Kellner & Campos, 2002
Rahiolisaurus gujaratensis	Novas *et al*., 2010	Novas *et al*., 2010
Rajasaurus narmadensis	Wilson *et al*., 2003	Wilson *et al*., 2003
Sinraptor dongi	Currie & Zhao, 1993	Currie & Zhao, 1993
Spectrovenator ragei	Zaher *et al*., 2020	Zaher *et al*., 2020

Thanos simonattoi	Delcourt & Iori, 2018	Delcourt & Iori, 2018
Tyrannosaurus rex	Brochu, 2003	Osborn, 1905
Abelisauroidea indet. cpp 893	Novas *et al*., 2008	Novas *et al*., 2008

2

Figure 1

Axial skeleton of *Aucasaurus garridoi*

Lateral right view of the axial elements of the holotype MCF-PVPH-236. Scale bar: 1 m. Silhouette modified from Scott Hartman (https://www.skeletaldrawing.com/).

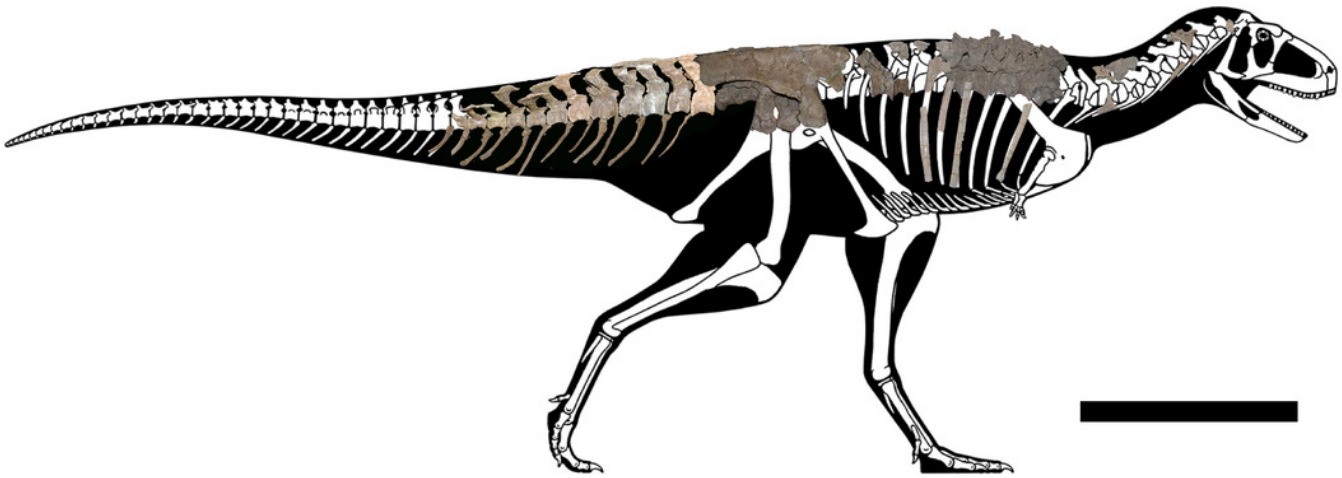

Figure 2

Atlas of *Aucasaurus garridoi* MCF-PVPH-236.

In anterior (A), posterior (B), right lateral (C), ventral (D), and dorsal (E) views. Abbreviations: amp, anteromedial process; ic, intercentrum; nrp, neurapophysis; od, odontoid; vp, ventral process. Scale bar: 5 cm.

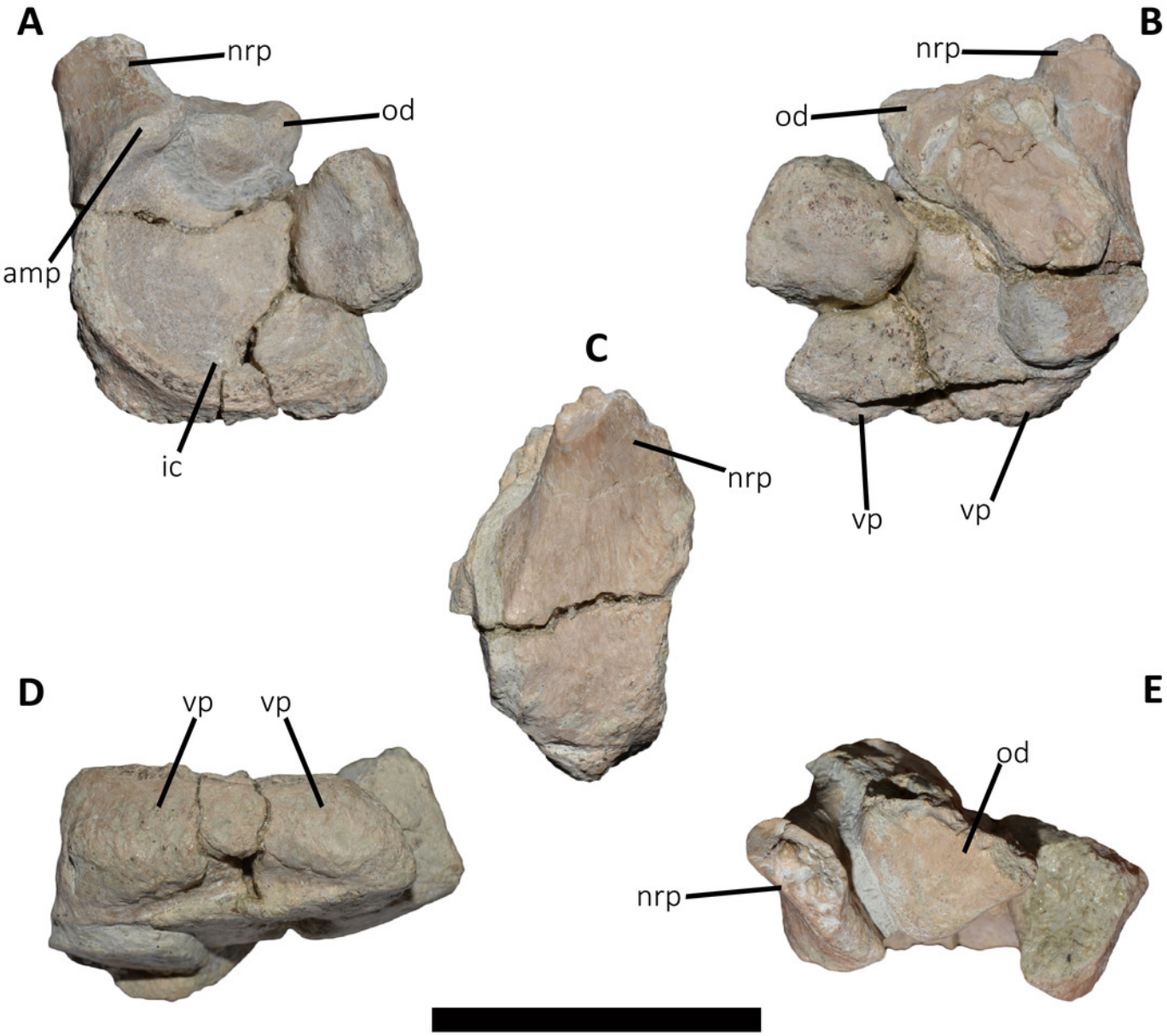

Figure 3

Cervical vertebra fragments of *Aucasaurus garridoi* MCF-PVPH-236.

In lateral (A, G, E), ventral (B), dorsal (C), and medial (D, F) views. Abbreviations: ape, anterior process of epipophysis; eprl, epipophyseal prezygapophyseal lamina; podl, postzygodiapophyseal lamina; poz, postzygapophysis; ppe, posterior process of epipophysis; prz, prezygapophysis; sprl, spinoprezigapophyseal lamina; tp, transverse process. Scale bar: 5 cm.

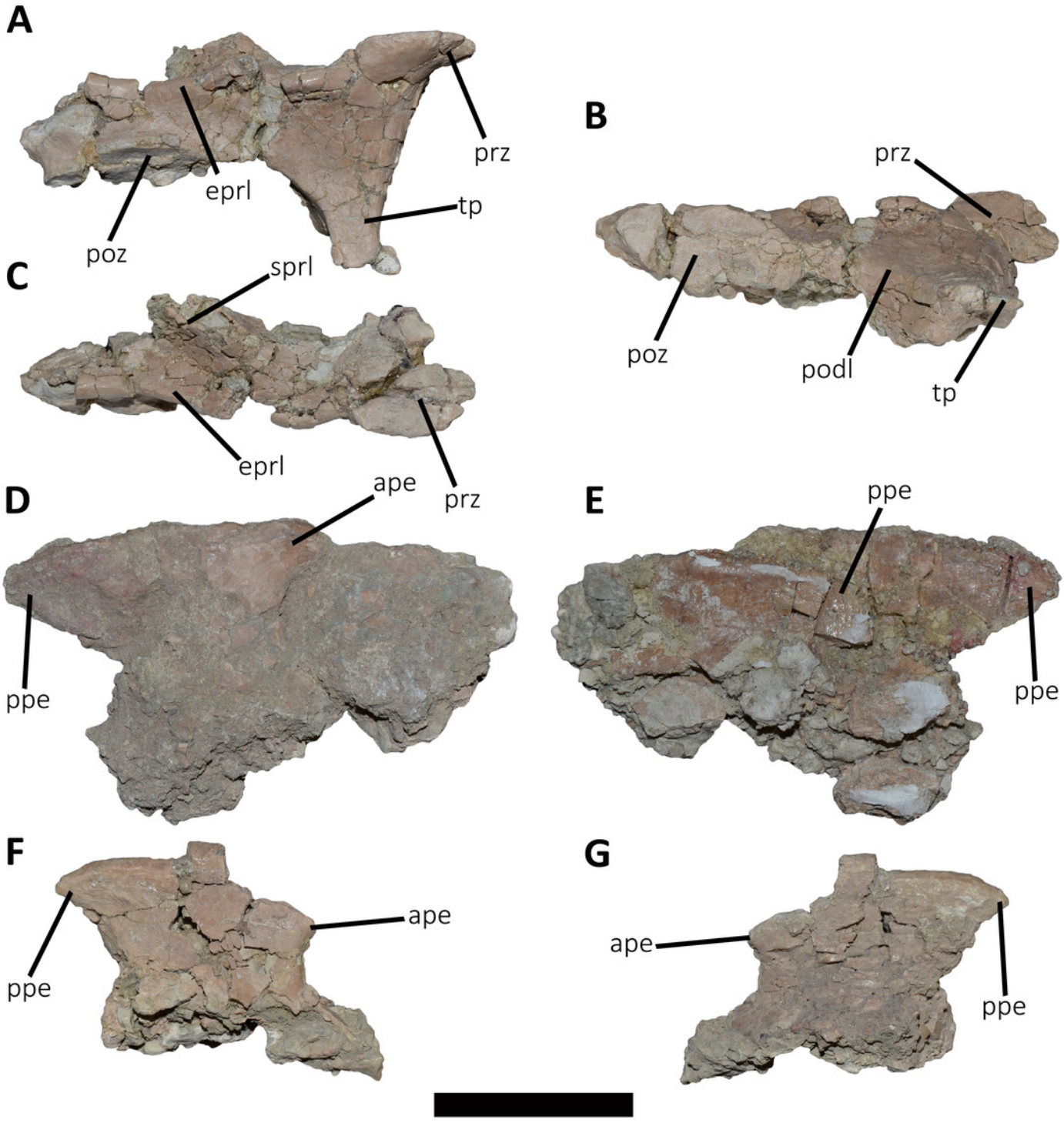
A
prz
eprl
tp
poz
B
prz
poz
podl
tp
C
sprl
eprl
prz
D
ape
ppe
E
ppe
ppe
F
ape
ppe
G
ape
ppe

Figure 4

Photographs and line drawings of the anterior dorsal vertebrae of *Aucasaurus garridoi* MCF-PVPH-236.

In lateral (A) view. Abbreviations: 2dns, second dorsal neural spine; 7dns, seventh dorsal neural spine; acpl, anterior centroparapophyseal lamina; D2-D6, second to seventh dorsal vertebrae; iap, interspinous accessory process; ilp, interspinous ligament process; pl, pleurocoel; pp, parapophysis; prz, prezygapophysis; tp, transverse process. Scale bar: 5 cm.

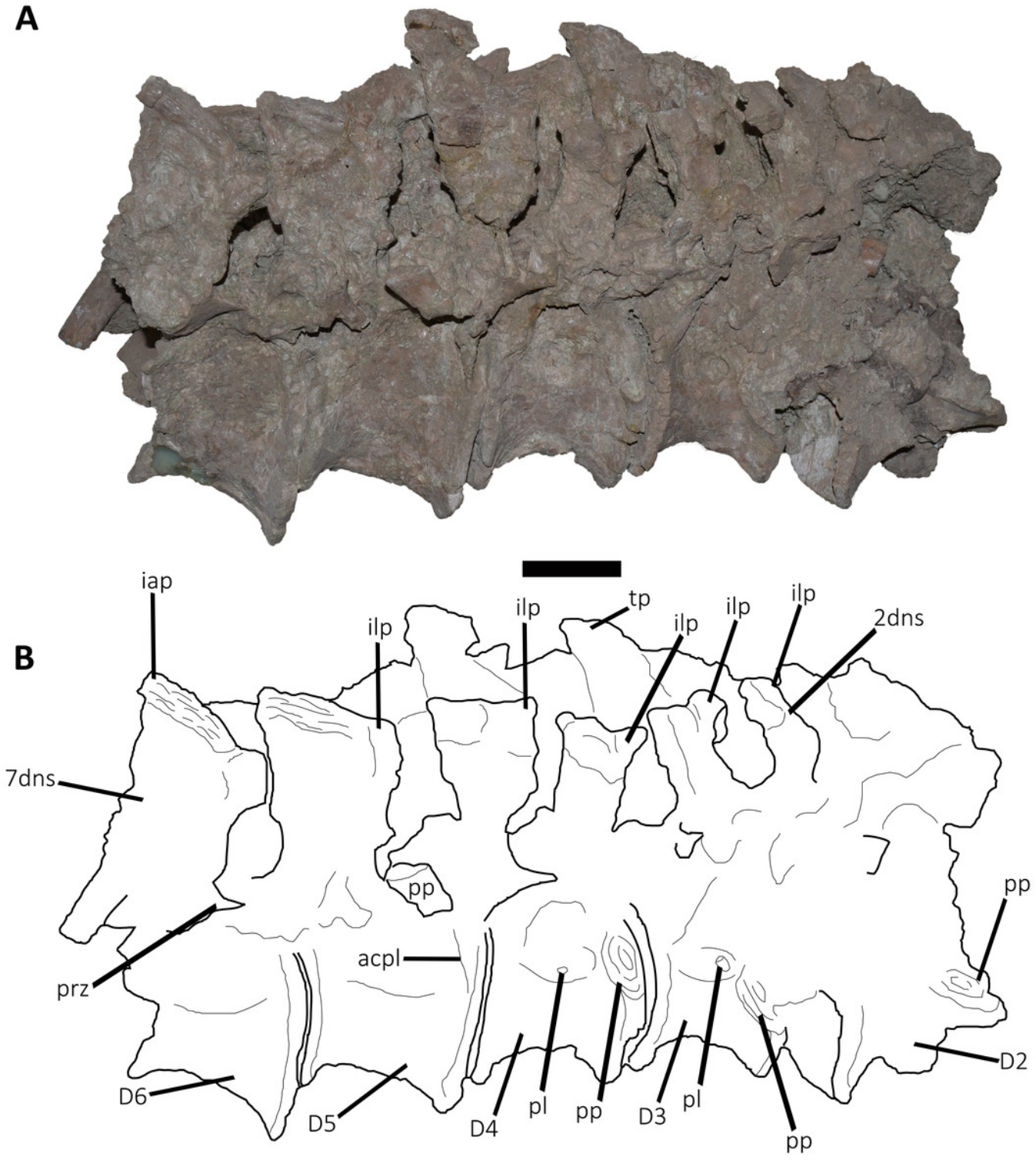
A
B
iap
ilp
ilp
tp
ilp
ilp
ilp
2dns
7dns
pp
pp
acpl
prz
D6
D5
D4
pl
pp
D3
pl
pp
D2

Figure 5

Photographs and line drawings of the anterior dorsal vertebrae of *Aucasaurus garridoi* MCF-PVPH-236.

In ventral (A, B), and dorsal (C, D) views. Abbreviations: D2-D7, second to seventh dorsal vertebrae; iap, interspinous accessory process; ilp, interspinous ligament process. Scale bar: 5 cm.

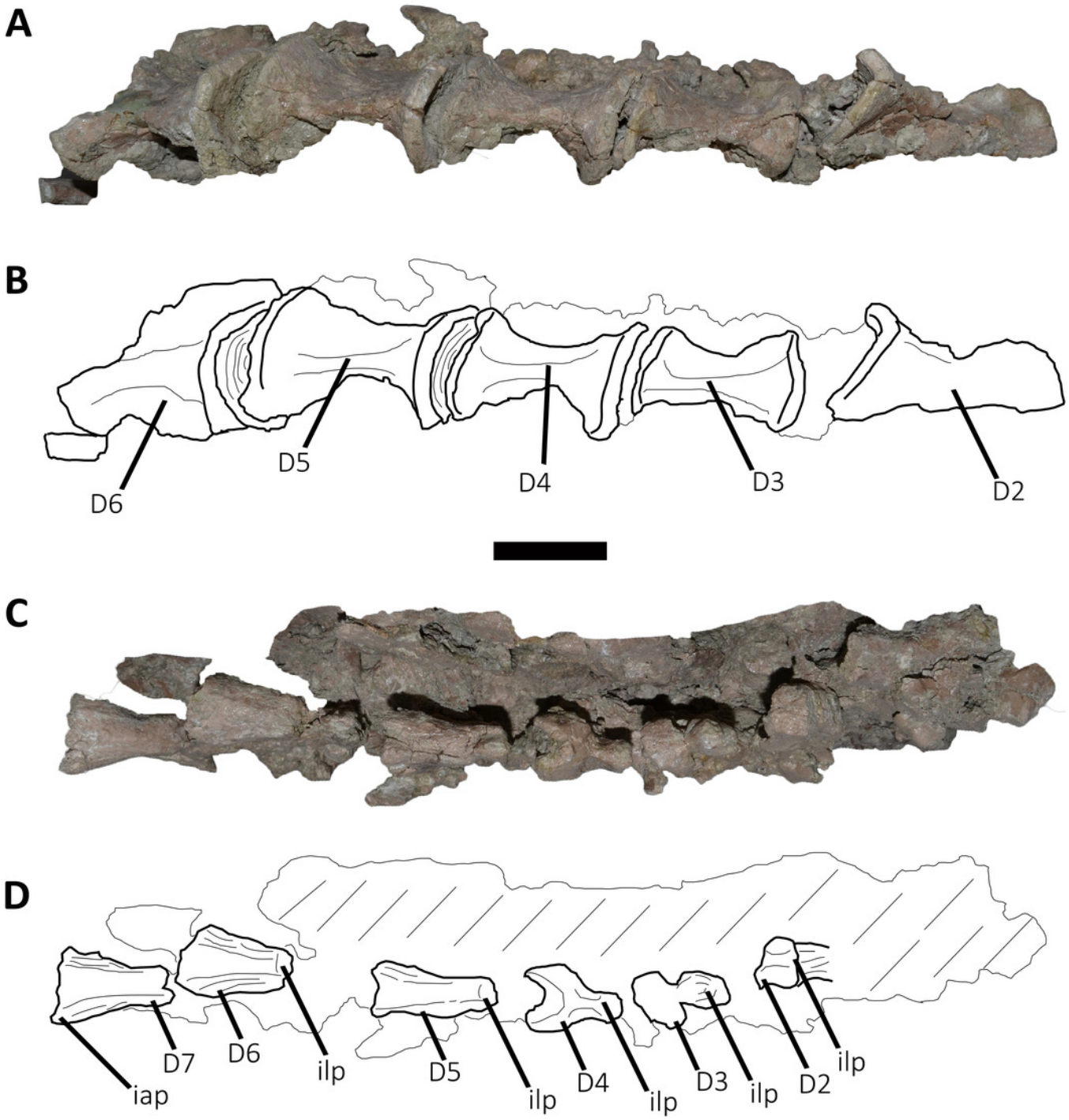
A
B
D6
D5
D4
D3
D2
C
D
iap
D7
D6
ilp
D5
ilp
D4
ilp
D3
ilp
D2
ilp

Figure 6

Posterior dorsal vertebrae of *Aucasaurus garridoi* MCF-PVPH-236.

In anterior (A, G), posterior (B, H), lateral (C, D, I, J), dorsal (E), and ventral (F, K) views. Abbreviations: ns, neural spine; pl, pleurocoel. Scale bar: 5 cm.

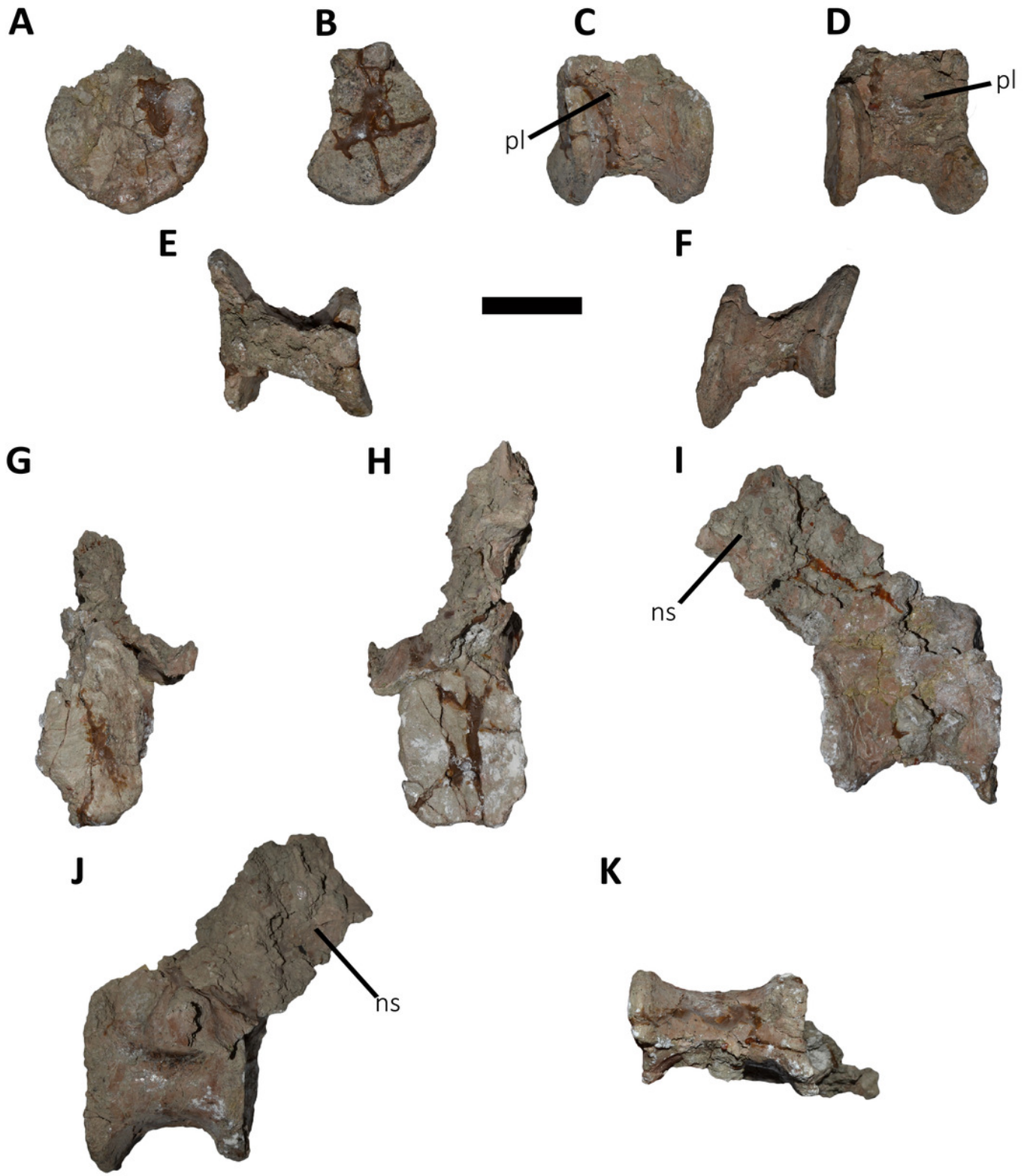
A
B
C
pl
D
pl
E
F
G
H
I
ns
J
ns
K

Figure 7

Distal fragments of dorsal neural spines of *Aucasaurus garridoi* MCF-PVPH-236.

In dorsal (A-C), and left lateral (D-F) views. Abbreviations: iap, interspinous accessory process; ilp, interspinous ligament process. Scale bar: 5 cm.

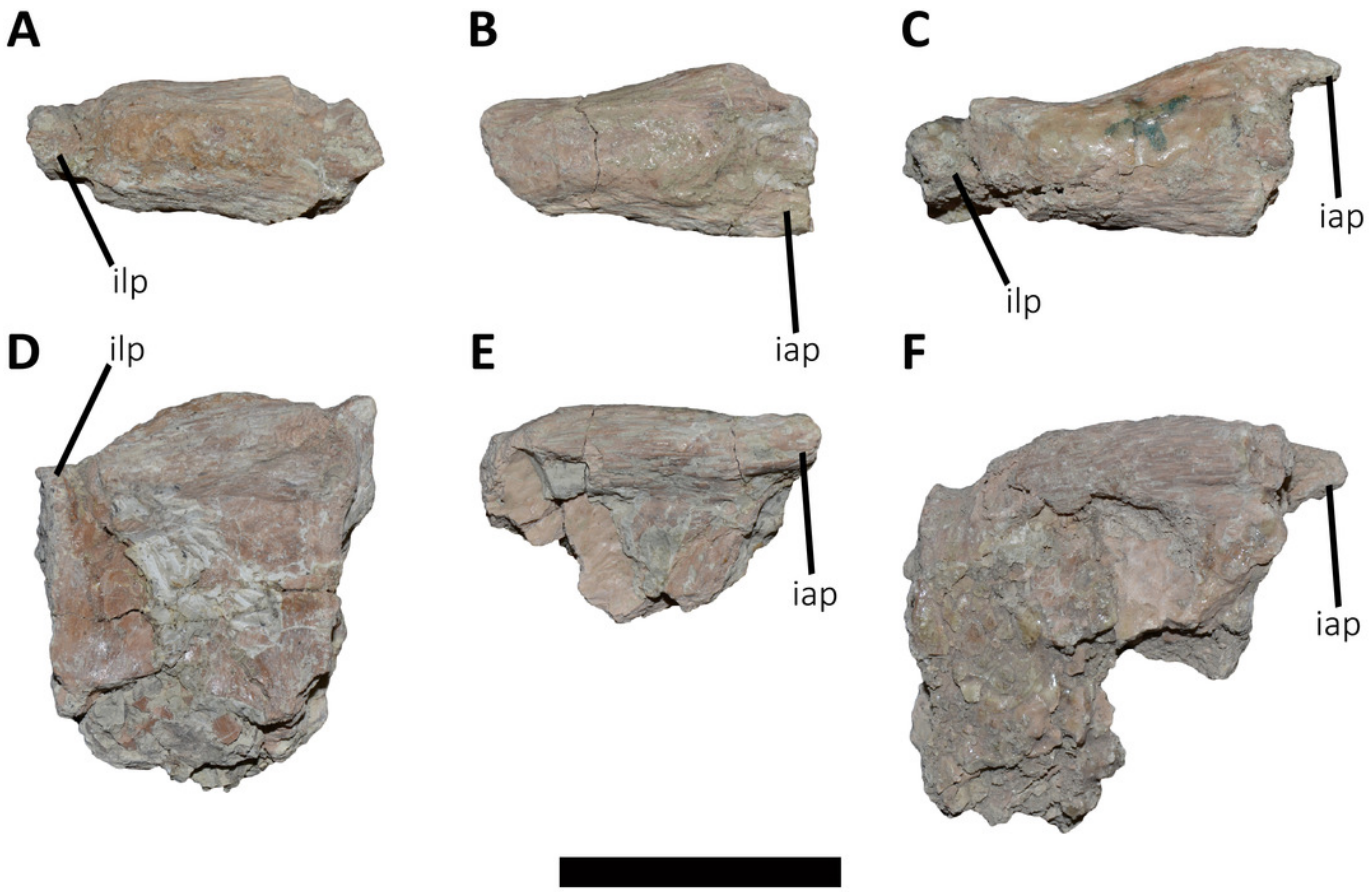

Figure 8

Sacrum of *Aucasaurus garridoi* MCF-PVPH-236.

In lateral (A, B), ventral (C), posterior (D), and dorsal (E, F) views. Colored dashed lines marking the anterior and posterior rims of the third to fifth transverse processes. Abbreviations: 1sc-6sc, first to sixth sacral centra; 4sr, fourth sacral rib; 1stp-5stp, first to fifth sacral transverse processes; IL, ilion; ns, neural spine. Scale bar: 10 cm.

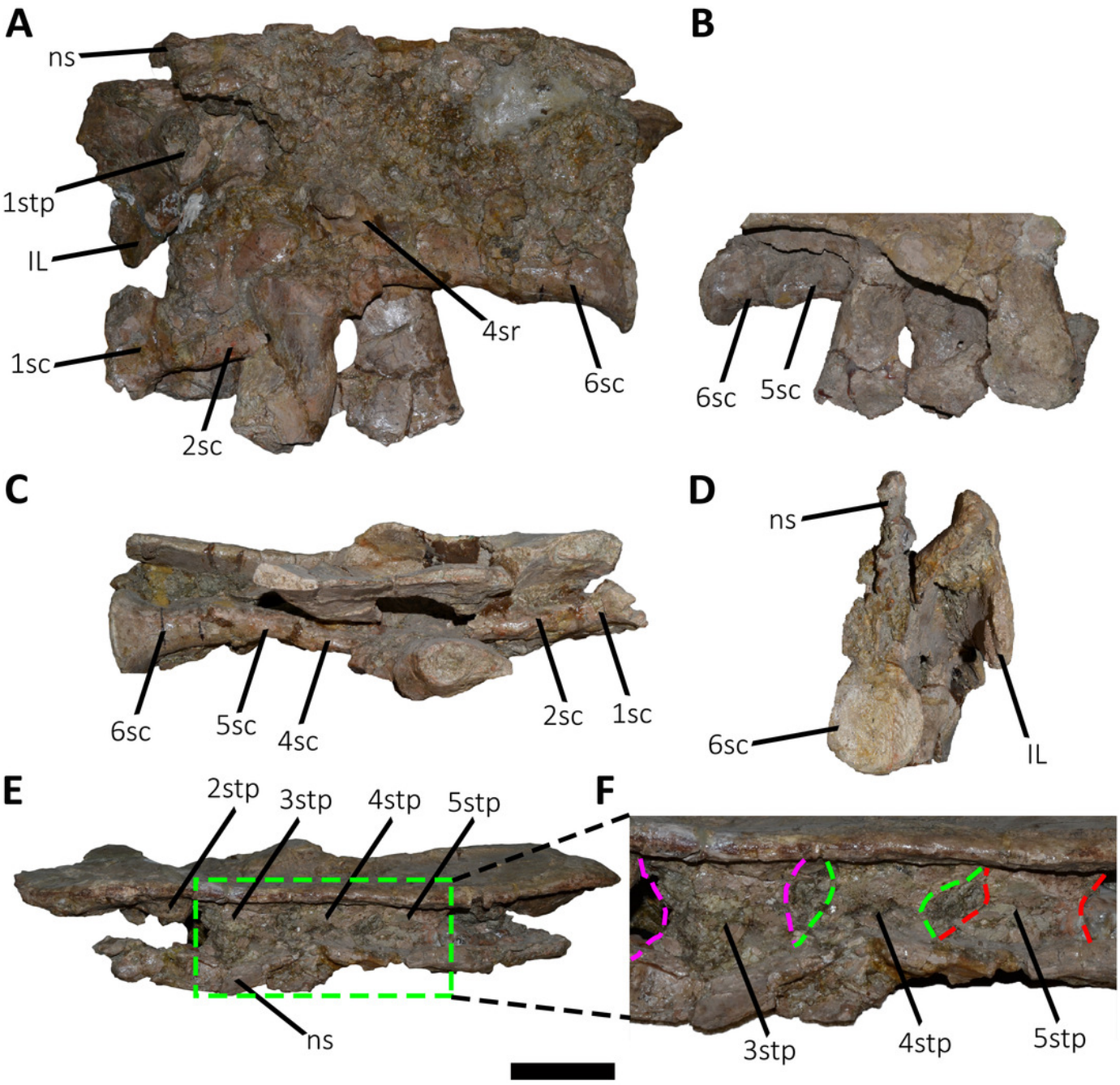
A
ns
1stp
lL
1sc
2sc
4sr
6sc
B
6sc
5sc
C
6sc
5sc
4sc
2sc
1sc
D
ns
6sc
lL
E
2stp
3stp
4stp
5stp
ns
F
3stp
4stp
5stp

Figure 9

First caudal vertebra of *Aucasaurus garridoi* MCF-PVPH-236.

In anterior (A), lateral (B, E), dorsal (C), posterior (D), and ventral (F) views. Abbreviations: acdl, anterior centrodiapophyseal lamina; apltp, anterior process of lateral transverse process; cdl, centrodiapophyseal lamina; dr, dorsal roughness; ha, hypantrum; hy, hyposphene; iap, interspinous accessory process; ldvc, lateral depression of vertebral centrum; lrcdl, lateral ridge of centrodiapophyseal lamina; nc, neural canal; ns, neural spine; pcdl, posterior centrodiapophyseal lamina; pf, pneumatic foramen; poz, postzygapophysis; prz, prezygapophysis; spof, spinopostzigapophyseal fossa; spol, spinopostzigapophyseal lamina; sprf, spinoprezigapophyseal fossa; tp, transverse process; vlrtp, ventrolateral ridge of the transverse process. Scale bar: 10 cm.

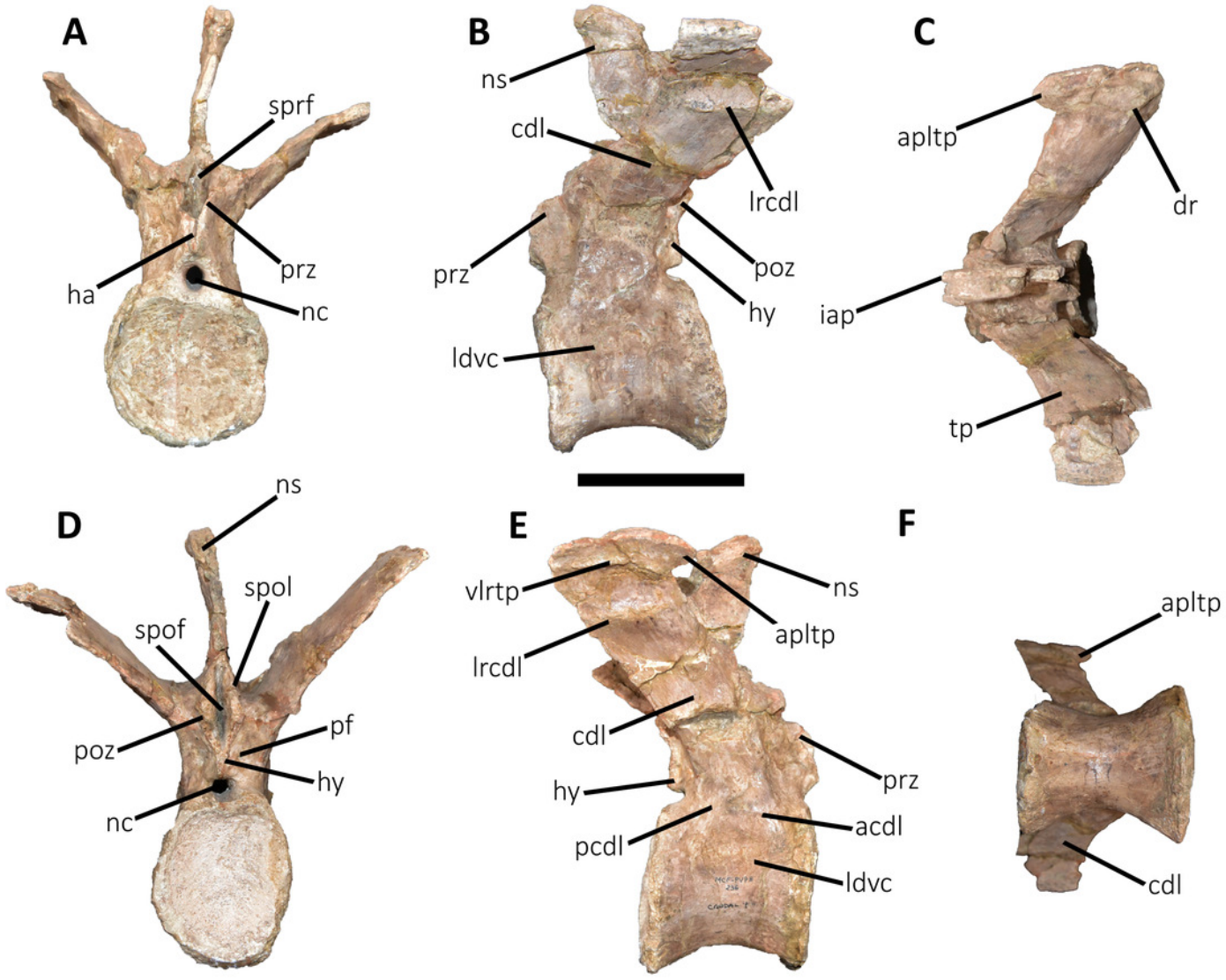
A
sprf
prz
ha
nc
B
ns
cdl
lrcdl
prz
poz
hy
ldvc
C
apltp
dr
iap
tp
D
ns
spol
spof
poz
pf
hy
nc
E
vlrtp
ns
apltp
lrcdl
cdl
prz
hy
acdl
pcdl
ldvc
F
apltp
cdl

Figure 10

Second caudal vertebra of *Aucasaurus garridoi* MCF-PVPH-236.

In anterior (A), lateral (B, E), dorsal (C), posterior (D), and ventral (F) views. Abbreviations: acdl, anterior centrodiapophyseal lamina; apltp, anterior process of lateral transverse process; cdl, centrodiapophyseal lamina; ha, hypantrum; haaf, haemal arch articular facet; hy, hyposphene; ldvc, lateral depression of vertebral centrum; lrcdl, lateral ridge of centrodiapophyseal lamina; nc, neural canal; ns, neural spine; pcdl, posterior centrodiapophyseal lamina; pf, pneumatic foramen; poz, postzygapophysis; ppltp, posterior process of lateral transverse process; prz, prezygapophysis; spof, spinopostzigapophyseal fossa; spol, spinopostzigapophyseal lamina; sprf, spinoprezigapophyseal fossa; tp, transverse process; vg, ventral groove; vlrtp, ventrolateral ridge of the transverse process. Scale bar: 10 cm.

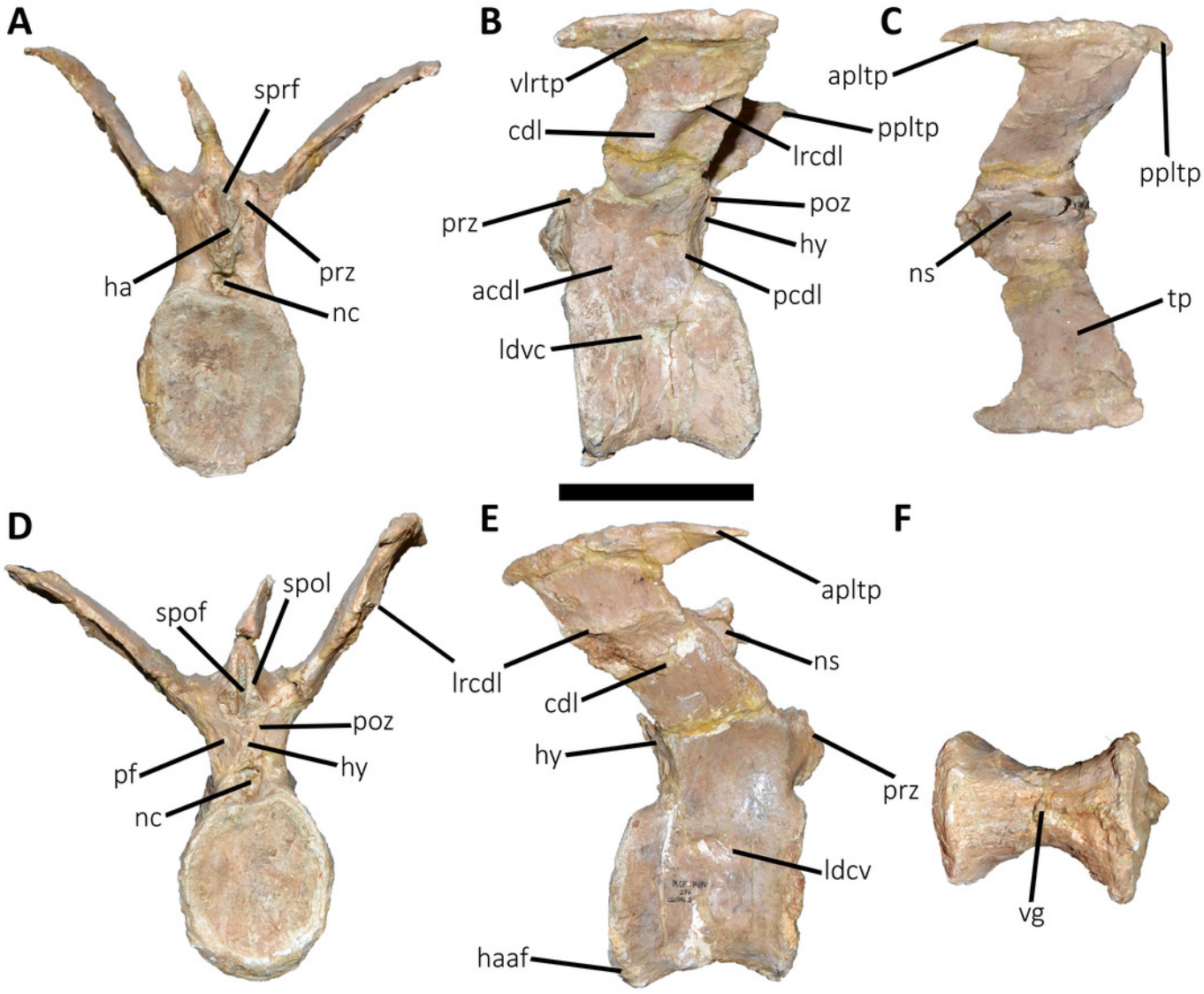
A
sprf
ha
prz
nc
B
vlrtp
cdl
lrcdl
prz
poz
hy
acdl
pcdl
ldvc
C
apltp
ppltp
ppltp
ns
tp
D
spol
spof
lrcdl
poz
pf
hy
nc
E
apltp
ns
lrcdl
cdl
hy
prz
ldcv
haaf
F
vg

Figure 11

Third caudal vertebra of *Aucasaurus garridoi* MCF-PVPH-236.

In anterior (A), lateral (B, E), dorsal (C), posterior (D), and ventral (F) views. Abbreviations: acdl, anterior centrodiapophyseal lamina; apltp, anterior process of lateral transverse process; cdf, centrodiapophyseal fossa; cdl, centrodiapophyseal lamina; dr, dorsal roughness; ha, hypantrum; haaf, haemal arch articular facet; hy, hyposphene; ldvc, lateral depression of vertebral centrum; lrcdl, lateral ridge of centrodiapophyseal lamina; lrtp, lateral rugosity of transverse process; nc, neural canal; ns, neural spine; pcdl, posterior centrodiapophyseal lamina; pocdf, postzygapophyseal centrodiapophyseal fossa; poz, postzygapophysis; prcdf, prezygapophyseal centrodiapophyseal fossa; prz, prezygapophysis; spof, spinopostzigapophyseal fossa; spol, spinopostzigapophyseal lamina; sprf, spinoprezigapophyseal fossa; vg, ventral groove; vlrtp, ventrolateral ridge of the transverse process. Scale bar: 10 cm.

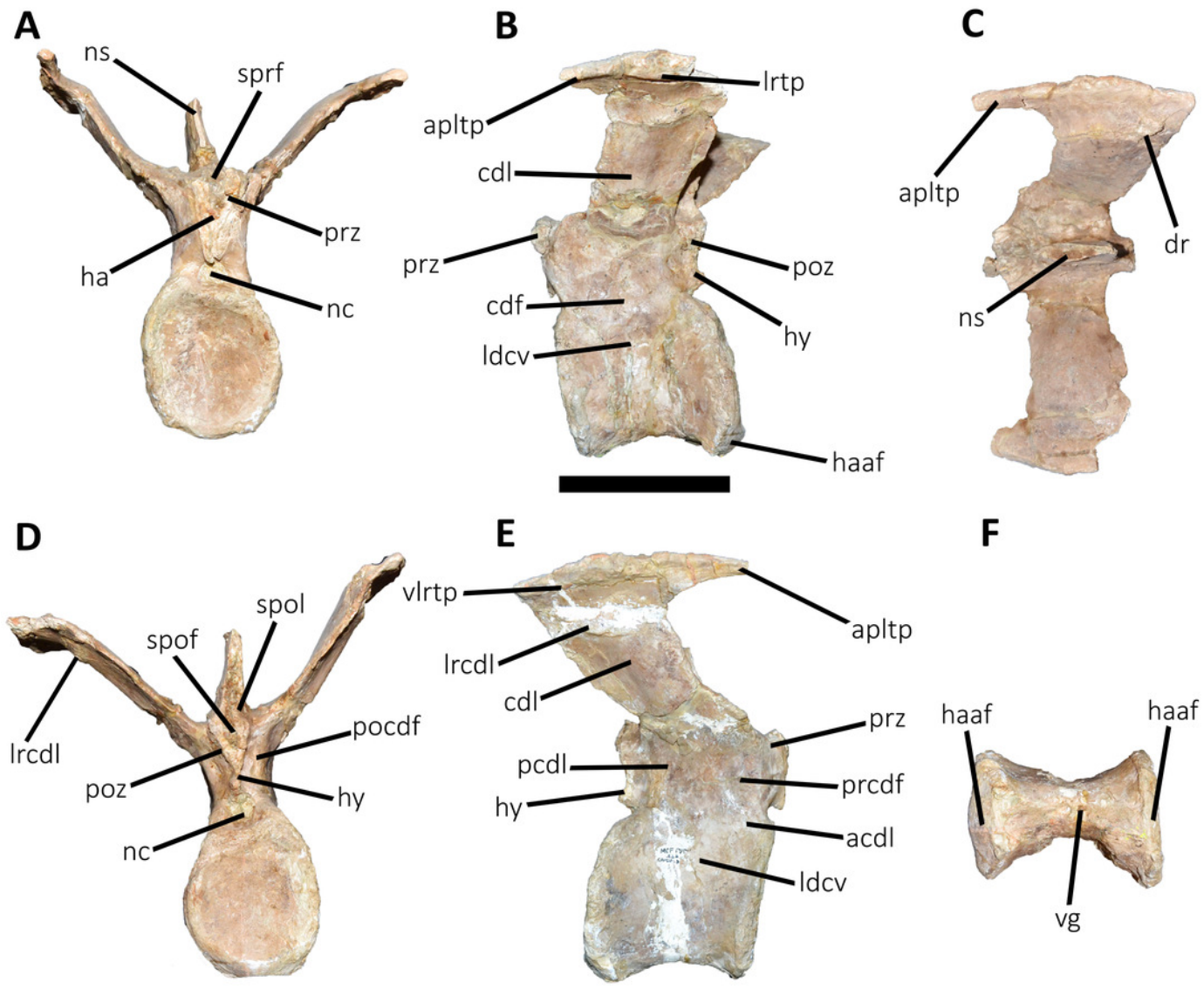
A
ns
sprf
prz
ha
nc
B
lrtp
apltp
cdl
prz
poz
cdf
hy
ldcv
haaf
C
apltp
dr
ns
D
spol
spof
pocdf
lrcdl
poz
hy
nc
E
vlrtp
apltp
lrcdl
cdl
prz
pcdl
prcdf
hy
acdl
ldcv
F
haaf
haaf
vg

Figure 12

Fourth caudal vertebra of *Aucasaurus garridoi* MCF-PVPH-236.

In anterior (A), lateral (B, E), dorsal (C), posterior (D), and ventral (F) views. Abbreviations: acdl, anterior centrodiapophyseal lamina; apltp, anterior process of lateral transverse process; cdf, centrodiapophyseal fossa; cdl, centrodiapophyseal lamina; dr, dorsal roughness; haaf, haemal arch articular facet; hy, hyposphene; ldvc, lateral depression of vertebral centrum; lrcdl, lateral ridge of centrodiapophyseal lamina; lrtp, lateral rugosity of transverse process; nc, neural canal; ns, neural spine; pcdl, posterior centrodiapophyseal lamina; pocdf, postzygapophyseal centrodiapophyseal fossa; poz, postzygapophysis; prcdf, prezygapophyseal centrodiapophyseal fossa; prz, prezygapophysis; spof, spinopostzigapophyseal fossa; spol, spinopostzigapophyseal lamina; sprf, spinoprezigapophyseal fossa; vg, ventral groove. Scale bar: 10 cm.

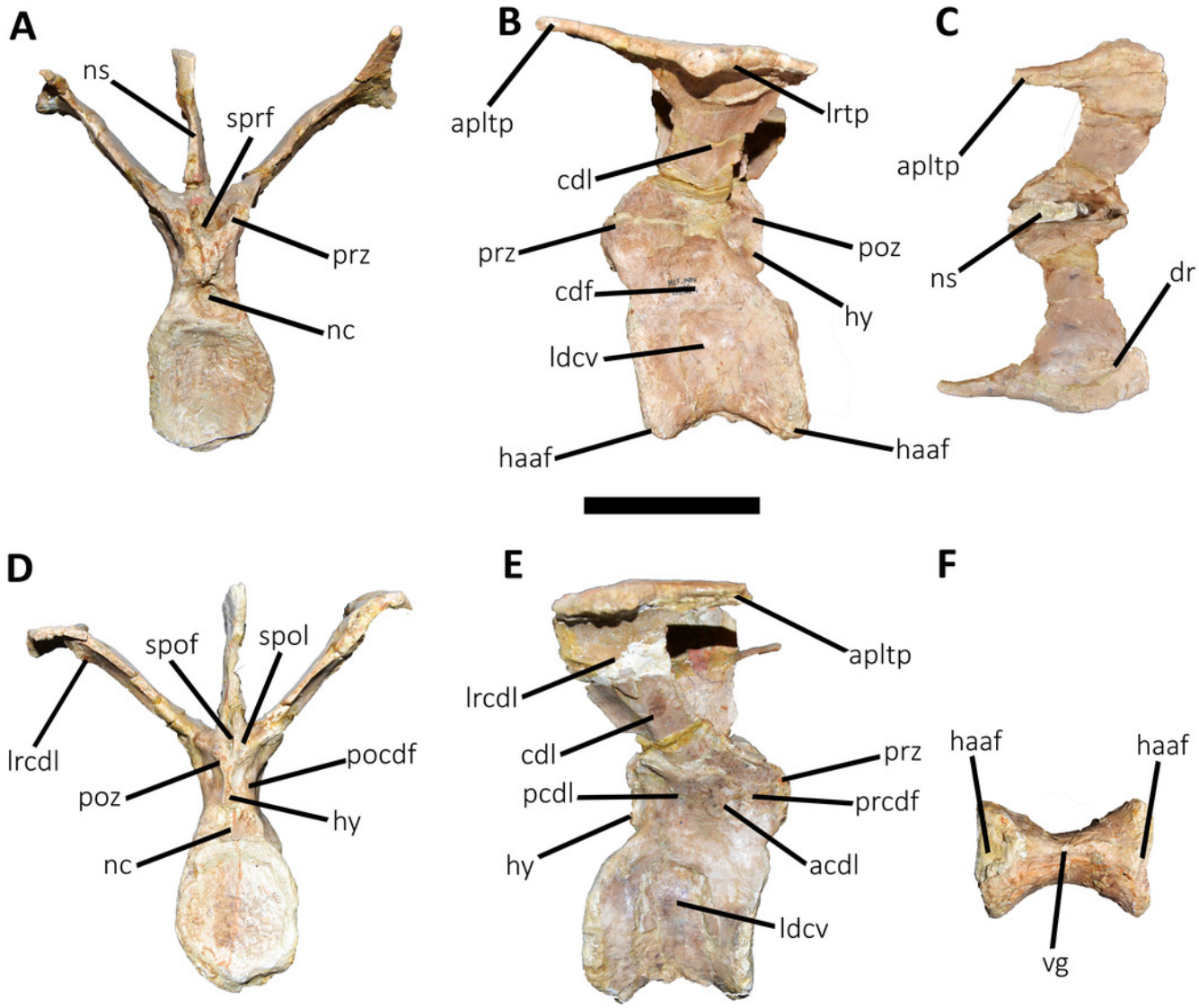
A
ns
sprf
prz
nc
B
apltp
lrtp
cdl
prz
poz
cdf
hy
ldcv
haaf
haaf
C
apltp
ns
dr
D
spof
spol
lrcdl
pocdf
poz
hy
nc
E
apltp
lrcdl
cdl
prz
pcdl
prcdf
hy
acdl
ldcv
F
haaf
haaf
vg

Figure 13

Fifth and sixth caudal vertebrae of *Aucasaurus garridoi* MCF-PVPH-236.

In anterior (A), lateral (B, E), dorsal (C), posterior (D), and ventral (F) views. Abbreviations: 5cv, fifth caudal vertebra; 6cv, sixth caudal vertebra; apltp, anterior process of lateral transverse process; cdl, centrodiapophyseal lamina; dr, dorsal roughness; ha, hypantrum; har, haemal arch; haaf, haemal arch articular facet; hy, hyposphene; iap; interspinous accessory process; lrcdl, lateral ridge of centrodiapophyseal lamina; lrtp, lateral rugosity of transverse process; nc, neural canal; ns, neural spine; pf, pneumatic foramen; poz, postzygapophysis; prcdf, prezygapophyseal centrodiapophyseal fossa; prz, prezygapophysis; spof, spinopostzigapophyseal fossa; spol, spinopostzigapophyseal lamina; sprf, spinoprezigapophyseal fossa; tp, transverse process; vg, ventral groove; vlrtp, ventrolateral ridge of the transverse process. Scale bar: 10 cm.

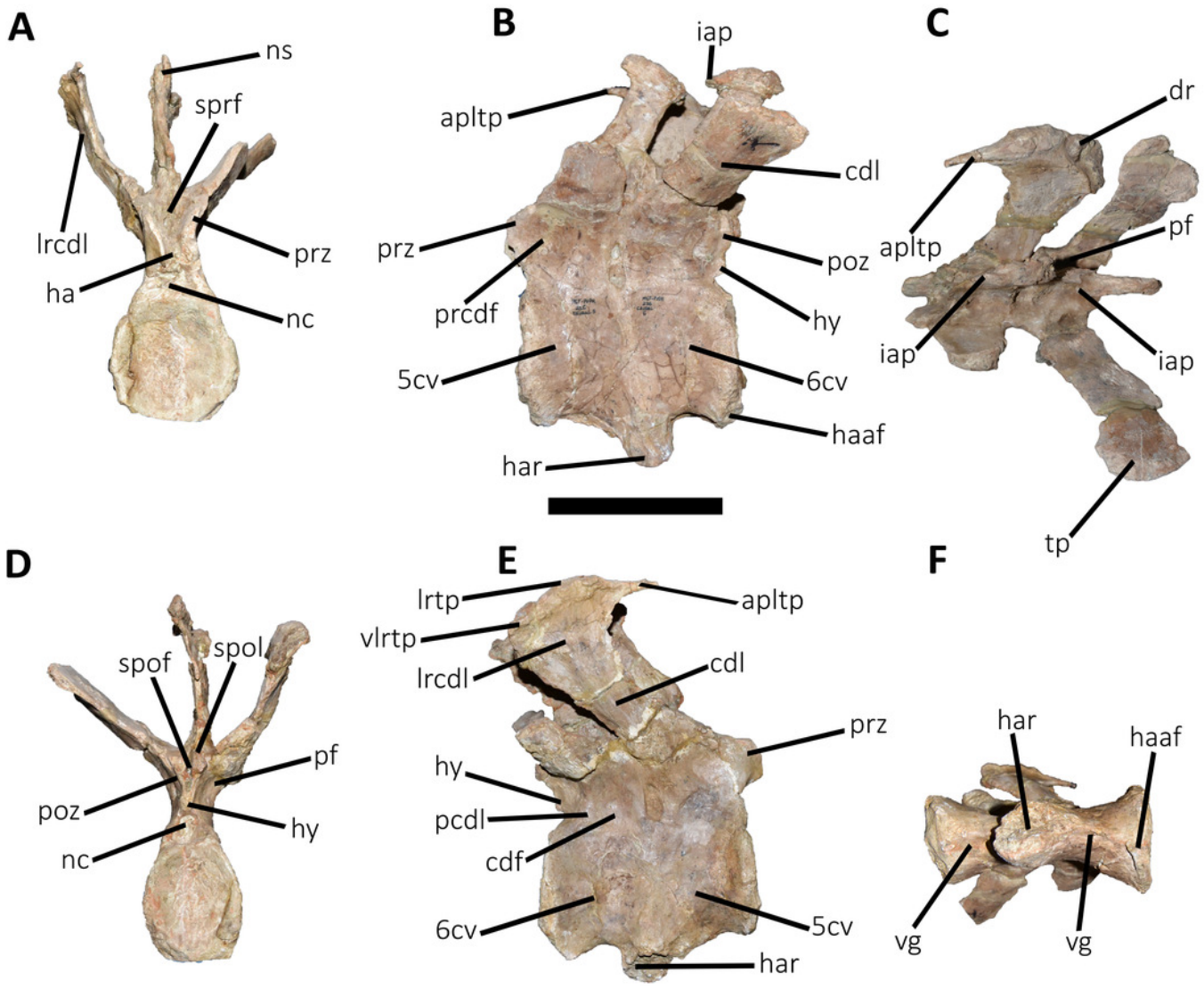
A
ns
sprf
lrcdl
prz
ha
nc
B
iap
apltp
cdl
prz
poz
prcdf
hy
5cv
6cv
haaf
har
C
dr
apltp
pf
iap
iap
tp
D
spof
spol
pf
poz
hy
nc
E
lrtp
apltp
vlrtp
lrcdl
cdl
prz
hy
pcdl
cdf
6cv
5cv
har
F
har
haaf
vg
vg

Figure 14

Seventh caudal vertebra of *Aucasaurus garridoi* MCF-PVPH-236.

In anterior (A), lateral (B, E), dorsal (C), posterior (D), and ventral (F) views. Abbreviations: acdl, anterior centrodiapophyseal lamina; apltp, anterior process of lateral transverse process; cdf, centrodiapophyseal fossa; cdl, centrodiapophyseal lamina; dr, dorsal roughness; ha, hypantrum; haaf, haemal arch articular facet; hy, hyposphene; iap; interspinous accessory process; lrcdl, lateral ridge of centrodiapophyseal lamina; lrtp, lateral rugosity of transverse process; nc, neural canal; ns, neural spine; pcdl, posterior centrodiapophyseal lamina; pf, pneumatic foramen; poz, postzygapophysis; prcdf, prezygapophyseal centrodiapophyseal fossa; prz, prezygapophysis; spof, spinopostzigapophyseal fossa; sprf, spinoprezigapophyseal fossa; sprl, spinoprezigapophyseal lamina; vg, ventral groove. Scale bar: 10 cm.

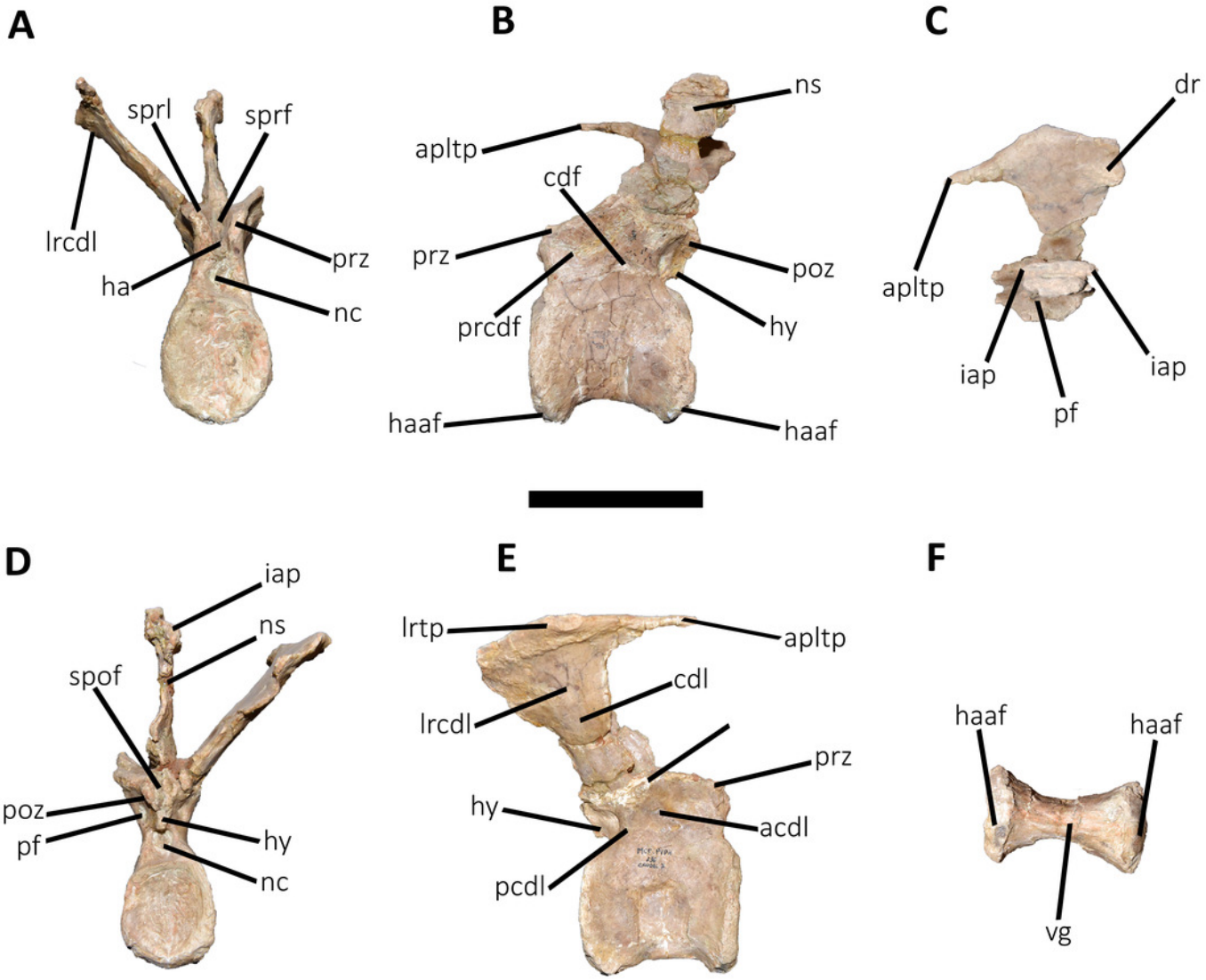
A
sprl
sprf
lrcdl
prz
ha
nc
B
ns
apltp
cdf
prz
poz
prcdf
hy
haaf
haaf
C
dr
apltp
iap
iap
pf
D
iap
ns
spof
poz
pf
hy
nc
E
lrtp
apltp
cdl
lrcdl
prz
hy
acdl
pcdl
F
haaf
haaf
vg

Figure 15

Eighth caudal vertebra of *Aucasaurus garridoi* MCF-PVPH-236.

In anterior (A), lateral (B, E), dorsal (C), posterior (D), and ventral (F) views. Abbreviations: apbns, anterior process of basal neural spine; apltp, anterior process of lateral transverse process; cdl, centrodiapophyseal lamina; dr, dorsal roughness; haaf, haemal arch articular facet; hy, hyposphene; lrcdl, lateral ridge of centrodiapophyseal lamina; lrtp, lateral rugosity of transverse process; nc, neural canal; ns, neural spine; pocdf, postzygapophyseal centrodiapophyseal fossa; poz, postzygapophysis; prcdf, prezygapophyseal centrodiapophyseal fossa; prz, prezygapophysis; spof, spinopostzigapophyseal fossa; spol, spinopostzigapophyseal lamina; sprf, spinoprezigapophyseal fossa; sprl, spinoprezigapophyseal lamina; vg, ventral groove. Scale bar: 10 cm.

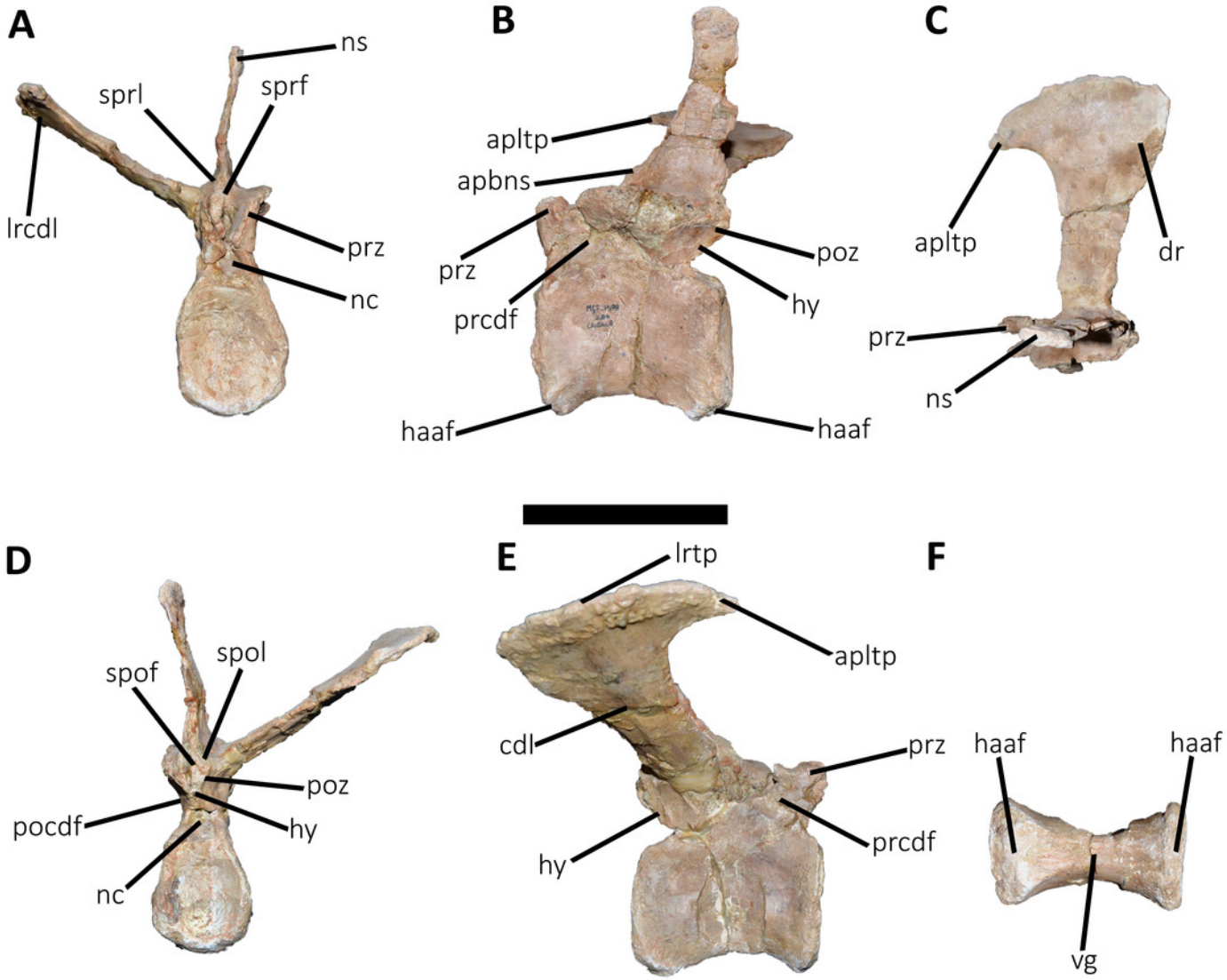
A
ns
sprl
sprf
lrcdl
prz
nc
B
apltp
apbns
prz
poz
prcdf
hy
haaf
haaf
C
apltp
dr
prz
ns
D
spof
spol
poz
pocdf
hy
nc
E
lrtp
apltp
cdl
prz
prcdf
hy
F
haaf
haaf
vg

Figure 16

Ninth caudal vertebra of *Aucasaurus garridoi* MCF-PVPH-236.

In anterior (A), lateral (B, E), dorsal (C), posterior (D), and ventral (F) views. Abbreviations: apltp, anterior process of lateral transverse process; cdl, centrodiapophyseal lamina; haaf, haemal arch articular facet; hy, hyposphene; lrtp, lateral rugosity of transverse process; nc, neural canal; ns, neural spine; pf, pneumatic foramen; pocdf, postzygapophyseal centrodiapophyseal fossa; poz, postzygapophysis; prcdf, prezygapophyseal centrodiapophyseal fossa; prz, prezygapophysis; spof, spinopostzigapophyseal fossa; spol, spinopostzigapophyseal lamina; sprf, spinoprezigapophyseal fossa; sprl, spinoprezigapophyseal lamina; vg, ventral groove. Scale bar: 10 cm.

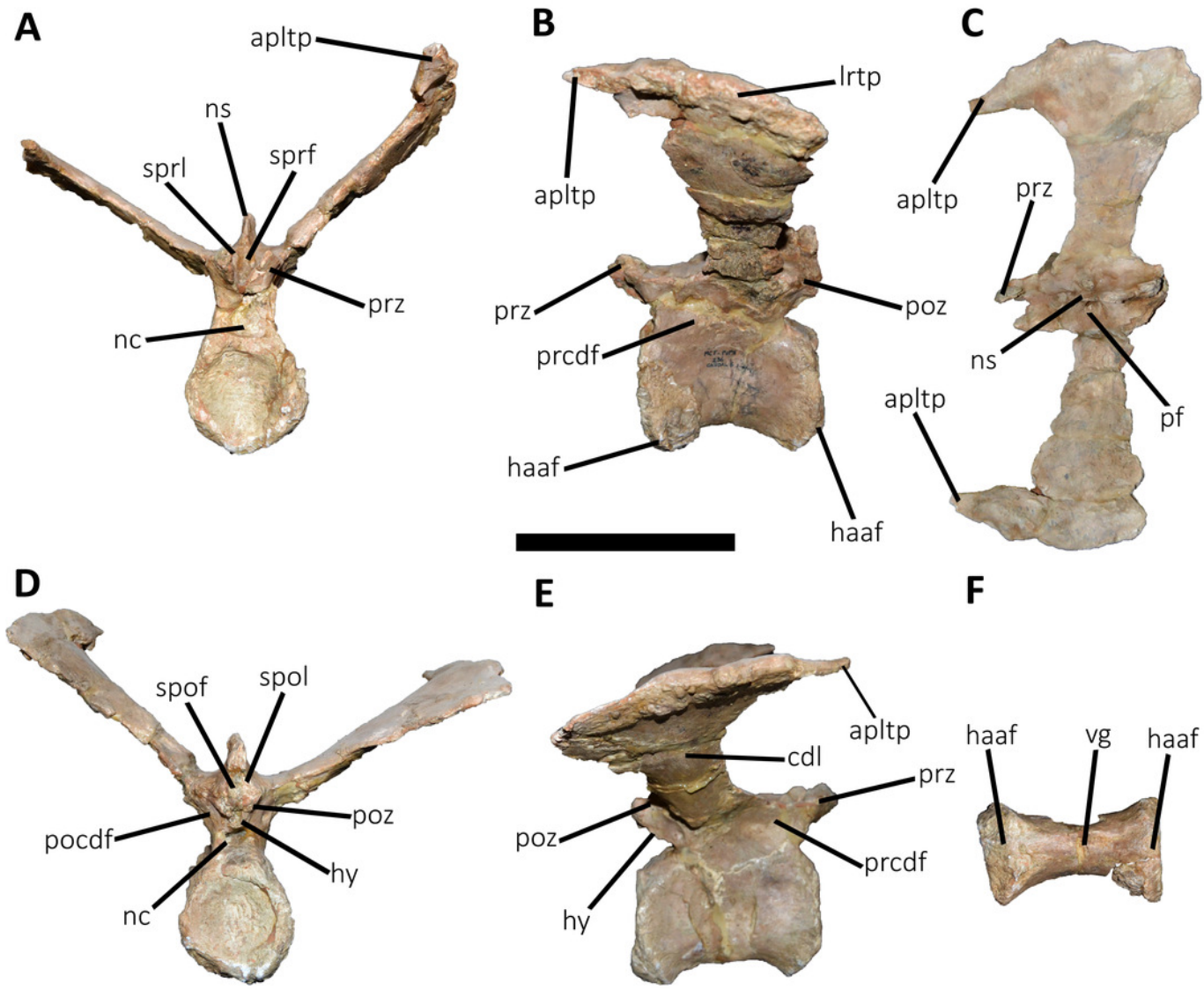
A
apltp
ns
sprl
sprf
prz
nc
B
lrtp
apltp
prz
poz
prcdf
haaf
haaf
C
apltp
prz
ns
pf
apltp
D
spof
spol
pocdf
poz
hy
nc
E
apltp
cdl
prz
poz
prcdf
hy
F
haaf
vg
haaf

Figure 17

Tenth caudal vertebra of *Aucasaurus garridoi* MCF-PVPH-236.

In anterior (A), lateral (B, E), dorsal (C), posterior (D), and ventral (F) views. Abbreviations: apltp, anterior process of lateral transverse process; cdl, centrodiapophyseal lamina; dr, dorsal roughness; haaf, haemal arch articular facet; lrcdl, lateral ridge of centrodiapophyseal lamina; lrtp, lateral rugosity of transverse process; nc, neural canal; ns, neural spine; pf, pneumatic foramen; prcdf, prezygapophyseal centrodiapophyseal fossa; prz, prezygapophysis; sprf, spinoprezigapophyseal fossa. Scale bar: 10 cm.

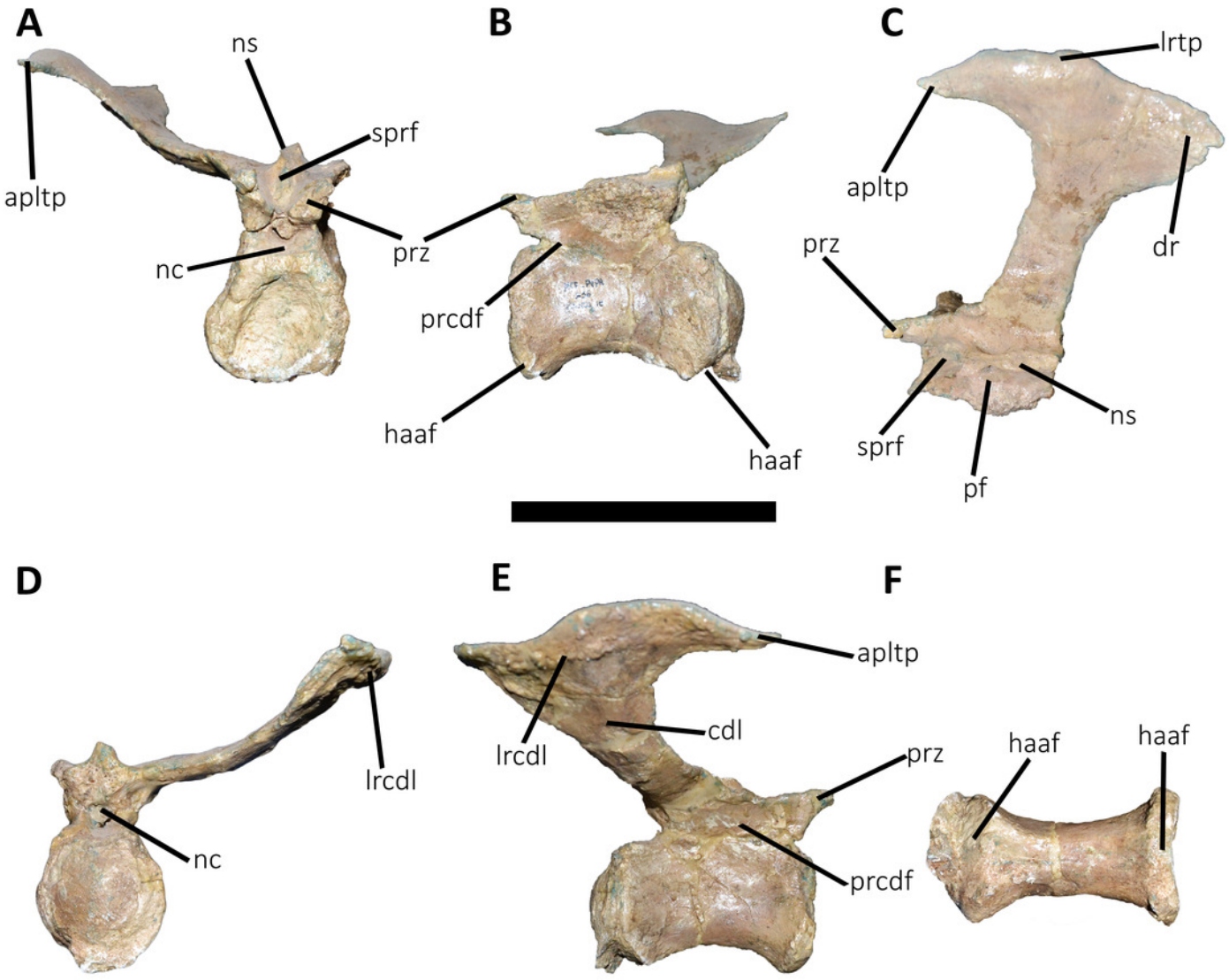
A
ns
sprf
apltp
nc
prz
B
prcdf
haaf
haaf
C
lrtp
apltp
dr
prz
ns
sprf
pf
D
lrcdl
nc
E
apltp
cdl
lrcdl
prz
prcdf
F
haaf
haaf

Figure 18

Eleventh caudal vertebra of *Aucasaurus garridoi* MCF-PVPH-236.

In anterior (A), lateral (B, E), dorsal (C), posterior (D), and ventral (F) views. Abbreviations: apltp, anterior process of lateral transverse process; dr, dorsal roughness; haaf, haemal arch articular facet; lrtp, lateral rugosity of transverse process; nc, neural canal; ns, neural spine; pf, pneumatic foramen; poz, postzygapophysis; prz, prezygapophysis; vg, ventral groove. Scale bar: 10 cm.

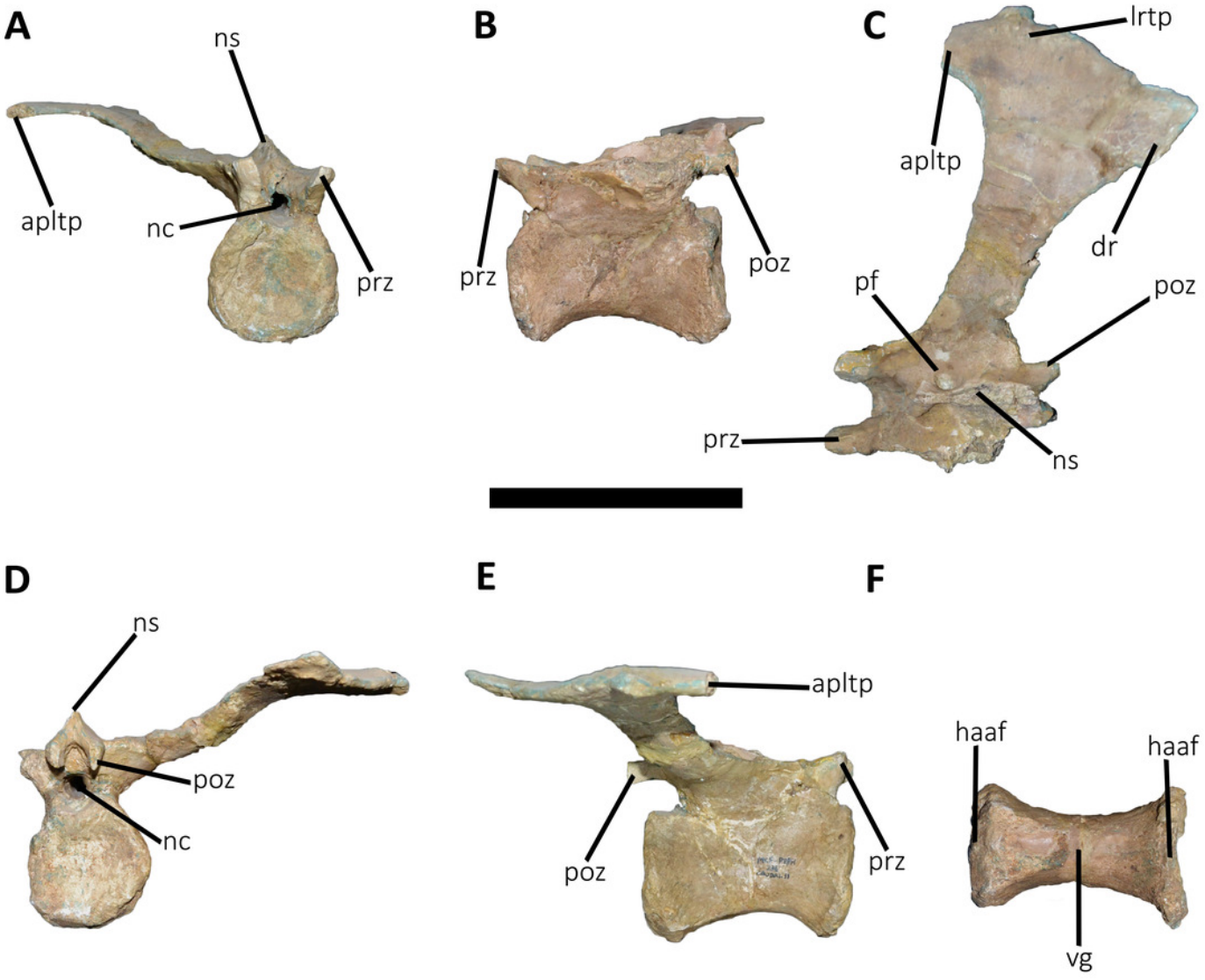

Figure 19

Twelfth and thirteenth caudal vertebrae of *Aucasaurus garridoi* MCF-PVPH-236.

In anterior (A), lateral (B, E), dorsal (C), posterior (D), and ventral (F) views. Abbreviations: 12cv, twelfth posterior vertebra; 13cv, thirteenth posterior vertebra; apltp, anterior process of lateral transverse process; dr, dorsal roughness; haaf, haemal arch articular facet; ltprz, lateral tubercle of prezygapophysis; lrtp, lateral rugosity of transverse process; nc, neural canal; ns, neural spine; poz, postzygapophysis; prz, prezygapophysis; vg, ventral groove. Scale bar: 10 cm.

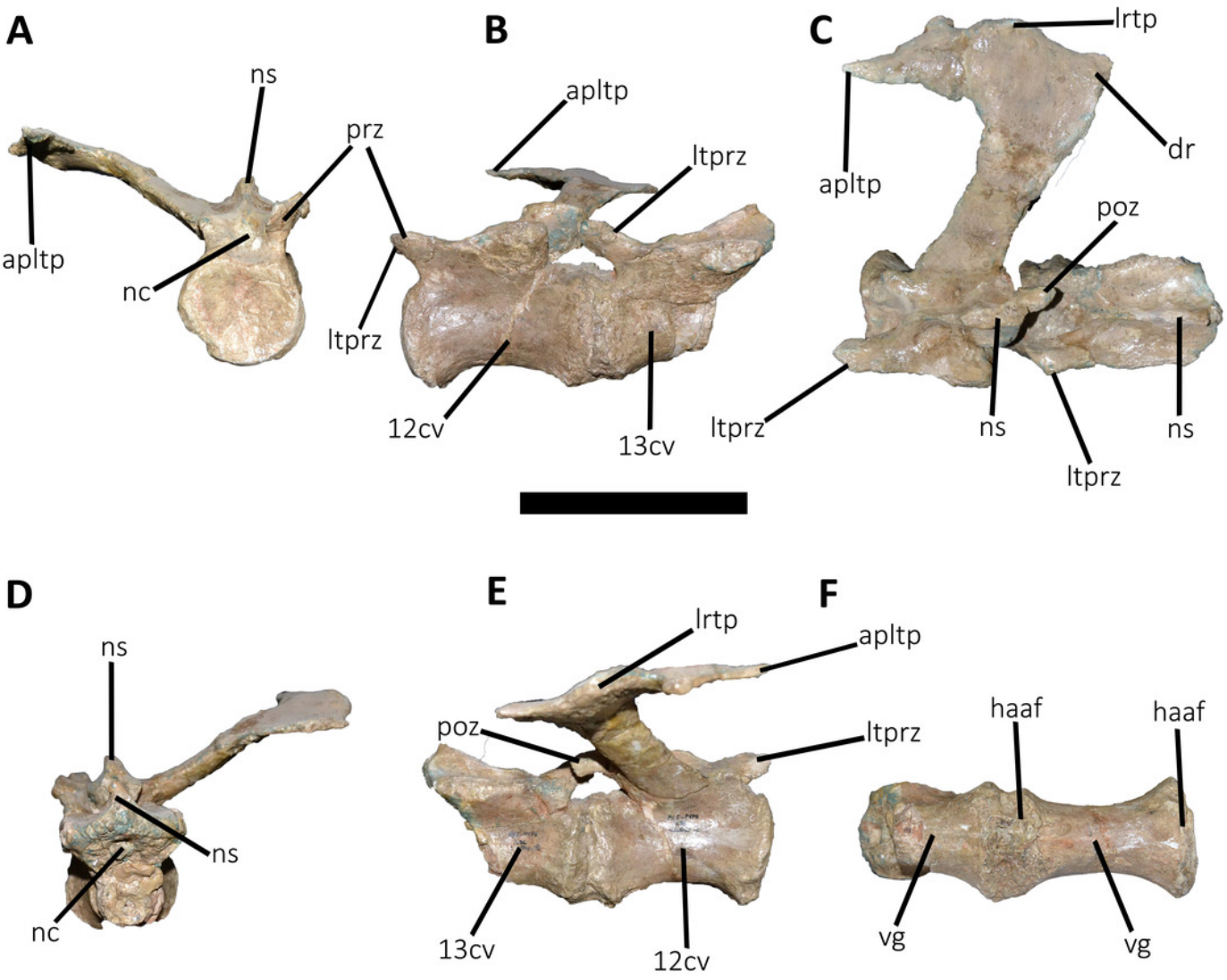
A
ns
prz
apltp
nc
B
apltp
ltprz
ltprz
12cv
13cv
C
lrtp
dr
apltp
poz
ltprz
ns
ns
ltprz
D
ns
ns
nc
E
lrtp
apltp
poz
ltprz
13cv
12cv
F
haaf
haaf
vg
vg

Figure 20

Caudal neural spines of *Aucasaurus garridoi* MCF-PVPH-236.

In lateral (A, B) and dorsal (C, D) views. Abbreviations: iap; interspinous accessory process. Scale bar: 5 cm.

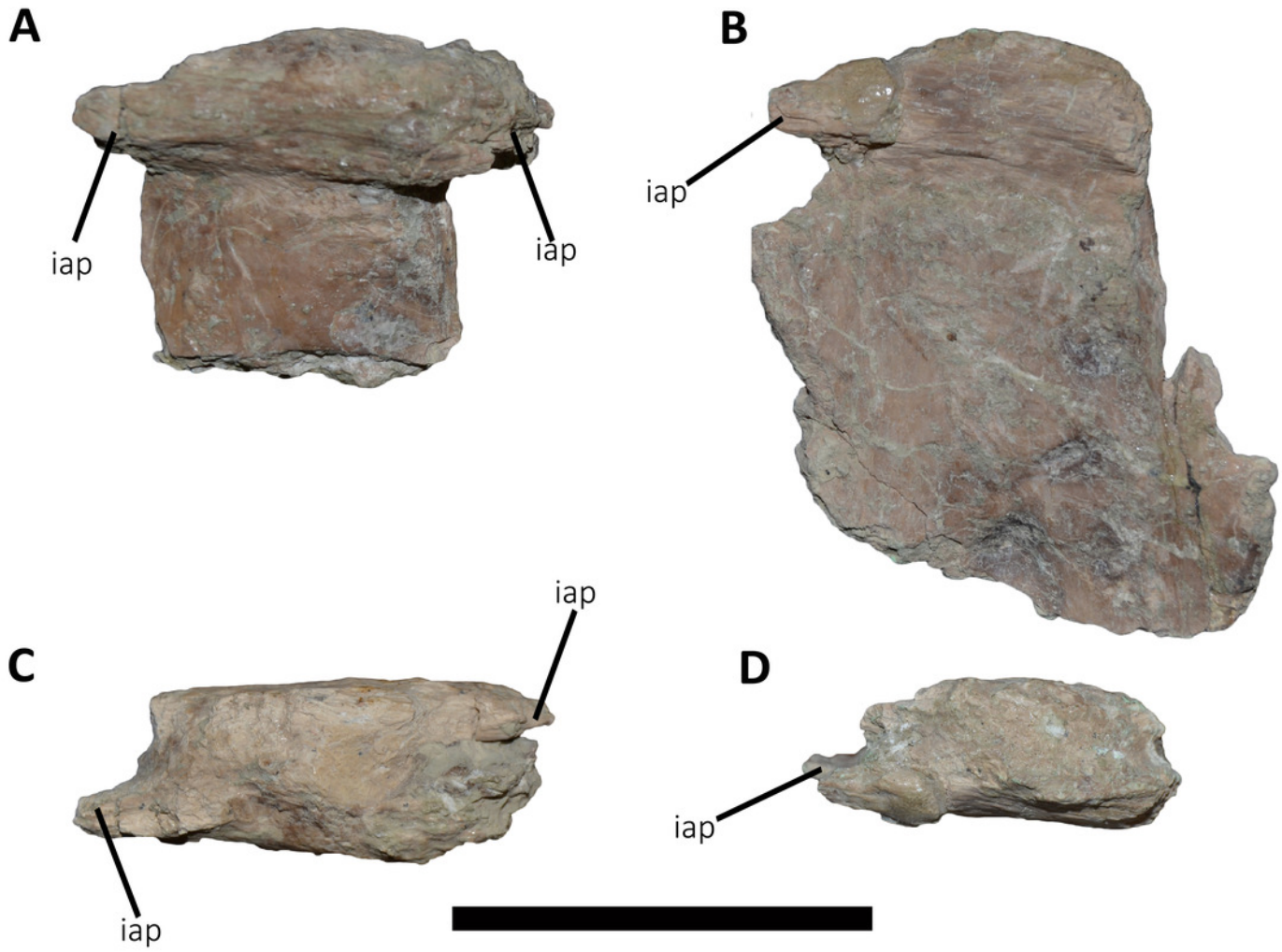

Figure 21

Caudal transverse processes of *Aucasaurus garridoi* MCF-PVPH-236.

In dorsal (A, B) and ventral (C, D) views. Abbreviations: apltp, anterior process of lateral transverse process; cdl, centrodiapophyseal lamina; dr, dorsal roughness; lrcdl, lateral ridge of centrodiapophyseal lamina; lrtp, lateral rugosity of transverse process. Scale bar: 5 cm.

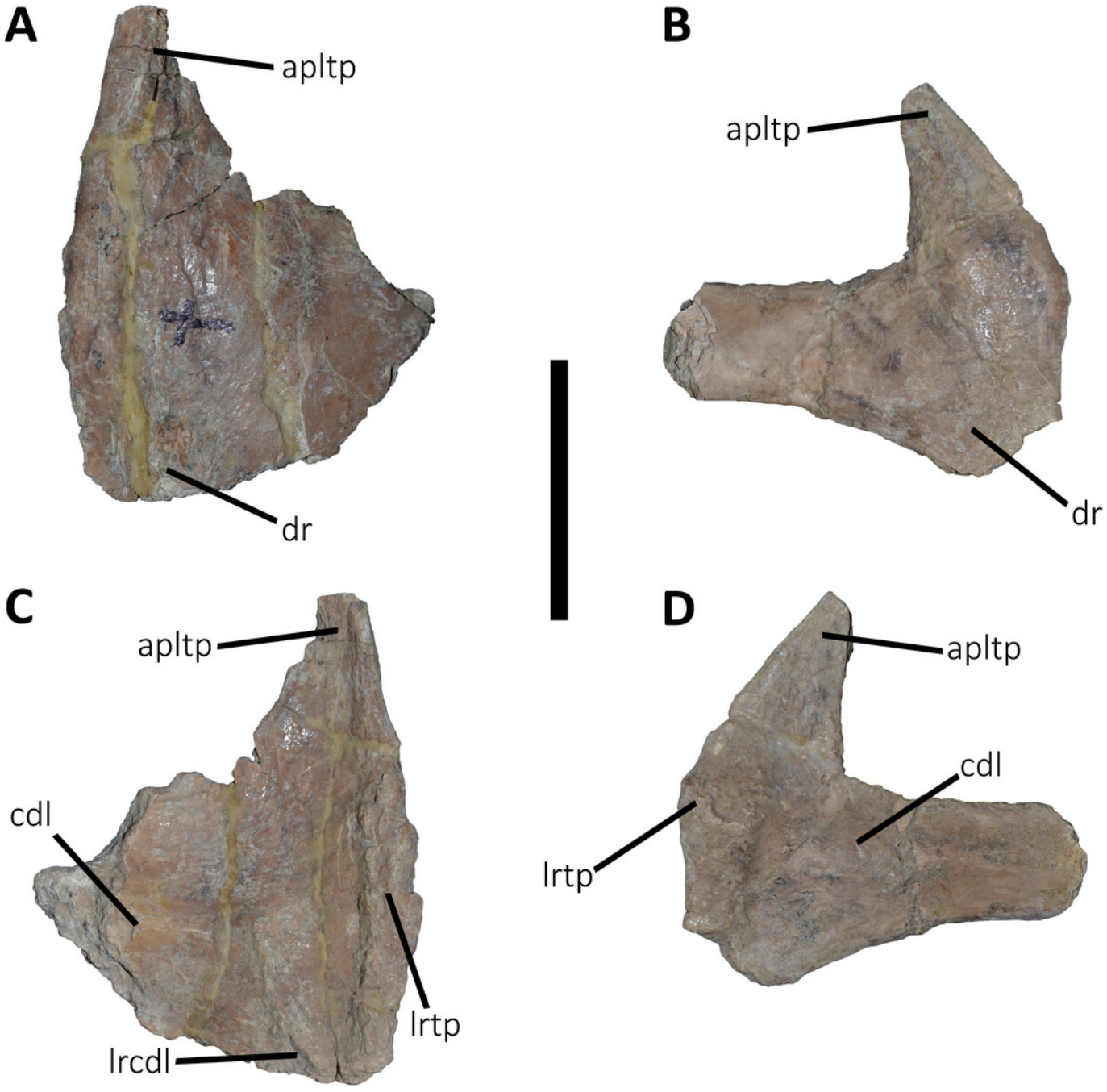
A
apltp
dr
B
apltp
dr
C
apltp
cdl
lrtp
lrcdl
D
apltp
cdl
lrtp

Figure 22

Proximal fragments of two cervical ribs of *Aucasaurus garridoi* MCF-PVPH-23.

In lateral (A, B) views. Abbreviations: alp, anterolateral process; cap, capitulum; dlp, dorsolateral process; tub, tuberculum. Scale bar: 5 cm.

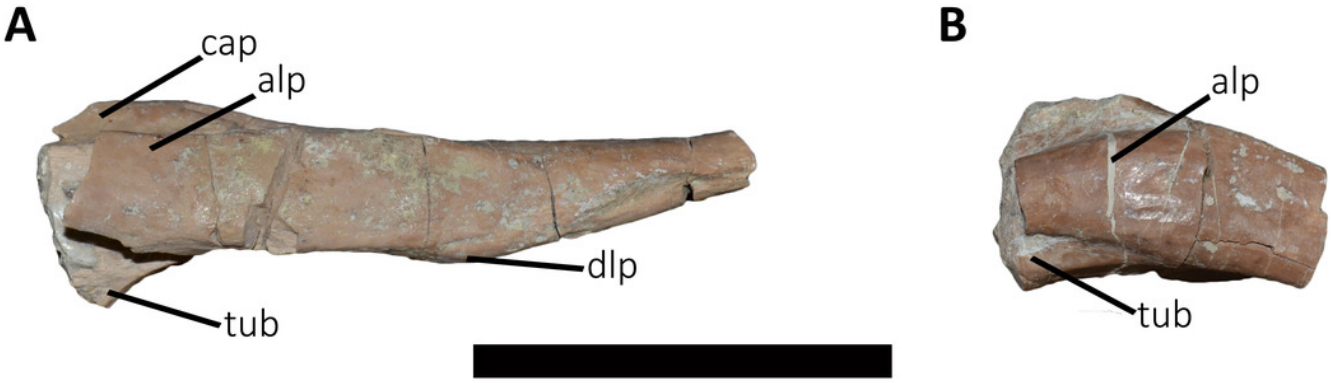

Figure 23

Fragments of dorsal ribs of *Aucasaurus garridoi* MCF-PVPH-236.

In lateral (A, C-G) and medial (B) views. Abbreviations: cap, capitulum; ctw, capitotuberculum web; der, distal expansion of rib; drcap, distal ridge of capitulum; ir, intercostal ridge; tub, tuberculum. Scale bar: 5 cm.

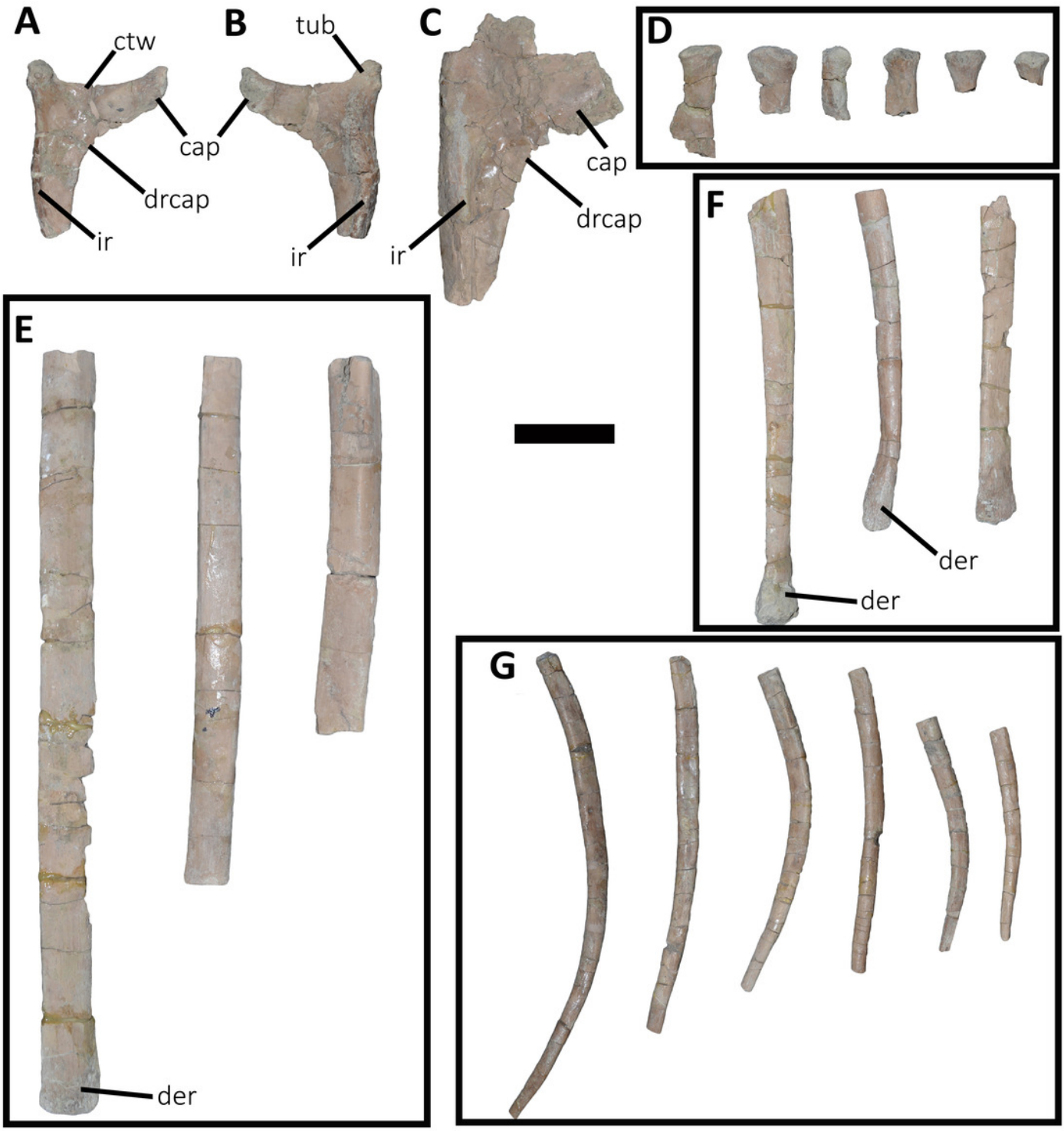
A
ctw
cap
drcap
ir
B
tub
ir
C
cap
drcap
ir
D
E
der
F
der
der
G

Figure 24

Gastralia of *Aucasaurus garridoi* MCF-PVPH-236.

In ventral (A, C, D) and dorsal (B) views. Abbreviations: dpg, distal process of gastralia; g, groove; mfg, medial fusion of gastralia; mpg, medial process of the gastralium. Scale bar: 5 cm.

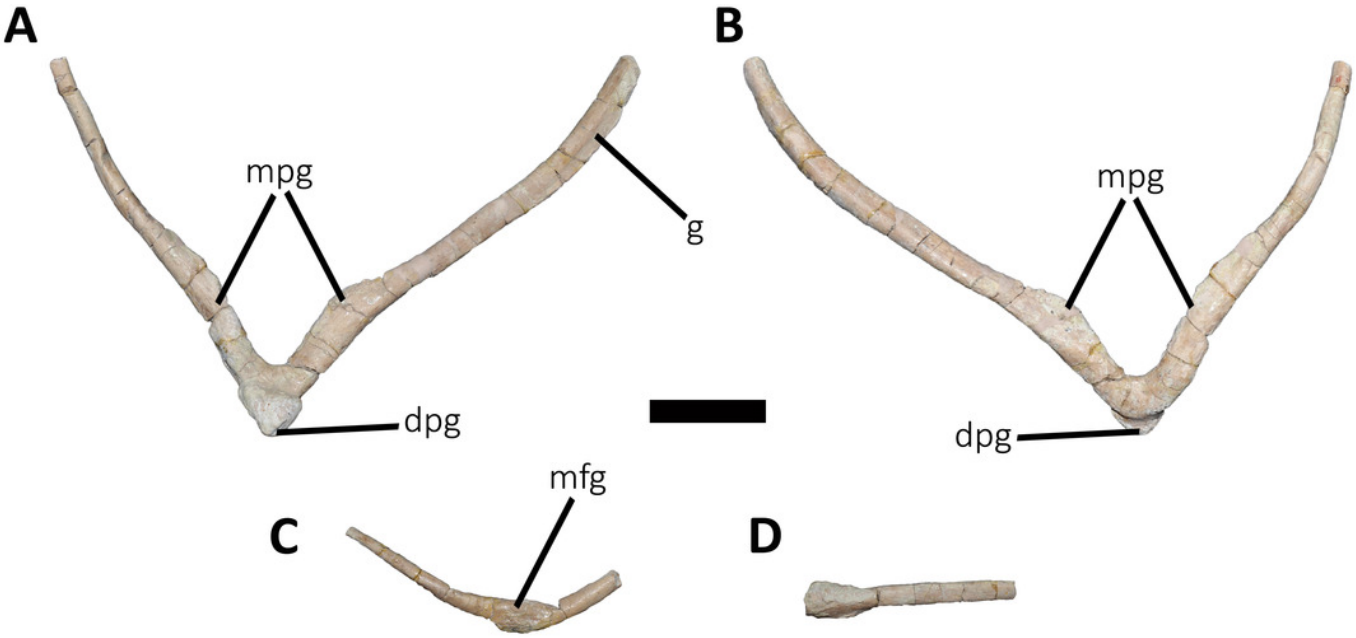

Figure 25

First to eighth haemal arches of *Aucasaurus garridoi* MCF-PVPH-236.

In anterior (A-H), posterior (A1-H1), and lateral (A2-H2; A3-H3) views. Abbreviations: afcc, articular facet for the caudal centrum; arha, anterior ridge of haemal arch; hc, haemal canal; pgha, posterior groove of the haemal arch; prha, posterior ridge of the haemal arch. Scale bar: 5 cm.

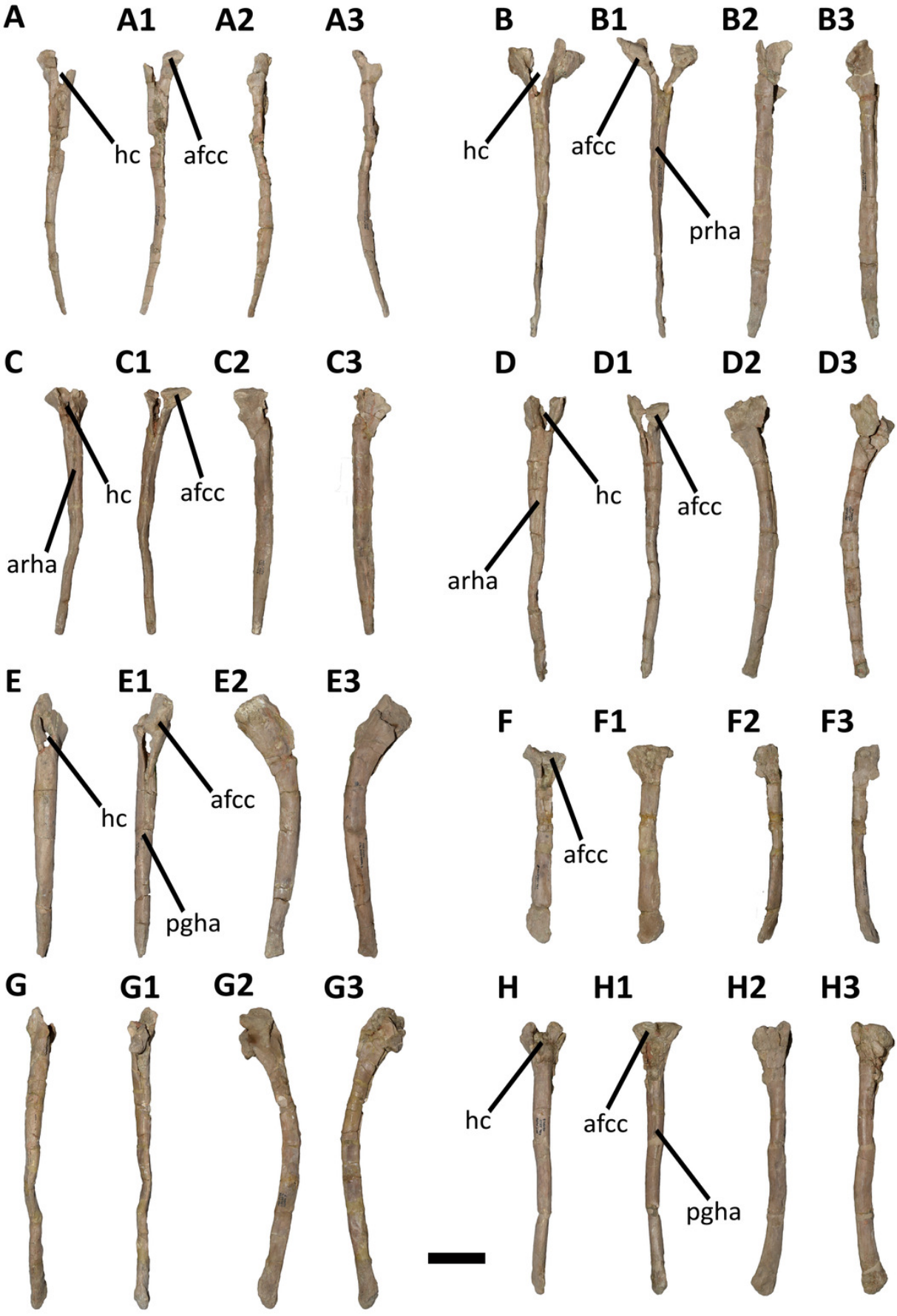
A
A1
A2
A3
hc
afcc
B
B1
B2
B3
hc
afcc
prha
C
C1
C2
C3
hc
afcc
arha
D
D1
D2
D3
hc
afcc
arha
E
E1
E2
E3
hc
afcc
pgha
F
F1
F2
F3
afcc
G
G1
G2
G3
H
H1
H2
H3
hc
afcc
pgha

Figure 26

Ninth to thirteenth haemal arches of *Aucasaurus garridoi* MCF-PVPH-236.

In anterior (A-E), posterior (A1-E1), and lateral (A2-E2; A3-E3) views. Abbreviations: hc, haemal canal; pgha, posterior groove of the haemal arc. Scale bar: 5 cm.

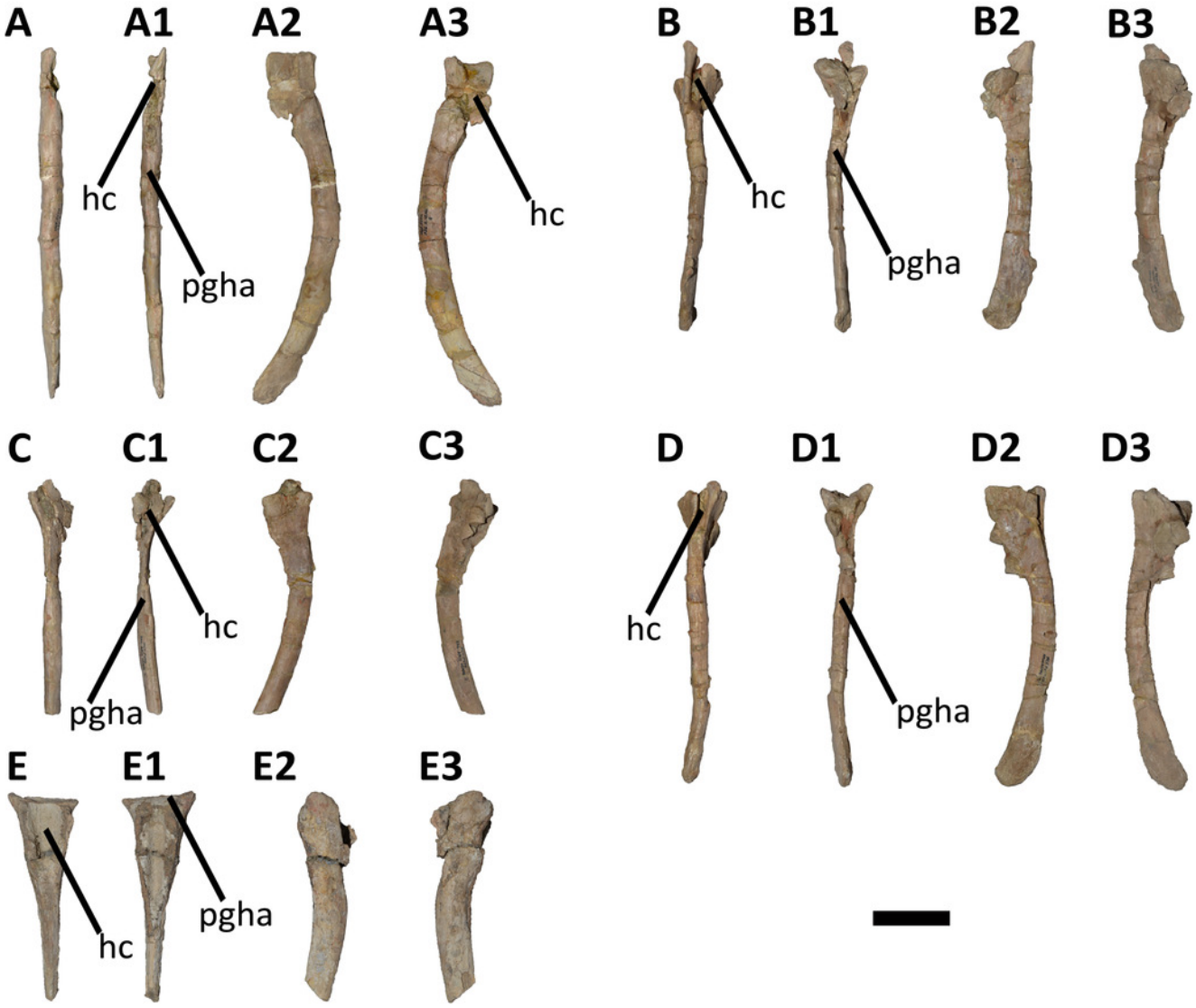

Figure 27

Phylogenetic relationships of *Aucasaurus garridoi* MCF-PVPH-236.

The results show a quite unresolved strisct consensus (A), and a more resolved topology of the reduced consensus (B). Colored dots were used for node-based taxa, colored arrows for stem-based taxa.

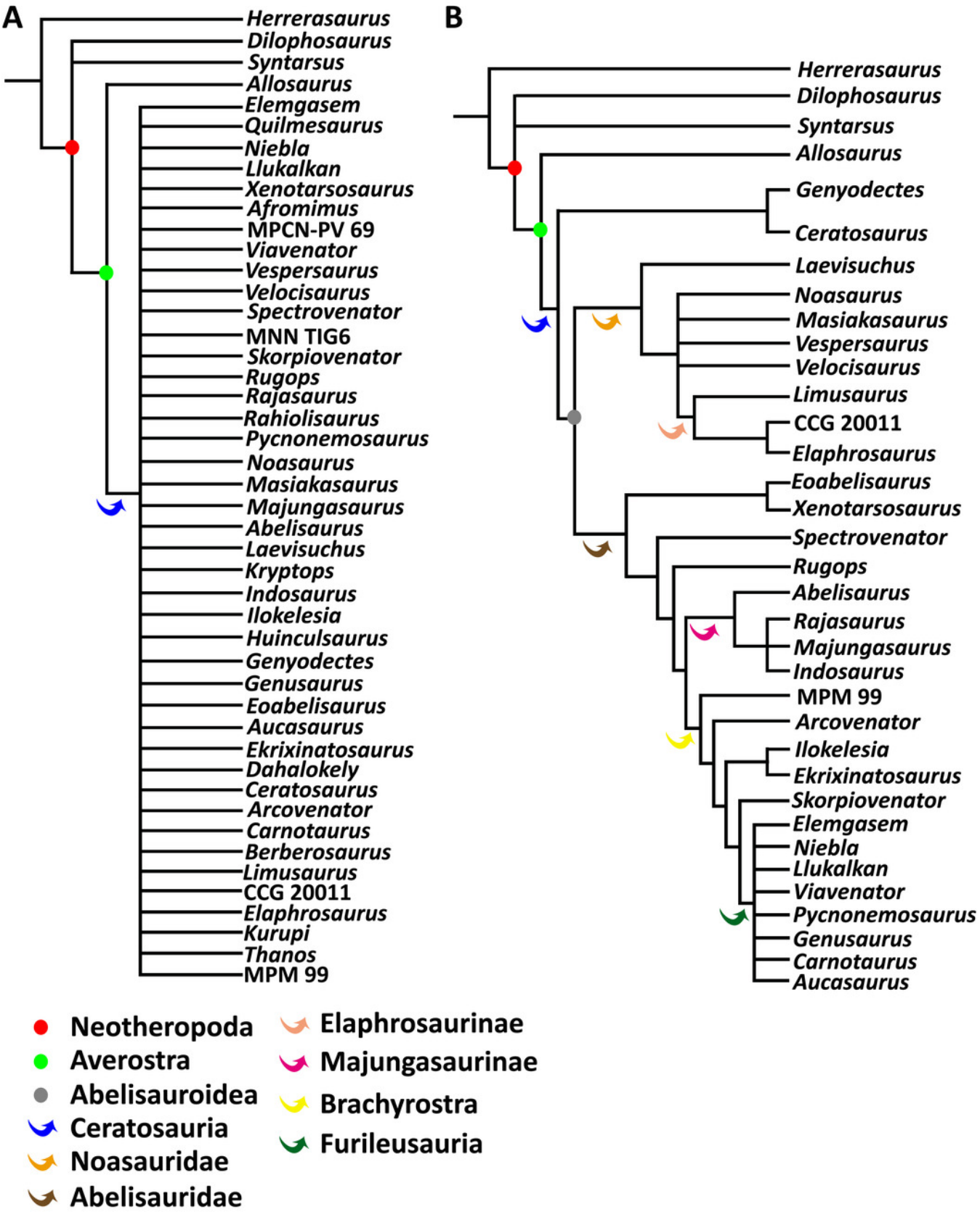
A
Herrerasaurus
Dilophosaurus
Syntarsus
Allosaurus
Elemgasem
Quilmesaurus
Niebla
Llukalkan
Xenotarsosaurus
Afromimus
MPCN-PV 69
Viavenator
Vespersaurus
Velocisaurus
Spectrovenator
MNN TIG6
Skorpiovenator
Rugops
Rajasaurus
Rahiolisaurus
Pycnonemosaurus
Noasaurus
Masiakasaurus
Majungasaurus
Abelisaurus
Laevisuchus
Kryptops
Indosaurus
Ilokelesia
Huinculsaurus
Genyodectes
Genusaurus
Eoabelisaurus
Aucasaurus
Ekrixinatosaurus
Dahalokely
Ceratosaurus
Arcovenator
Carnotaurus
Berberosaurus
Limusaurus
CCG 20011
Elaphrosaurus
Kurupi
Thanos
MPM 99
B
Herrerasaurus
Dilophosaurus
Syntarsus
Allosaurus
Genyodectes
Ceratosaurus
Laevisuchus
Noasaurus
Masiakasaurus
Vespersaurus
Velocisaurus
Limusaurus
CCG 20011
Elaphrosaurus
Eoabelisaurus
Xenotarsosaurus
Spectrovenator
Rugops
Abelisaurus
Rajasaurus
Majungasaurus
Indosaurus
MPM 99
Arcovenator
Ilokelesia
Ekrixinatosaurus
Skorpiovenator
Elemgasem
Niebla
Llukalkan
Viavenator
Pycnonemosaurus
Genusaurus
Carnotaurus
Aucasaurus
Neotheropoda
Averostra
Abelisauroidea
Ceratosauria
Noasauridae
Abelisauridae
Elaphrosaurinae
Majungasaurinae
Brachyrostra
Furileusauria

Figure 28

Photographs of autapomorphies of *Aucasaurus garridoi*.

Dorsal view of the odontoids of *Aucasaurus* (A), *Carnotaurus* (B), *Thanos* (C), *Majungasaurus* (modified by O'Connor, 2007) (E), and *Masiakasaurus* (modified by Carrano, Loewen & Sertich, 2011) (D). Image not to scale.

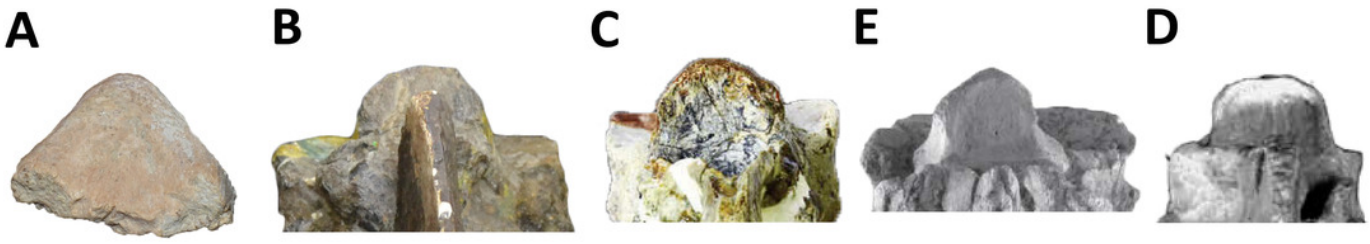

Figure 29

Photographs of autapomorphies of *Aucasaurus garridoi*.

Outline (in red dashed line) of the anterior articular surface of the atlas of *Aucasaurus* (A), *Viavenator* (B), and *Carnotaurus* (C). Interspinous accessory processes on the dorsal (D), sacral (E), and caudal (F) neural spines of *Aucasaurus*. Lateral tubercle of prezygapophysis in the middle caudal vertebrae of *Aucasaurus* (G), and ventral bulge on prezygapophysis of the posterior caudal vertebrae of *Alioramus* (modified by Brusatte, Carr & Norell, 2012) (H). Foramina on the dorsal surface of the caudal neural arch in *Meraxes* (I). Whereas, *Aucasaurus* holds pneumatic foramina on the dorsal surface of the neural arches (framed by blue dashed lines) of the ninth (J) and eleventh (K) caudal vertebrae. Image not to scale.

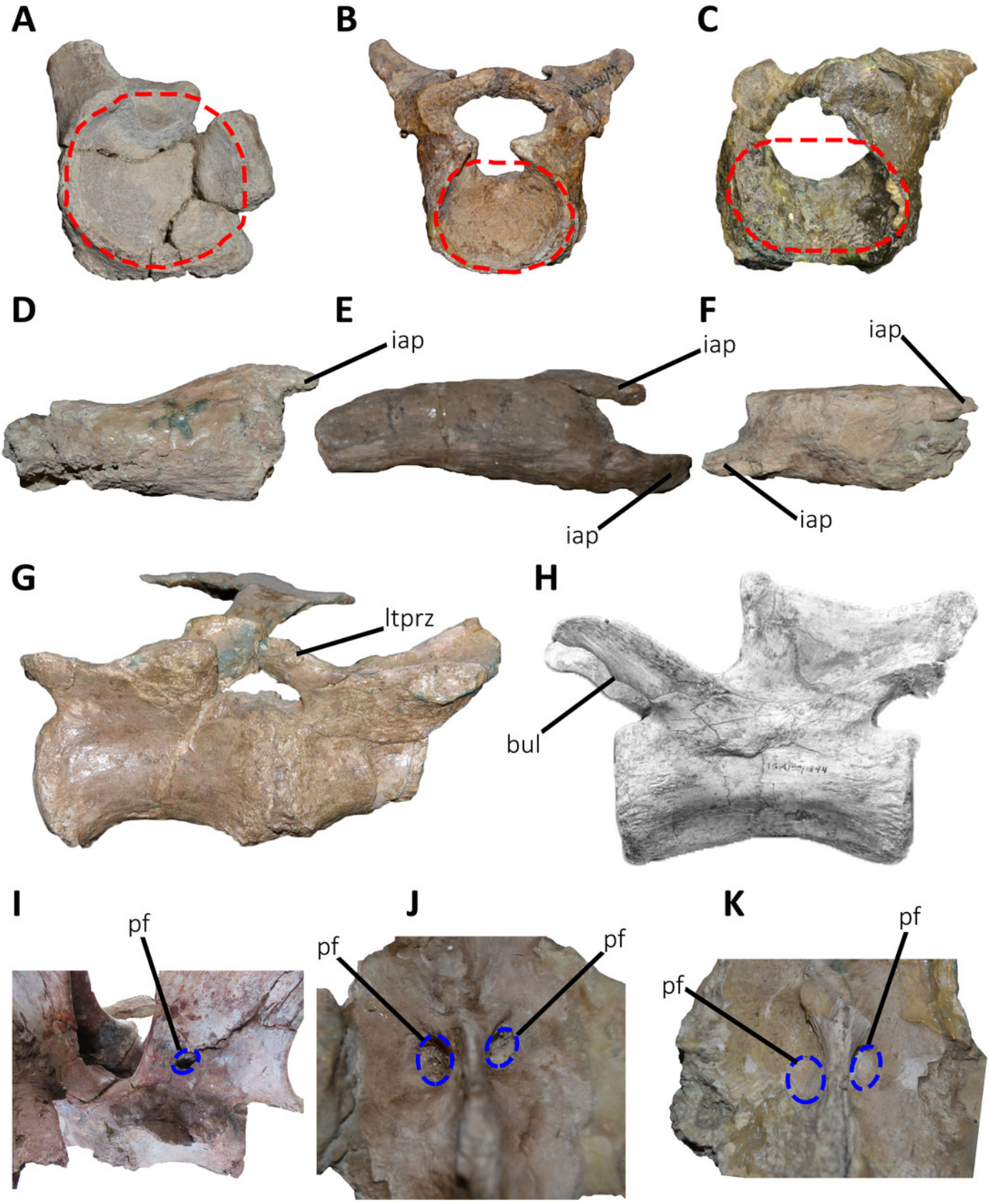
A
B
C
D
E
iap
iap
iap
F
iap
iap
G
ltprz
H
bul
I
pf
J
pf
pf
K
pf
pf

Figure 30

Photographs of autapomorphies of *Aucasaurus garridoi*.

Lateral rugosity and tubercle of the transverse processes of the fourth (A), ninth (B), and eleventh (C) caudal vertebrae of *Aucasaurus* in dorsal (upper) and lateral (lower) views. Anterodorsal scar (black arrows) of the transverse processes of the first (D), and second (E) caudal vertebrae of *Aucasaurus*, and cuneiform process (black arrow) on the anterodorsal surface of the anterior caudal vertebra of *Kurupi* (F). Triangular distal process (red lines) of posterior gastralia in ventral (G), and dorsal (H) views. Proximal portion of the first (I), and second (J) haemal arches showing a dorsally open haemal canal. Image not to scale.

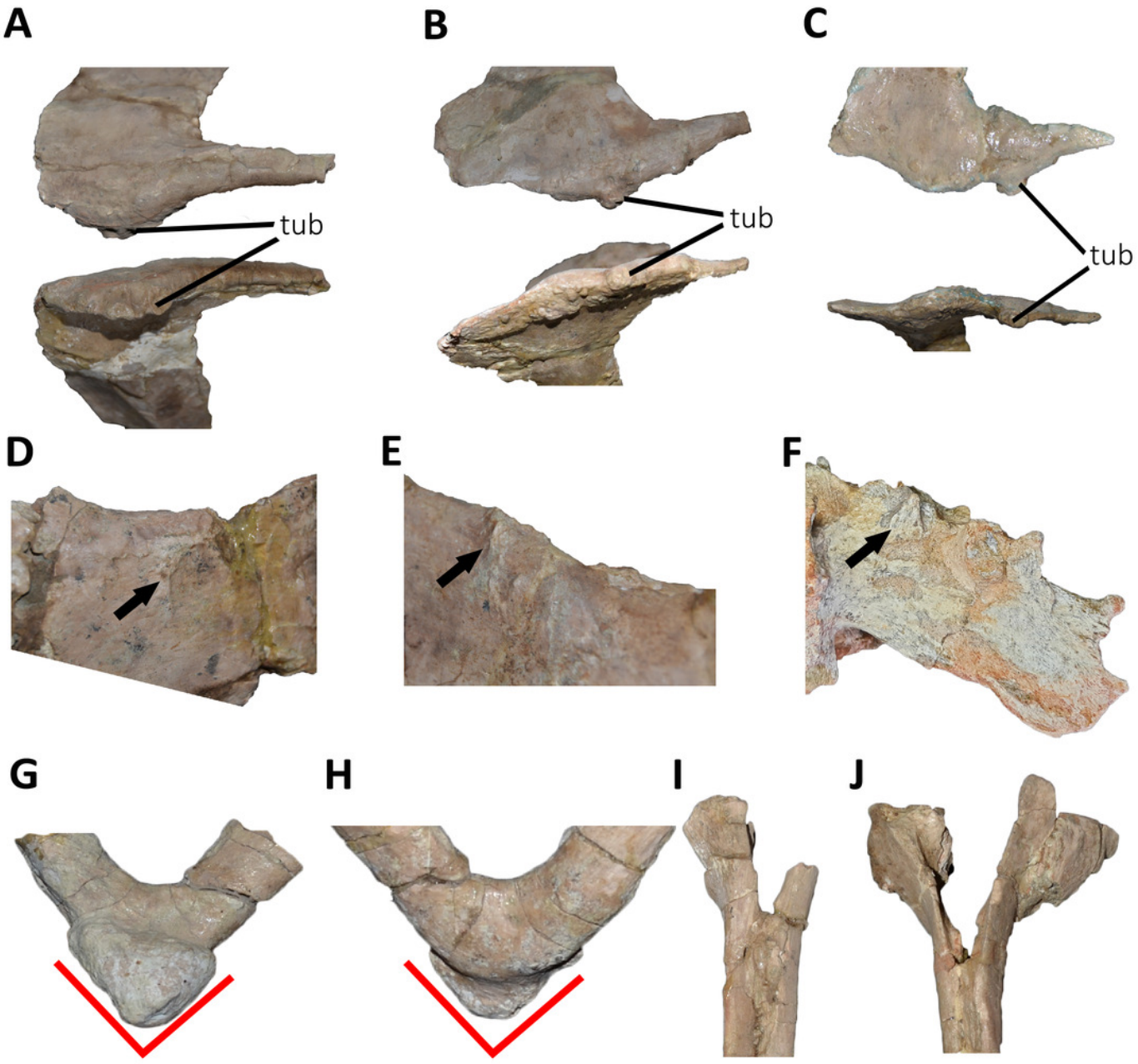
A
tub
B
tub
C
tub
D
E
F
G
H
I
J

Figure 31

Select computed tomography sections of selected caudal vertebrae of *Aucasaurus garridoi*.

First (A, B, I, J), fifth and sixth (C, D, K, L), ninth (E, F, N, O), and twelfth and thirteenth (G, H, P, Q) caudal vertebrae in anterior (A, C, E, G), and posterior (B, D, F, H) views. Red lines indicate sagittal sections, while blu lines indicate transverse sections. Abbreviations: ct, camellate tissue.

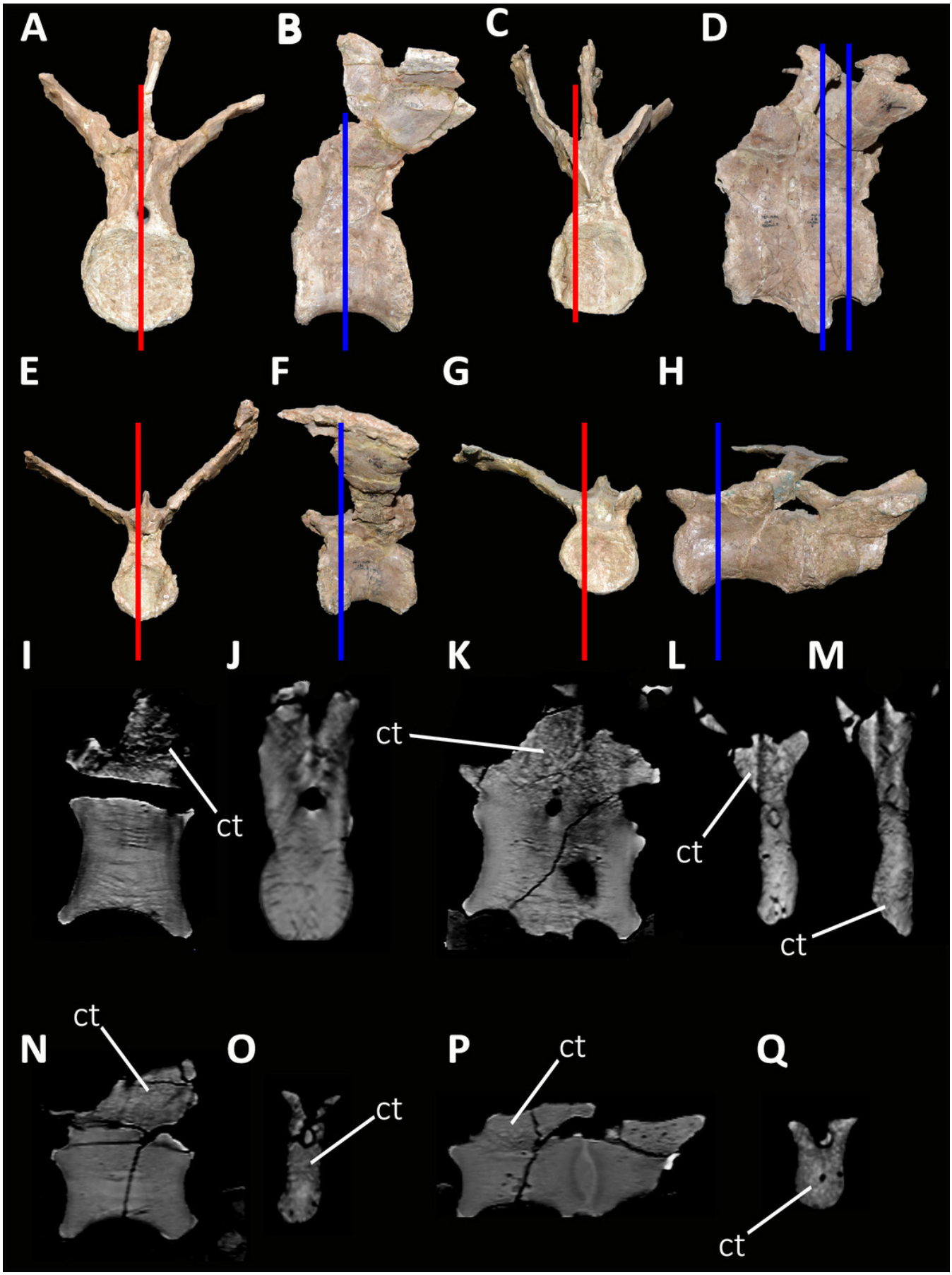
A
B
C
D
E
F
G
H
I
J
K
L
M
ct
ct
ct
ct
ct
N
O
P
Q
ct
ct
ct
ct

Figure 32

Photographs of possible external correlates of pneumaticity in *Aucasaurus garridoi*.

Foramina (black arrows) whitin the pocdf of the first (A), fourth (B), and ninth (C) caudal vertebrae of *Aucasaurus*.

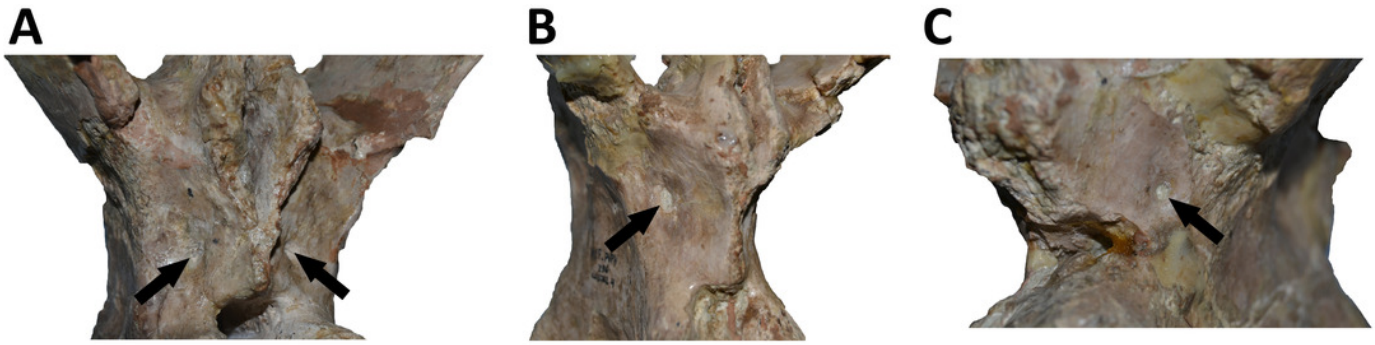

Figure 33

Internal tissue in caudal vertebrae of two brachyrostran abelisaurids.

The camellate tissues is visible in the centrum of Abelisauridae indet. MPM 99 (A), and the transverse process of *Kurupi* (B). On the right, details of the camellate tissues in both specimens. Image not to scale.

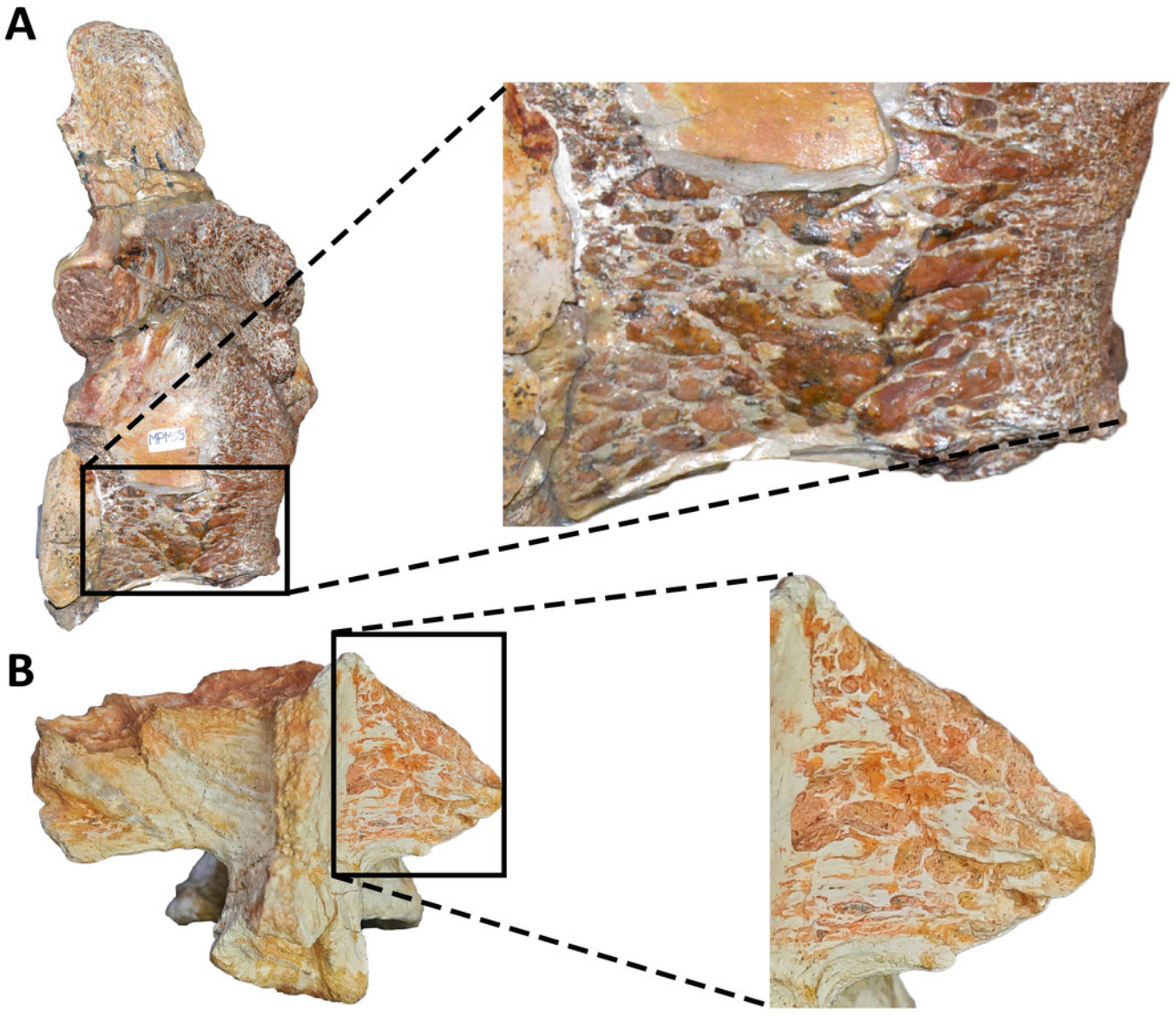

Figure 34

Details of the dorsal and caudal vertebrae of several abelisaurids.

Structures on the dorsal surface of the transverse process in the second dorsal vertebra of *Viavenator* (A, B), and anterior dorsal vertebra of MAU-Pv-LI 665 (C, D). Interspinous accessory process on the dorsal neural spine of the fourth dorsal vertebra of *Viavenator* (E), and *Aucasaurus* (F). Scar (black arrows) on the dorsal surface of the mid caudal transverse processes of *Aucasaurus* (G, H), *Viavenator* (I, J), and MAU-Pv-LI 547 (K). Ventrolateral ridge (black arrows) of the transverse process in *Aucasaurus* (L), and *Viavenator* (M) (lateral ridges of centrodiapophyseal lamina indicate by red arrows). Image not to scale.

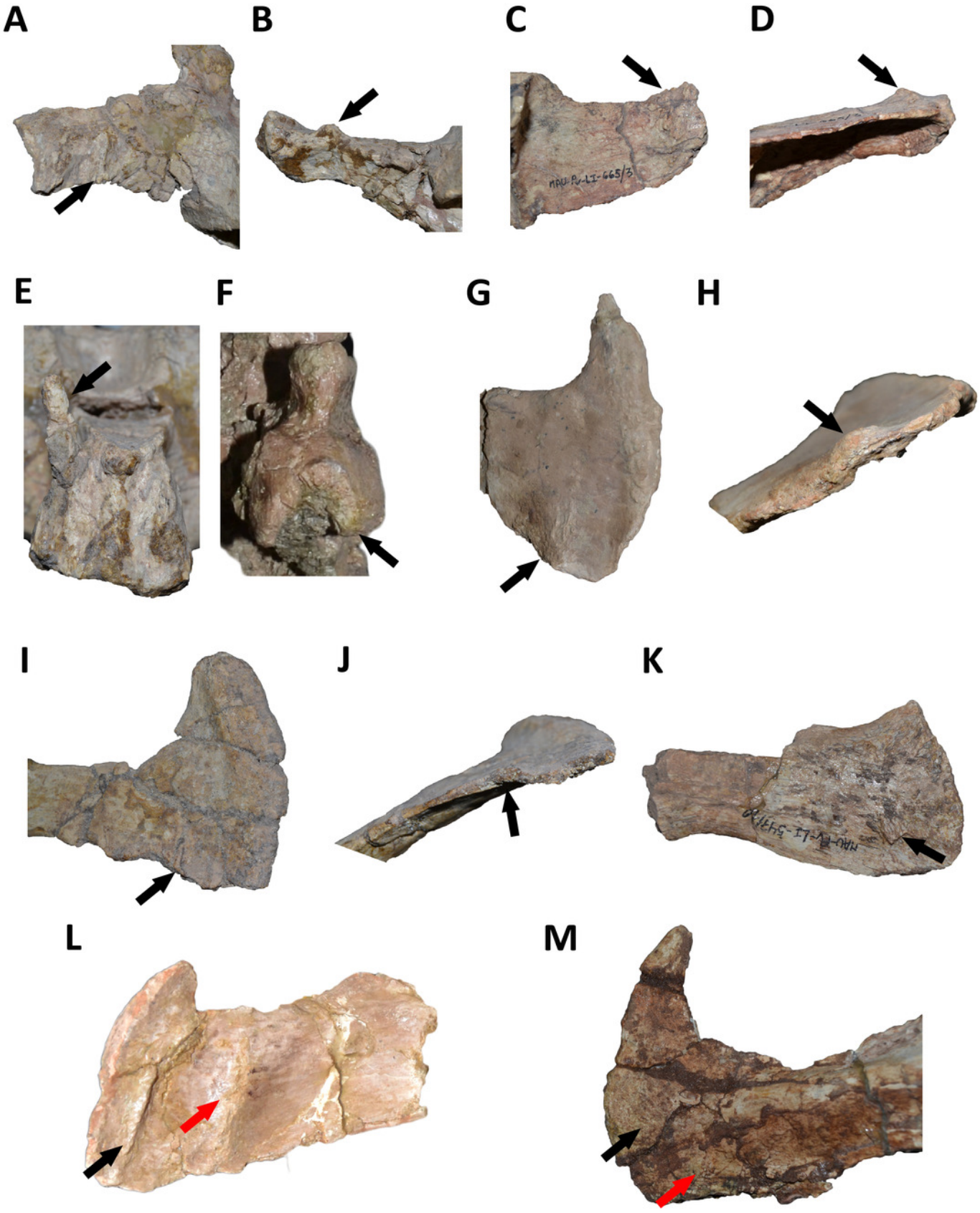
A
B
C
D
E
F
G
H
I
J
K
L
M